A Front Tracking Method for Modelling Thermal Growth

Thesis by

Elizabeth Anne Howard

In Partial Fulfillment of the Requirements
for the Degree of
Doctor of Philosophy

California Institute of Technology
Pasadena, California

2002
(Submitted 25 July 2002)

Acknowledgements

I could not have finished this thesis without the support of my friends and family. Although I cannot list all of the people who have helped to encourage and guide me, a few do deserve a special mention. First and foremost, I want to express my love and appreciation for my partner and husband, Bryan Howard. Bryan has helped me, supported me, loved me, and kept me working when I didn't think that I could do anymore. I would like to thank my advisor, Professor Dan Meiron, for his patience and guidance. I am also extremely grateful to David Camp for the many and lengthy discussions about the material in this thesis. My family has been supportive without pressuring me through a very long graduate career. To my parents, Wilbur and Winona, and my brother and his family, Chris, Kris, Phillip, Emily, Katie, and Colin. I want to thank you for your encouragement and acceptance. I have made many special friends during the course of my work, but I would like to thank Cynthia Kiser, Michelle Weinberger, and Tim Conrow for keeping me sane during the end of my graduate career. I know that it wasn't easy. I would also like to thank Brunella Lahey, for her insightful comment that kept me working on this when I was prepared to stop. Thank you all.

Abstract

Several important thermal growth problems involve a solid growing into an undercooled liquid. The heat that is released at the interface diffuses into both the solid and the liquid phases. This is a free boundary problem where the position of the interface is an unknown which must be found as part of the solution. The problem can conveniently be represented as an integral equation for the unknown interface. However, a history integral must be evaluated at each time step which requires information about the boundary position at all previous times. The time and memory required to perform this calculation quickly becomes unreasonable. We develop an alternative way to deal with the problems that the history integral presents. By taking advantage of properties of the diffusion equation, we can use a method with a constant operation count and amount of memory required for each time step. We show that a numerical algorithm can be implemented for a two-dimensional, symmetric problem with equal physical parameters in both phases. The results agree well with the exact solution for the expanding circle case and microscopic solvability theory. We also extend the method to the nonsymmetric case. Additionally, a stability analysis is done of a simple, parabolic moving front to perturbations on the surface. As the eigenvalues of our problem increase, the interface becomes more increasingly oscillatory.

Contents

Acknowledgements **iii**

Abstract **iv**

1 Introduction **1**

1.1 Introducing the Solidification Problem 1

1.2 Mathematical Description of the Problem 1

1.3 Challenges of the Problem 5

1.4 Previous Work 6

1.5 Preview of this Thesis 9

2 Integral Equation Formulation **11**

2.1 Derivation 11

2.2 Symmetric Case 18

2.3 Nonsymmetric Case 20

3 Numerical Algorithm for the 2-D Symmetric Case **23**

3.1 Numerical Formulation 23

3.1.1 Step 1: Separate Singular and Smooth Parts 27

3.1.2 Step 2: Approximate the Singular Integral 29

3.1.3 Step 3: Find the Interface Position 34

3.1.4 Step 4: Diffuse the Smooth Temperature Field 38

3.1.5 Step 5: Find the New Contribution 43

3.2 Analytic Solutions 44

3.2.1 Advancing Planar Front 44

3.2.2 Expanding Circle 46

4 Numerical Stability Analysis of the Ivantsov Solution **49**

4.1 Introduction 49

4.2 Ivantsov Solution 50

4.3 Linear Stability Analysis 52

4.4 Discretization 54

4.5 Implicitly Restarted Arnoldi Method 56

4.6 Numerical Results 60

5 Application to 2-D Solidification **65**

5.1 Expanding Circle Case 65

5.2 Convergence in the 2-D Symmetric Case 71

5.3 Velocity Selection for a Needle Crystal 92

6 Numerical Algorithm for the 2-D nonsymmetric Case **105**

6.1 Two-Sided Case 105

6.1.1 Step 1: Separate into Singular and Smooth Parts 106

6.1.2 Step 2: Approximate the Singular Integrals 109

6.1.3 Step 3: Find the Interface Position 117

6.1.4 Step 4: Diffuse the Smooth Temperature Field 120

6.1.5 Step 5: Find the New Contribution 121

6.2 One-Sided Model 123

7 Summary and Ideas for Future Work **125**

Bibliography **126**

List of Figures

1.1 A stable system where the liquid bath is initially at a uniform tempearture above the freezing temperature. The walls of the system are then lowered to a temperature below the freezing temperature and held there. Solidification begins at the walls and progresses inward. 2

1.2 An unstable system where the liquid bath is initially at a uniform temperature below the freezing temperature. Solidification begins at a central seed and proceeds outward. 4

2.1 Solidification into an undercooled melt where the liquid bath is initially at a uniform temperature below the freezing temperature. Solidification is started at a central seed and proceeds outward into the undercooled liquid. 12

2.2 The angle used for determination of anisotropy is measured as the deviation from the outward pointing normal to the advancing solidification surface. 13

3.1 Segmentation of the interface into I segments of equal length starting at the negative real axis (angle $= -\pi$). 30

4.1 $\eta - \xi$ orthogonal coordinate system 51

4.2 The computed interface position N associated with the positive eigenvalue $\sigma = 0.005$ of our matrix A. Positive eigenvalues imply that the solidification of the needle crystal is unstable. 61

4.3 The computed interface position N associated with the positive eigenvalue $\sigma = 0.102$ of our matrix A. Positive eigenvalues imply that the solidification of the needle crystal is unstable. 62

4.4 The computed interface position N associated with the positive eigenvalue $\sigma = 0.186$ of our matrix A. Positive eigenvalues imply that the solidification of the needle crystal is unstable. 63

4.5 The temperature field U in both phases corresponding to the positive eigenvalue $\sigma = 0.186$. 64

5.1 The similarity solution is used to test our code with a similarity constant $\lambda = 0.5$, a constant for diffusion $\kappa = 1$, the number of steps held in memory $N = 2$, and the outer radius of the system $r_{\max}/r_0 = 60$. . 66

5.2 The similarity solution is used to test our code with a similarity constant $\lambda = 0.5$, a constant for diffusion $\kappa = 1$, the number of steps held in memory $N = 2$, and the outer radius of the system $r_{\max} = 60$. . . . 67

5.3 The similarity solution is used to test our code with a similarity constant $\lambda = 0.5$, a constant for diffusion $\kappa = 1$, and the number of steps held in memory $N = 2$. 68

5.4 The similarity solution is used to test our code with a similarity constant $\lambda = 0.5$, a constant for diffusion $\kappa = 1$, the number of steps held in memory $N = 2$, and the outer radius of the system $r_{\max} = 60$. . . . 69

5.5 Runs for different time step sizes with similarity constant $\lambda = 0.5$, constant for diffusion $\kappa = 1$, the number of steps held in memory $N = 2$, and $d_0 = 0.04$. 70

5.6 Runs for different time step sizes with similarity constant $\lambda = 0.5$, constant for diffusion $\kappa = 1$, the number of steps held in memory $N = 2$, and $d_0 = 0.04$. 71

5.7 Surface position determined when starting with a circular contour with anisotropy $\alpha = 0.60$ and undercooling $\Delta = 0.56$. 72

5.8 Surface position determined when starting with a circular contour with anisotropy $\alpha = 0.70$ and undercooling $\Delta = 0.56$. 72

5.9 Surface position determined when starting with a circular contour with anisotropy $\alpha = 0.80$ and undercooling $\Delta = 0.56$. 73

5.10 Surface position determined when starting with a circular contour with anisotropy $\alpha = 0.70$ and undercooling $\Delta = 0.48$. 74
5.11 Surface position determined when starting with a circular contour with anisotropy $\alpha = 0.70$ and undercooling $\Delta = 0.52$. 74
5.12 Surface position determined when starting with a circular contour with anisotropy $\alpha = 0.70$ and undercooling $\Delta = 0.56$. 75
5.13 Surface position determined when starting with a perturbed circular contour with a perturbation constant of $p = 0.10$ with anisotropy $\alpha = 0.00$ and undercooling $\Delta = 0.60$ and $d_0 = 0.04$. 77
5.14 Surface position determined when starting with a perturbed circular contour with a perturbation constant of $p = 0.10$ with anisotropy $\alpha = 0.00$ and undercooling $\Delta = 0.60$ and $d_0 = 0.02$. 78
5.15 Initial perturbation of the $d_0 = 0.0$ similarity solution with a perturbation constant $p = 0.10$. 79
5.16 Tip position determined with anisotropy $\alpha = 0.30$ and undercooling $\Delta = 0.64$. 80
5.17 Tip velocity determined with anisotropy $\alpha = 0.30$ and undercooling $\Delta = 0.64$. 81
5.18 Difference from converged tip position determined with anisotropy $\alpha = 0.30$, and undercooling $\Delta = 0.64$. 82
5.19 Tip position determined with anisotropy $\alpha = 0.40$ and undercooling $\Delta = 0.60$. 83
5.20 Tip velocity determined with anisotropy $\alpha = 0.40$ and undercooling $\Delta = 0.60$. 84
5.21 Tip position determined with anisotropy $\alpha = 0.40$ and undercooling $\Delta = 0.60$. 86
5.23 Tip velocity determined with anisotropy $\alpha = 0.40$ and undercooling $\Delta = 0.60$. 87
5.22 Tip position determined with anisotropy $\alpha = 0.40$ and undercooling $\Delta = 0.60$. 88

5.24 Difference in tip position from assumed converged solution with changing radial grid sizes as determined with anisotropy $\alpha = 0.40$ and undercooling $\Delta = 0.60$. 89
5.25 Tip position determined with anisotropy $\alpha = 0.45$ and undercooling $\Delta = 0.60$. 90
5.26 Tip velocity determined with anisotropy $\alpha = 0.45$ and undercooling $\Delta = 0.60$. 91
5.27 Difference from converged tip position determined with anisotropy $\alpha = 0.45$ and undercooling $\Delta = 0.60$. 93
5.28 Plot of (tip velocity) $\times$ (tip radius)^2 vs. anisotropy for various undercoolings. 98
5.29 Plot of (tip velocity) $\times$ (tip radius)^2 vs. anisotropy for various undercoolings. 99
5.30 Plot of tip velocity vs. undercooling for various values of anisotropy. . 100
5.31 Plot of tip velocity vs. undercooling for various values of anisotropy. . 101
5.32 Plot of tip velocity vs. anisotropy for various values of undercooling. . 102
5.33 Plot of tip velocity vs. anisotropy for various values of undercooling. . 103

Chapter 1 Introduction

1.1 Introducing the Solidification Problem

Snowflakes are a common example of unstable solidification in nature. You can easily see the sixfold symmetry demonstrating the effect of anisotropy (preferential solidification based on direction) in the formation of dendrites and side branches in snowflakes. Although each snowflake has six similar branches, each branch is unique. Slightly different initial conditions and differences in forcing are expected to produce these different structures. The growth of a solid from an undercooled or supersaturated melt gives rise to dendritic pattern formation, a process characterized by propagation of a needle-shaped tip and the persistent emission of side branches [8]. The phenomenon of dendritic crystal growth is a particularly elegant example of a process in which an instability of a simple system generates complex but highly structured new patterns [26].

1.2 Mathematical Description of the Problem

Consider a container of a pure substance which is initially at a temperature, T, above the freezing temperature of water [Figure 1.1].

$$\lim_{\mathbf{x}\to 0} T > T_{melting}. \tag{1.1}$$

If you lower the temperature of the walls to below the freezing temperature,

$$\lim_{\mathbf{x}\to \infty} T < T_{melting}, \tag{1.2}$$

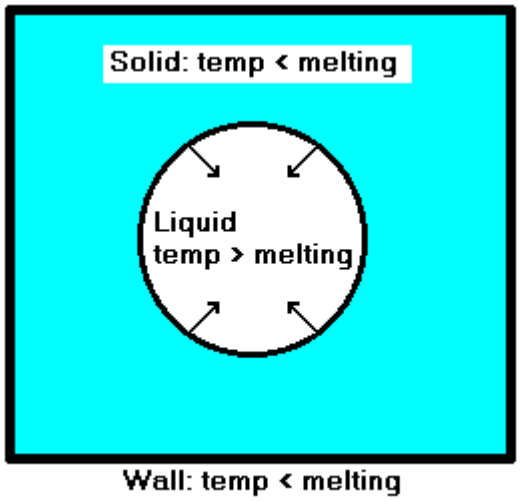

Figure 1.1: A stable system where the liquid bath is initially at a uniform tempearture above the freezing temperature. The walls of the system are then lowered to a temperature below the freezing temperature and held there. Solidification begins at the walls and progresses inward.

the solid will begin to form at the walls of the container. Heat is being removed at the walls of the container and the solid grows into the liquid from all sides. This stable solidification is characterized by conduction of heat away from the solid-liquid interface through the solid. The velocity of the moving interface is controlled by the speed of conduction of the excess heat through the solid which is in turn modelled by the classic diffusion equation:

$$\frac{\partial T}{\partial t} = \kappa \nabla^2 T \quad \text{in the solid and liquid,} \tag{1.3}$$

where κ is the thermal diffusivity. The boundary conditions imposed at the interface are given by a condition on heat conservation:

$$L\mathbf{v}\cdot\mathbf{n} = \left[k_S\left(\mathbf{n}\cdot\nabla T_S\right) - k_L\left(\mathbf{n}\cdot\nabla T_L\right)\right], \tag{1.4}$$

where $\mathbf{v}\cdot\mathbf{n}$ is the normal velocity of the interface, k_S and k_L are the thermal conductivities in the solid and liquid, respectively, T_S and T_L are the temperatures in

the solid and liquid, respectively, and L is the latent heat of solidification. The other boundary condition is a statement of local thermodynamic equilibrium

$$T = T_{melting} - d_0 K \quad \text{at the interface.} \tag{1.5}$$

The second term on the right-hand side of (1.5) is a correction to the melting temperature for a curved surface often called the Gibbs-Thomson correction, where K describes the curvature and anisotropy of the system. The Gibbs-Thomson correction will be defined in more detail in Chapter 2. The interface generally remains smooth and any protrusions of the solid into the liquid are retarded [18]. The solidification front will move smoothly and uniformly towards the center. This is a smooth, stable phenomenon which can be modelled by the classical two-phase Stefan problem. The temperature field satisfies the heat equation in each phase separately, the normal velocity is the jump in the normal component of the heat flux across the interface, and the temperature on the interface is the equilibrium melting temperature. The motion of the interface is determined by the rate at which the excess energy of the solidifying fluid can be conducted out through the surrounding solid [29].

Alternatively, we look at the case of unstable solidification [Figure 1.3]. Here, a liquid bath of a pure substance is slowly cooled to below its normal freezing temperature without initiating freezing.

$$T < T_{melting} \quad \text{for all } \mathbf{x} \text{ at time } t_0 \tag{1.6}$$

and

$$\lim_{\mathbf{x}\to\infty} T < T_{melting}. \tag{1.7}$$

Starting with this undercooled melt, solidification can be started at a central nucleating point in the solid. The solid will advance rapidly into the undercooled liquid. The latent heat generated at the interface must now be conducted away from the interface through the liquid in order for the crystal to grow. The process is controlled by the

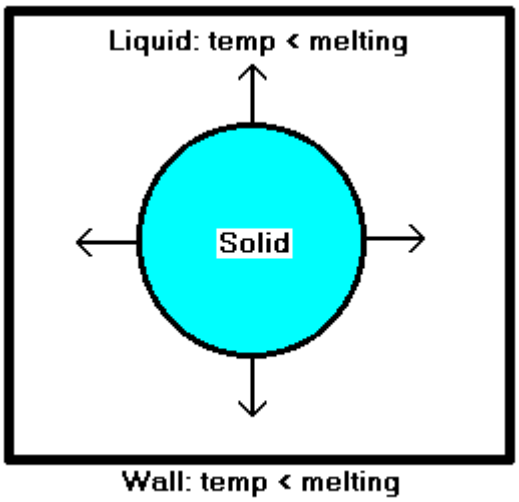

Figure 1.2: An unstable system where the liquid bath is initially at a uniform temperature below the freezing temperature. Solidification begins at a central seed and proceeds outward.

amount of heat that can be removed from the interface surface [29]. Here again,

$$\frac{\partial T}{\partial t} = \kappa \nabla^2 T \quad \text{in the solid and liquid.} \tag{1.8}$$

The boundary conditions (1.4) and (1.5) from the stable case are applicable to this case as well. This situation is intrinsically unstable and the interface breaks up into dendrites which grow relatively rapidly out from the central seed [29].

Both the stable and unstable systems can be modelled by a moving boundary problem. As in most crystal growth problems, this involves solving the diffusion equation in the two domains representing solid and liquid phases. The diffusion equations are coupled by boundary conditions describing the production of latent heat at the interface during the freezing process and the Gibbs-Thomson correction to the melting temperature at the interface. The interface position is unknown and must be determined as a part of the solution [4].

1.3 Challenges of the Problem

The equations for either the stable or unstable case are highly nonlinear due to the conditions on the interface. Few exact solutions to these problems have been found and this has lead to interest in numerical solutions to these problems. The problem is often converted to an integral equation. Because the integral equations only need to be evaluated on the interface, the dimension of the problem is reduced. The integral equations are derived in detail in Chapter 2. Often, a simplified version of the system is investigated where the physical properties (thermal conductivity and diffusivity) of the liquid and solid are assumed to be the same. However, we will find that even in this case, called the symmetric case, the integral equation is quite complex and will be seen to be of the form:

$$\begin{aligned}\Delta = d_0 f\left(s,t,\alpha\right) K\left(s,t\right) + \int_V u_S\left(\mathbf{x}',t_0\right) G\left(\mathbf{x}',t;\zeta\left(s,t\right),t_0\right) dV' \\ + \kappa \int_{t_0}^{t} \int_{S(t')} G\left(\mathbf{x}',t;\zeta\left(s,t\right),t'\right) \left[\mathbf{v}'\cdot\mathbf{n}'\right] dS'dt'\end{aligned} \tag{1.9}$$

where

$$\begin{aligned} G\left(\mathbf{x},t;\mathbf{x}',t'\right) &= \frac{\exp\left(-\left|\mathbf{x}-\mathbf{x}'\right|^2/\left(4\kappa\left(t-t'\right)\right)\right)}{\left[4\pi\kappa\left(t-t'\right)\right]^{d/2}} \qquad \text{for } t' < t \\ G\left(\mathbf{x},t;\mathbf{x}',t'\right) &= 0 \qquad\qquad\qquad\qquad\qquad\qquad\quad \text{for } t' > t. \end{aligned} \tag{1.10}$$

A direct approach to solving the integral equation can be problematic. First, it can be seen that the integrand (1.9) contains a singularity at the current time. Therefore, evaluation of the integral equations must be approached with care. Additionally, the integral equation formulation of the problem contains a history integral which tracks the release of latent heat since the initial time. The surface integrals are evaluated over the entire history of the system. For each time step, the entire history of the system must be retained. The increasing memory and time required may prohibit direct evaluation, especially in higher dimensions.

We propose an alternative numerical method for modelling the unstable problem which requires both a constant amount of time and memory for each time step. We take advantage of properties of the heat equation to avoid holding the entire history

of the system in memory for each time step. The proposed method splits the history integral into two pieces. The first and, as time increases, larger piece is smooth and can be advanced independently because it satisfies the heat equation. The remaining, smaller piece as time increases contains the singularity in the kernel and must be approximated. This method provides a constant operation count for each time step. However, it does require the introduction of an underlying spatial grid for the smooth temperature field.

1.4 Previous Work

Dendritic solidification is a challenging problem, but there are several general approaches which have been used to model the problem. Successful methods must be robust enough to handle highly deformed interface geometries.

Phase field models introduce an order parameter, $\phi(x,t)$, which identifies the phase of a point x. The order parameter, $\phi(x,t)$, takes on given and different constant values in the solid and liquid phases; $\phi = 1$ in the solid and $\phi = -1$ in the liquid are a common choice. Values of $\phi(x)$ in the range $(-1,1)$ indicate points which lie on the interface. In the case where $\phi = 1$ in the solid and $\phi = -1$ in the liquid, the dimensionless temperature field, u, of the system is coupled to the order parameter by the relationship [5]:

$$\frac{\partial u}{\partial t} = \kappa \nabla^2 u + \frac{1}{2}\frac{\partial \phi}{\partial t}. \tag{1.11}$$

Because of this smoothed step function $\phi(x,t)$, there is never a sharp boundary. And, therefore, the boundary conditions are never explicitly applied. However, Caginalp [6] has shown that the sharp-interface boundary conditions are recovered as the width of the interfacial region vanishes. Numerical computations by Kobayashi [22] using such an approach show the expected large scale dendritic features. However, Juric and Tryggvason [18] suggest that smaller-scale features of Kobayashi's model are dependent on the underlying mesh used. Simulations by Karma and Rappel [19], [20], and [21] using a new thin-interface limit version of the phase field equations also

demonstrate the promise of this method.

The immersed boundary technique described by Juric and Tryggvason [18] uses a fixed grid to track the temperature field for the problem and explicit tracking of the solid-liquid interface position. This technique uses a single heat equation for both phases which adds a forcing term at the boundary to incorporate the liberation of heat at the interface during solidification:

$$\frac{\partial (cT)}{\partial t} = \nabla \cdot k \nabla T + Q, \tag{1.12}$$

where T is the temperature field, c is the heat capacity, and k is the thermal conductivity. The source term Q at the solid-liquid interface is given by

$$Q = \int_S \left[L + (c_L - c_S) \left(T_{surface} - T_{melting} \right) \right] \delta \left(\mathbf{x} - \mathbf{x}_S \right) dS, \tag{1.13}$$

where L is the latent heat of solidification, c_L and c_S are heat capacities in the liquid and solid, and the delta function is nonzero only at the interface. This formulation of the heat source at the interface is derived in [1]. The Gibbs-Thomson equation is additionally applied as a boundary condition at the interface. Solution of the problem in this formulation requires knowledge of the interface position and a numerical representation of the delta function. The interface is represented using a series of marker particles. The method is able to track highly complex interface geometries. However, Lahey [24] shows that the method is only first-order accurate and does not agree well with linear stability theory.

Lahey [24] uses an immersed interface method where a custom finite difference stencils are constructed to allow second-order accurate calculations of derivatives of nonsmooth functions at the interface. Knowledge of the jumps in the value of the function of interest and its derivatives at the interface are used to reduce the error of the stencil. The resulting front tracking method was found able to simulate dendritic solidification in the presence of convection. The method was shown to be second-order accurate and could be extended to even higher orders of accuracy.

Level set methods have become viable for modelling dendritic solidification. Level

set methods introduce a variable ϕ which is defined to be the distance from the interface. Therefore, the interface position can be established by finding the position (level set) where:

$$\phi = 0.$$

The interface position can be updated through the solution of the equation found in [24]:

$$\frac{\partial \phi}{\partial t} + \mathbf{v} \cdot \nabla \phi = 0, \tag{1.14}$$

where $\mathbf{v}$ is the normal velocity of the interface. Chen, Merriman, Osher, and Smereka show agreement in [12] with stability theory and a capability to model deformed interface geometries.

Finite element methods have been used by many researchers to model the dendritic solidification problem. One approach allows the finite element mesh to deform as the interface moves so that elements are in either the solid or liquid phase, but not both. This is quite difficult to implement because the interface is of an irregular shape and continuously deforming in time. Also, since the interface position must be determined as a part of the solution, setting up the mesh itself becomes a part of the problem. Linear stability theory is shown to be satisfied in [44]. Another method is presented by Schmidt in [38], which does not require that mesh elements be entirely in either phase. This allows extremely complex interface shapes to be modelled. However, because elements can contain both solid and liquid phases, the method is restricted to only symmetric problems (where the physical parameters of the system are the same in both the solid and liquid phases.)

Brattkus and Meiron [4] have used a variant of the method that we outline here to look at the one-dimensional, symmetric case of an advancing planar front. We will discuss the method in greater detail in Chapter 2. However, they were able to achieve second-order accuracy in comparison to the known, exact similarity solution to the one-dimensional, symmetric model. Another possible simplification of our system is also explored, a one-sided model. In a one-sided model, no diffusion takes place in the solid phase. This method again leads to a single integral equation, but one that

contains more terms than that found for the symmetric model. The one-dimensional, one-sided method is applied to the problem of rapid solidification. Banded structures observed in rapidly solidified alloys represent essentially one-dimensional growth. The transition point is found to be accurate to within 1 percent and the value of the initial oscillation frequency agrees even more closely to that found by linear theory. The numerical algorithm works well for one-dimensional problems and we will extend this method to two-dimensional problems.

1.5 Preview of this Thesis

We show that the numerical algorithm, suggested by Brattkus and Meiron in [4], can be implemented for the symmetric case in two dimensions. The results obtained agree with theory as well as with the exact solution for the expanding circle case. We have also derived a numerical method which can be used to extend this method to the nonsymmetric case.

Additionally, an analysis is done of the stability of the Ivantsov solution, a simple parabolic moving front representing a dendrite tip, to perturbations on the surface. Our computation found many eigenvalues of our matrix with positive real parts and saw that as the eigenvalue increases, the interface becomes more oscillatory.

In Chapter 2, we look at the mathematical formulation of our problem in terms of partial differential equations and conditions at the interface. An integral equation reformulation of the problem can reduce the order of the problem we are trying to solve. We discuss in detail how our system can be converted to one using integral equations. Our system can be greatly simplified by assuming that we have a symmetric system and we explore the resulting integral equation for the symmetric problem. Two exact similarity solutions are introduced, an advancing planar front and an expanding circle. The case of the advancing planar front is included to motivate the method used to determine the expanding circle solution. However, the expanding circle solution is a valuable and direct check for our two-dimensional, numerical method.

In Chapter 3, we present the outline of the numerical method for the symmetric

case. We look specifically at the two-dimensional case and show the details of the numerical implementation. We introduce the underlying temperature field for our problem. We discuss how the smooth temperature field evaluated over the entire domain can reduce the difficulty inherent in determining the interface position with a history integral.

In Chapter 4, we look at the derivation of the Ivantsov solution. We then look at the stability of a single dendrite tip advancing into an undercooled melt. We perform a numerical stability analysis of the known Ivantsov solution to small perturbations of the interface. This is used to set the stage for our simulations of unstable solidification.

In Chapter 5, the exact similarity solution for the expanding circle case will be compared against the output from the numerical method outlined in Chapter 3. The Ivantsov solution provides a continuous family of solutions for any undercooling. Experimentally, a particular velocity and tip radius are chosen for a given undercooling. Linear stability analysis around these solutions identifies the dynamically selected needle crystal. Our output of our simulation is compared to these theoretical relationships between undercooling, velocity, and tip radius. Our results appear to validate the theory of microscopic solvability as put forth in [2], [31], [37]. Our method is shown to converge with second-order accuracy.

Chapter 6, we expand our view to include the nonsymmetric case. This gives us two integral equations coupled by our boundary conditions. Each of the integral equations is more complex than the one integral equation needed for the symmetric case. However, our method can still be applied independently to these two coupled integral equations. We present the outline of the numerical method for the more complex, nonsymmetric case. We look specifically at the two-dimensional case and show the details of the numerical implementation.

Chapter 2 Integral Equation Formulation

2.1 Derivation

We consider the problem of crystal growth from a melt of a pure substance initially cooled to a temperature, T_∞, which is below the melting temperature, T_M (see Figure 2.1). Heat conduction moves the latent heat, which is produced at the surface during solidification, away from the interface. The temperatures in the solid, $T_S(\mathbf{x}, t)$, and liquid, $T_L(\mathbf{x}, t)$, satisfy

$$\frac{\partial T_S}{\partial t} = \kappa_S \nabla^2 T_S \qquad \text{in the solid,} \tag{2.1}$$

$$\frac{\partial T_L}{\partial t} = \kappa_L \nabla^2 T_L \qquad \text{in the liquid,} \tag{2.2}$$

where κ_S and κ_L are the thermal diffusivities in the solid and liquid, respectively.

One boundary condition deals with the absorption or liberation of latent heat at the interface. When the interface grows with a normal velocity $\mathbf{v} \cdot \mathbf{n}$, then the latent heat produced is transported away from the interface by conduction in the normal direction. Equation (2.3) is often called the Stefan condition:

$$L\mathbf{v} \cdot \mathbf{n} = \left[k_S \left(\mathbf{n} \cdot \nabla T_S\right) - k_L \left(\mathbf{n} \cdot \nabla T_L\right)\right], \tag{2.3}$$

where k_S and k_L are the thermal conductivities in the solid and liquid, respectively, and L is the amount of heat released produced during the solidification process.

We can now re-scale our system to work in terms of dimensionless quantities. We will define a scaled temperature field, $u(\mathbf{x}, t)$,

$$u = \frac{T - T_\infty}{\kappa L / k}. \tag{2.4}$$

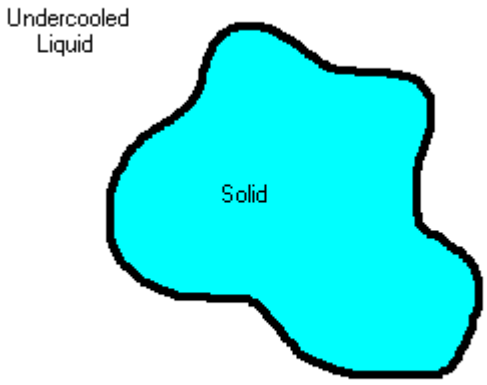

Figure 2.1: Solidification into an undercooled melt where the liquid bath is initially at a uniform temperature below the freezing temperature. Solidification is started at a central seed and proceeds outward into the undercooled liquid.

The equations for heat conduction in each phase become

$$\frac{\partial u_S}{\partial t} = \kappa_S \nabla^2 u_S, \tag{2.5}$$

$$\frac{\partial u_L}{\partial t} = \kappa_L \nabla^2 u_L. \tag{2.6}$$

The equation describing conservation of heat at the interface becomes

$$\mathbf{v} \cdot \mathbf{n} = \kappa_S \nabla u_S (s,t) \cdot \mathbf{n} - \kappa_L \nabla u_L (s,t) \cdot \mathbf{n}, \tag{2.7}$$

where s is the parameterized position on the interface and t is the current time.

Additionally, the temperature of the interface should be equal to the melting temperature with a Gibbs-Thomson surface tension correction. The Gibbs-Thomson effect (2.8) predicts the increasing depression of the melting point of a substance on a curved interface as the pressure and, therefore, the amount of curvature increases. A detailed discussion of the Gibbs-Thomson effect can be found in [31]. The Gibbs-

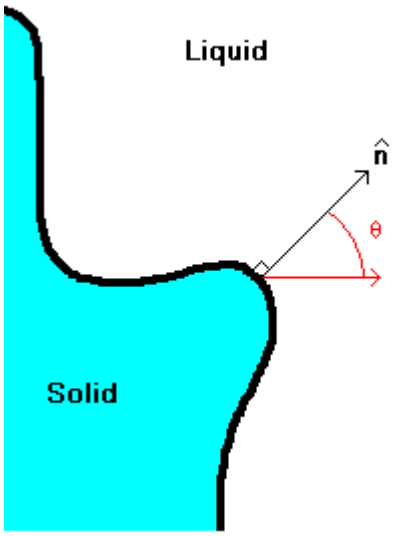

Figure 2.2: The angle used for determination of anisotropy is measured as the deviation from the outward pointing normal to the advancing solidification surface.

Thomson condition is given by:

$$u_\zeta = \Delta - d_0 f(s,t,\alpha) K(s,t), \tag{2.8}$$

where u_ζ is the temperature at a point on the interface, Δ is the transformed value of the melting temperature, and d_0 is a capillarity length as defined, for example, by Langer [31] and which is defined in greater detail below, and K refers to the curvature of the surface. d_0 is not a good length scale. We will scale with values from the initial value problem. The term $f(s,t,\alpha)$ is used to model directionally preferred solidification or anisotropy. In the case where $\alpha = 0$, there would be no preference for any particular direction of solidification. As α increases, the strength of the directional preference increases. The function $f(s,t,\alpha)$ is used to model the direction of preference for growth of the solid. We will assume a simple form of angular dependence with an $m-$fold symmetry where $\theta = \theta(s,t)$ as in Figure 2.2:

$$f(s,t,\alpha) = 1 - \alpha\cos(m\theta). \tag{2.9}$$

In the definition of d_0, we have physical parameters where γ is the surface tension, c_p is the specific heat per unit volume in the liquid, and L is the latent heat per unit volume. The parameter is given by

$$d_0 = \gamma c_p T_M / L^2. \tag{2.10}$$

The resulting free-boundary problem is often represented as a pair of integral equations. An integral equation representation of the system is often most convenient because the dimension of the original problem is reduced to the dimension of the interface. The heat equation operator and its corresponding adjoint operator are

$$L = \frac{\partial}{\partial t} - \kappa \nabla^2, \tag{2.11}$$

$$L^* = -\frac{\partial}{\partial t} - \kappa \nabla^2. \tag{2.12}$$

The adjoint Green's function for this problem is given in d dimensions by

$$G^*(\mathbf{x}, t; \mathbf{x}', t') = \frac{\exp\left(-|\mathbf{x} - \mathbf{x}'|^2 / (4\kappa(t' - t))\right)}{[4\pi\kappa(t' - t)]^{d/2}} \qquad \text{for } t' > t, \tag{2.13}$$

$$G^*(\mathbf{x}, t; \mathbf{x}', t') = 0 \qquad \text{for } t' < t.$$

A simple relationship exists between the Green's function and its adjoint:

$$G(\mathbf{x}, t; \mathbf{x}', t') = G^*(\mathbf{x}, t'; \mathbf{x}', t), \tag{2.14}$$

and, therefore,

$$G(\mathbf{x}, t; \mathbf{x}', t') = \frac{\exp\left(-|\mathbf{x} - \mathbf{x}'|^2 / (4\kappa(t - t'))\right)}{[4\pi\kappa(t - t')]^{d/2}} \qquad \text{for } t' < t, \tag{2.15}$$

$$G(\mathbf{x}, t; \mathbf{x}', t') = 0 \qquad \text{for } t' > t.$$

To obtain a coupled set of integral equations, we look at the integral of $uL^*(G^*) - G^*L(u)$ or, because we know the relationship between G^* and G, we can examine

$uL^*(G) - GL(u)$. For simplicity, we will look only at the equation in the solid. A similar method can be used to derive the equation in the liquid. We look at the complete integral of $uL^*(G) - GL(u)$ over time and the volume of the solid:

$$\int_{t_0}^{t} \int_{V_S(t')} \left[u_S L^*(G_S) - G_S L(u_S) \right] dV' dt'. \tag{2.16}$$

We know that $L(u_S) = 0$ and $L^*(G_S) = \delta(t' - t)\,\delta(\mathbf{x} - \mathbf{x}')$. Therefore, we have the identity at the interface $\mathbf{x}$:

$$\frac{1}{2} u_S(\mathbf{x}, t) = \int_{t_0}^{t} \int_{V_S(t')} \left[u_S L^*(G_S) - G_S L(u_S) \right] dV' dt'. \tag{2.17}$$

There is a factor of $1/2$ because $\mathbf{x}$ is on the edge of the solid region. We can then expand the operators to a more complete equation,

$$\begin{aligned} \frac{1}{2} u_S(\mathbf{x}, t) = & \int_{t_0}^{t} \int_{V_S(t')} u_S(\mathbf{x}', t') \left(-\frac{\partial G_S}{\partial t'}(\mathbf{x}', t; \mathbf{x}, t') \right) dV' dt' \\ & - \int_{t_0}^{t} \int_{V_S(t')} u_S(\mathbf{x}', t') \left(\kappa_S \nabla'^2 G_S(\mathbf{x}', t; \mathbf{x}, t') \right) dV' dt' \\ & - \int_{t_0}^{t} \int_{V_S(t')} G_S(\mathbf{x}', t; \mathbf{x}, t') \left(\frac{\partial u_S}{\partial t'}(\mathbf{x}', t') \right) dV' dt' \\ & + \int_{t_0}^{t} \int_{V_S(t')} G_S(\mathbf{x}', t; \mathbf{x}, t') \left(\kappa_S \nabla'^2 u_S(\mathbf{x}', t') \right) dV' dt'. \end{aligned} \tag{2.18}$$

Out volume integrals are parameterized by the variable V', which varies over the volume of the solid. The point $\mathbf{x}'$ in the volume integrals is the position in the domain. The position $\mathbf{x}'$ is directly determined by the position V' in the coordinate system of interest.

$$\mathbf{x}' = \mathbf{x}'(V'). \tag{2.19}$$

Grouping the integrands of (2.18) by type of derivative, we obtain

$$\begin{aligned}\frac{1}{2}u_S(\mathbf{x},t) = &-\int_{t_0}^{t}\int_{V_S(t')}\frac{\partial}{\partial t'}\left(u_S(\mathbf{x}',t')\,G_S(\mathbf{x}',t;\mathbf{x},t')\right)dV'dt' \\ &+\kappa_S\int_{t_0}^{t}\int_{V_S(t')}G_S(\mathbf{x}',t;\mathbf{x},t')\,\nabla'^2 u_S(\mathbf{x}',t')\,dV'dt' \\ &-\kappa_S\int_{t_0}^{t}\int_{V_S(t')}u_S(\mathbf{x}',t')\,\nabla'^2 G_S(\mathbf{x}',t;\mathbf{x},t')\,dV'dt'.\end{aligned} \tag{2.20}$$

Using Leibniz's Theorem for differentiation of an integral to move the partial derivative with respect to time outside of the volume integral, an additional term is introduced because the boundary of the volume of the solid is time dependent:

$$\begin{aligned}\frac{1}{2}u_S(\mathbf{x},t) = &-\int_{t_0}^{t}\frac{\partial}{\partial t'}\int_{V_S(t')}u_S(\mathbf{x}',t')\,G_S(\mathbf{x}',t;\mathbf{x},t')\,dV'dt' \\ &+\int_{t_0}^{t}\int_{S(t')}u_S(\mathbf{x}',t')\,G_S(\mathbf{x}',t;\mathbf{x},t')\,(\mathbf{v}'\cdot\mathbf{n}')\,dS'dt' \\ &+\kappa_S\int_{t_0}^{t}\int_{V_S(t')}G_S(\mathbf{x}',t;\mathbf{x},t')\,\nabla'^2 u_S(\mathbf{x}',t')\,dV'dt' \\ &-\kappa_S\int_{t_0}^{t}\int_{V_S(t')}u_S(\mathbf{x}',t')\,\nabla'^2 G_S(\mathbf{x}',t;\mathbf{x},t')\,dV'dt'.\end{aligned} \tag{2.21}$$

Here the surface integral is an integral parameterized by the variable S'. The point $\mathbf{x}'$ in the surface integral is a point on the interface. The position $\mathbf{x}'$ in our coordinate system of interest can be directly determined by the value of the parameter S'.

$$\mathbf{x}' = \mathbf{x}'(V'). \tag{2.22}$$

As S' varies, our entire interface surface is determined and can be displayed using our coordinates $\mathbf{x}'$. The first integral in (2.21) can then be evaluated with respect to

time. Knowing that G_S vanishes as $t' \to t$ reduces our system to

$$\begin{aligned}\frac{1}{2}u_S(\mathbf{x},t) &= \int_{V_S(t_0)} u_S(\mathbf{x}',t_0)\, G_S(\mathbf{x}',t;\mathbf{x},t_0)\, dV' \\ &+ \int_{t_0}^{t}\int_{S(t')} u_S(\mathbf{x}',t')\, G_S(\mathbf{x}',t;\mathbf{x},t')\,(\mathbf{v}'\cdot\mathbf{n}')\, dS'dt' \\ &+ \kappa_S \int_{t_0}^{t}\int_{V_S(t')} G_S(\mathbf{x}',t;\mathbf{x},t')\,\nabla'^2 u_S(\mathbf{x}',t')\, dV'dt' \\ &- \kappa_S \int_{t_0}^{t}\int_{V_S(t')} u_S(\mathbf{x}',t')\,\nabla'^2 G_S(\mathbf{x}',t;\mathbf{x},t')\, dV'dt'.\end{aligned} \tag{2.23}$$

The final integrals can then be simplified by using Green's second theorem.

$$\begin{aligned}\frac{1}{2}u_S(\mathbf{x},t) &= \int_{V_S(t_0)} u_S(\mathbf{x}',t_0)\, G_S(\mathbf{x}',t;\mathbf{x},t_0)\, dV' \\ &+ \int_{t_0}^{t}\int_{S(t')} u_S(\mathbf{x}',t')\, G_S(\mathbf{x}',t;\mathbf{x},t')\,(\mathbf{v}'\cdot\mathbf{n}')\, dS'dt' \\ &+ \kappa_S \int_{t_0}^{t}\int_{S(t')} G_S(\mathbf{x}',t;\mathbf{x},t')\,(\nabla' u_S(\mathbf{x}',t')\cdot\mathbf{n}')\, dS'dt' \\ &- \kappa_S \int_{t_0}^{t}\int_{S(t')} u_S(\mathbf{x}',t')\,(\nabla' G_S(\mathbf{x}',t;\mathbf{x},t')\cdot\mathbf{n}')\, dS'dt'.\end{aligned} \tag{2.24}$$

A similar derivation leads to a similar integral equation in the liquid where the normal $\mathbf{n}$ is directed outward from the solid into the liquid.

$$\begin{aligned}\frac{1}{2}u_L(\mathbf{x},t) &= \int_{V_L(t_0)} u_L(\mathbf{x}',t_0)\, G_L(\mathbf{x}',t;\mathbf{x},t_0)\, dV' \\ &- \int_{t_0}^{t}\int_{S(t')} u_L(\mathbf{x}',t')\, G_L(\mathbf{x}',t;\mathbf{x},t')\,(\mathbf{v}'\cdot\mathbf{n}')\, dS'dt' \\ &- \kappa_L \int_{t_0}^{t}\int_{S(t')} G_L(\mathbf{x}',t;\mathbf{x},t')\,(\nabla' u_L(\mathbf{x}',t')\cdot\mathbf{n}')\, dS'dt' \\ &+ \kappa_L \int_{t_0}^{t}\int_{S(t')} u_L(\mathbf{x}',t')\,(\nabla' G_L(\mathbf{x}',t;\mathbf{x},t')\cdot\mathbf{n}')\, dS'dt'.\end{aligned} \tag{2.25}$$

The initial conditions $u_S(\mathbf{x},t_0)$ and $u_L(\mathbf{x},t_0)$ are required at the initial time $t_0 < t$ throughout the system as seen in the first integral in both (2.24) and (2.25). The remaining integrals have been reduced to ones which will only require information at

the interface. However, these integrals are history integrals and require evaluation and compilation of data over the time of the system. The amount of time and information needed for a straightforward evaluation grows quickly with increasing time. Additionally, each of these integrals has a singularity at the current time ($t' \to t$). This further complicates traditional methods of evaluation.

2.2 Symmetric Case

The system can be greatly simplified for a symmetric model having equal thermal diffusivities ($\kappa = \kappa_S = \kappa_L$) and conductivities ($k = k_S = k_L$) in the solid and liquid phases. By evaluating these equations at the interface, the problem can be reduced to a single integral equation. Although this is a dramatic simplification of the problem, a great deal of both theoretical and experimental work can be done on the symmetric problem. The plastic crystal succinonitrile is commonly used in solidification experiments because its physical parameters closely approximate a symmetric system [14] and its melting temperature is close to room temperature.

Evaluating the equations (2.24) and (2.25) at the interface gives

$$\begin{aligned}\frac{1}{2}u_\zeta(s,t) = &\int_{V_S(t_0)} u_S(\mathbf{x}',t_0)\, G(\mathbf{x}',t;\zeta(s,t),t_0)\, dV' \\ &+ \int_{t_0}^{t}\int_{S(t')} u_S(\mathbf{x}',t')\, G(\mathbf{x}',t;\zeta(s,t),t')\,(\mathbf{v}'\cdot\mathbf{n}')\, dS'dt' \\ &+ \kappa\int_{t_0}^{t}\int_{S(t')} G(\mathbf{x}',t;\zeta(s,t),t')\,(\nabla' u_S(\mathbf{x}',t')\cdot\mathbf{n}')\, dS'dt' \\ &+ \kappa\int_{t_0}^{t}\int_{S(t')} u_S(\mathbf{x}',t')\,(\nabla' G(\mathbf{x}',t;\zeta(s,t),t')\cdot\mathbf{n}')\, dS'dt'.\end{aligned} \tag{2.26}$$

$$\frac{1}{2}u_\zeta(s,t) = \int_{V_L(t_0)} u_L(\mathbf{x}',t_0)\, G(\mathbf{x}',t;\zeta(s,t),t_0)\, dV' \tag{2.27}$$
$$- \int_{t_0}^{t}\int_{S(t')} u_L(\mathbf{x}',t')\, G(\mathbf{x}',t;\zeta(s,t),t')\,(\mathbf{v}'\cdot\mathbf{n}')\, dS'dt'$$
$$- \kappa\int_{t_0}^{t}\int_{S(t')} G(\mathbf{x}',t;\zeta(s,t),t')\,(\nabla' u_L(\mathbf{x}',t')\cdot\mathbf{n}')\, dS'dt'$$
$$- \kappa\int_{t_0}^{t}\int_{S(t')} u_L(\mathbf{x}',t')\,(\nabla' G(\mathbf{x}',t;\zeta(s,t),t')\cdot\mathbf{n}')\, dS'dt'.$$

Our surface integral is parameterized by S'. As we evaluate our equations at a point on the interface, we should be able to determine our position on the interface in terms of a similar parameter s for the position on the surface. $\zeta(s,t)$ is a point in our coordinate system which is on the interface at a parameterized position on the interface s and at a time t.

Adding the two equations (2.26) and (2.27) gives a single integral equation:

$$u_\zeta(s,t) = \int_V u(\mathbf{x}',t_0)\, G(\mathbf{x}',t;\zeta(s,t),t_0)\, dV' \tag{2.28}$$
$$+ \kappa\int_{t_0}^{t}\int_{S(t')} G(\mathbf{x}',t;\zeta(s,t),t')\,[\nabla' u_S(\mathbf{x}',t')\cdot\mathbf{n}' - \nabla' u_L(\mathbf{x}',t')\cdot\mathbf{n}']\, dS'dt'.$$

The second integral can be simplified by using the conservation equation at the interface (2.7) giving:

$$u_\zeta(s,t) = \int_V u(\mathbf{x}',t_0)\, G(\mathbf{x}',t;\zeta(s,t),t_0)\, dV' \tag{2.29}$$
$$+ \kappa\int_{t_0}^{t}\int_{S(t')} G(\mathbf{x}',t;\zeta(s,t),t')\,[\mathbf{v}'\cdot\mathbf{n}']\, dS'dt'.$$

Incorporating the Gibbs-Thomson condition gives us the final equation to be solved for the symmetric case.

$$\Delta = d_0 f(s,t,\alpha)\, K(s,t) + \int_V u(\mathbf{x}',t_0)\, G(\mathbf{x}',t;\zeta(s,t),t_0)\, dV' \tag{2.30}$$
$$+ \kappa\int_{t_0}^{t}\int_{S(t')} G(\mathbf{x}',t;\zeta(s,t),t')\,[\mathbf{v}'\cdot\mathbf{n}']\, dS'dt'.$$

So the symmetric version has been reduced to a single-integral equation. The

position of the interface for a given undercooling of the system (Δ) can be determined by solving the integral equation.

The solution of these equations will be discussed in greater detail in Section 3.1.3, however, we can summarize the situation here. We can see that our integral equation for the symmetric case (2.30) involves two unknowns for each point on the interface. The unknown values in two dimensions are the current interface position $\zeta(s_j,t) = (x(s_j,t), y(s_j,t))$ in Cartesian coordinates or $\zeta(s_j,t) = (r(s_j,t), \theta(s_j,t))$. If we have I points on the interface, we have $2I$ unknowns. Our integral equation (2.30) will each be evaluated at each point on the interface providing us with I equations. The remaining I equations necessary will be provided by a prescription for interface point motion.

2.3 Nonsymmetric Case

Again, we will evaluate both equations (2.24) and (2.25) at the interface.

$$\begin{aligned}\frac{1}{2}u_\zeta(s,t) = &\int_{V_S(t_0)} u_S(\mathbf{x}',t_0)\, G_S(\mathbf{x}',t;\zeta(s,t),t_0)\, dV' \\ &+ \int_{t_0}^{t}\int_{S(t')} u_S(\mathbf{x}',t')\, G_S(\mathbf{x}',t;\zeta(s,t),t')\,(\mathbf{v}'\cdot\mathbf{n}')\, dS'dt' \\ &+ \kappa_S \int_{t_0}^{t}\int_{S(t')} G_S(\mathbf{x}',t;\zeta(s,t),t')\,(\nabla' u_S(\mathbf{x}',t')\cdot\mathbf{n}')\, dS'dt' \\ &- \kappa_S \int_{t_0}^{t}\int_{S(t')} u_S(\mathbf{x}',t')\,(\nabla' G_S(\mathbf{x}',t;\zeta(s,t),t')\cdot\mathbf{n}')\, dS'dt',\end{aligned} \tag{2.31}$$

$$\begin{aligned}\frac{1}{2}u_\zeta(s,t) = &\int_{V_L(t_0)} u_L(\mathbf{x}',t_0)\, G_L(\mathbf{x}',t;\zeta(s,t),t_0)\, dV' \\ &- \int_{t_0}^{t}\int_{S(t')} u_L(\mathbf{x}',t')\, G_L(\mathbf{x}',t;\zeta(s,t),t')\,(\mathbf{v}'\cdot\mathbf{n}')\, dS'dt' \\ &- \kappa_L \int_{t_0}^{t}\int_{S(t')} G_L(\mathbf{x}',t;\zeta(s,t),t')\,(\nabla' u_L(\mathbf{x}',t')\cdot\mathbf{n}')\, dS'dt' \\ &+ \kappa_L \int_{t_0}^{t}\int_{S(t')} u_L(\mathbf{x}',t')\,(\nabla' G_L(\mathbf{x}',t;\zeta(s,t),t')\cdot\mathbf{n}')\, dS'dt'.\end{aligned} \tag{2.32}$$

The simple addition of the unequal physical parameters κ_S and κ_L in these equations (and in the Green's functions) causes us to retain both an equation in the liquid and an equation in the solid for the nonsymmetric case. However, we can still apply the Gibbs-Thomson condition in both the solid and liquid to give us

$$\begin{aligned}\frac{1}{2}\Delta = &\frac{1}{2}d_0 f\left(s,t,\alpha\right)K\left(s,t\right) \\ &+\int_{V_S(t_0)} u_S\left(\mathbf{x}',t_0\right)G_S\left(\mathbf{x}',t;\zeta\left(s,t\right),t_0\right)dV' \\ &+\int_{t_0}^{t}\int_{S(t')} u_S\left(\mathbf{x}',t'\right)G_S\left(\mathbf{x}',t;\zeta\left(s,t\right),t'\right)\left(\mathbf{v}'\cdot\mathbf{n}'\right)dS'dt' \\ &+\kappa_S\int_{t_0}^{t}\int_{S(t')} G_S\left(\mathbf{x}',t;\zeta\left(s,t\right),t'\right)\left(\nabla' u_S\left(\mathbf{x}',t'\right)\cdot\mathbf{n}'\right)dS'dt' \\ &-\kappa_S\int_{t_0}^{t}\int_{S(t')} u_S\left(\mathbf{x}',t'\right)\left(\nabla' G_S\left(\mathbf{x}',t;\zeta\left(s,t\right),t'\right)\cdot\mathbf{n}'\right)dS'dt'.\end{aligned} \tag{2.33}$$

and

$$\begin{aligned}\frac{1}{2}\Delta = &\frac{1}{2}d_0 f\left(s,t,\alpha\right)K\left(s,t\right) \\ &+\int_{V_L(t_0)} u_L\left(\mathbf{x}',t_0\right)G_L\left(\mathbf{x}',t;\zeta\left(s,t\right),t_0\right)dV' \\ &-\int_{t_0}^{t}\int_{S(t')} u_L\left(\mathbf{x}',t'\right)G_L\left(\mathbf{x}',t;\zeta\left(s,t\right),t'\right)\left(\mathbf{v}'\cdot\mathbf{n}'\right)dS'dt' \\ &-\kappa_L\int_{t_0}^{t}\int_{S(t')} G_L\left(\mathbf{x}',t;\zeta\left(s,t\right),t'\right)\left(\nabla' u_L\left(\mathbf{x}',t'\right)\cdot\mathbf{n}'\right)dS'dt' \\ &+\kappa_L\int_{t_0}^{t}\int_{S(t')} u_L\left(\mathbf{x}',t'\right)\left(\nabla' G_L\left(\mathbf{x}',t;\zeta\left(s,t\right),t'\right)\cdot\mathbf{n}'\right)dS'dt'.\end{aligned} \tag{2.34}$$

We will leave our system as a pair of coupled integral equations (2.33) and (2.34). These two equations are coupled by the Stefan condition (2.7):

$$\mathbf{v}\cdot\mathbf{n} = \kappa_S\nabla u_S\left(s,t\right)\cdot\mathbf{n} - \kappa_L\nabla u_L\left(s,t\right)\cdot\mathbf{n} \tag{2.35}$$

describing conservation of heat at the interface.

The solution of these equations will be discussed in greater detail in Section 6.1.3, however, we can again summarize the situation here. We can see that our coupled

integral equations for the nonsymmetric case, (2.33) and (2.34), involve four unknowns for each point on the interface. The first two unknown values in two dimensions are the current interface position $\zeta(s_j,t) = (x(s_j,t), y(s_j,t))$ in Cartesian coordinates or $\zeta(s_j,t) = (r(s_j,t), \theta(s_j,t))$. Additionally in the nonsymmetric case, we also need to know the value of $\nabla u \cdot n$ at each point on the interface as approached from both the solid and liquid. We will represent these unknowns at each point as $\nabla u_S(s_j,t) \cdot n$ and $\nabla u_L(s_j,t) \cdot n$. If we have I points on the interface, we have $4I$ unknowns. Our integral equations (2.33) and (2.34) will each be evaluated at each point on the interface providing us with $2I$ equations. The Stefan condition (2.35) is applied at each point on the interface which gives us another I equations. The final I equations which we need will be provided by a prescription for motion of points on the interface.

Chapter 3 Numerical Algorithm for the 2-D Symmetric Case

3.1 Numerical Formulation

For the symmetric case, we are attempting to solve the equation (2.30):

$$\Delta = d_0 f(s,t,\alpha) K(s,t) + \int_V u(\mathbf{x}',t_0) G(\mathbf{x}',t;\zeta(s,t),t_0)\, dV' \qquad (3.1)$$
$$+ \kappa \int_{t_0}^{t} \int_{S(t')} G(\mathbf{x}',t;\zeta(s,t),t') [\mathbf{v}' \cdot \mathbf{n}']\, ds' dt',$$

with the Green's function:

$$G(\mathbf{x},t;\mathbf{x}',t') = \frac{\exp\left(-|\mathbf{x}-\mathbf{x}'|^2/(4\kappa(t-t'))\right)}{4\pi\kappa(t-t')} \qquad \text{for } t' < t \qquad (3.2)$$
$$G(\mathbf{x},t;\mathbf{x}',t') = 0 \qquad \text{for } t' > t.$$

The integration of the source gives us a discontinuity in the derivative of the temperature field at the moment the latent heat is released during freezing. However, due to the smoothing nature of the heat equation, if no further heat is released, the temperature field will have finite derivatives of any order thereafter. The liberation of heat at the interface during solidification may be thought of as a moving temperature source at the interface. We see the discontinuity in the second integral of (3.1). Because we are evaluating the system at some point s on the interface, there will be a point on the integral of the surface where s' will be equal to s. At that point, our Green's function will have a singularity. For this reason, the integrals in (3.1) will be broken into a contribution with a singularity in the integrand and a contribution

without a singularity in the integrand:

$$\Delta = d_0 f(s,t,\alpha) K(s,t) + \overline{u}(\zeta(s,t), t - N\Delta t, t) + Q(\mathbf{x}, \zeta(s,t), t - N\Delta t, t), \quad (3.3)$$

where N is the number of time steps held in the singular integral and Δt is the size of the time step. At the end of Section 3.1.1, we will discuss the ideas behind the selection of the number of time steps to hold in memory N and the size of each time step Δt.

These new values are defined by

$$\begin{aligned} \overline{u}(\mathbf{x}, t_1, t) = &\int_V u_S(\mathbf{x}', t_0) G(\mathbf{x}', t; \mathbf{x}, t_0) dV' \\ &+ \kappa \int_{t_0}^{t_1} \int_{S(t')} G(\mathbf{x}', t; \mathbf{x}, t') [\mathbf{v}' \cdot \mathbf{n}'] ds' dt' \end{aligned} \quad (3.4)$$

and

$$Q(\mathbf{x}, t_1, t) = \kappa \int_{t_1}^{t} \int_{S(t')} G(\mathbf{x}', t; \mathbf{x}, t') [\mathbf{v}' \cdot \mathbf{n}'] ds' dt'. \quad (3.5)$$

Because our temperature fields, u_S and u_L, and our Green's function satisfy the heat equation, we are not surprised to find that our underlying temperature field $\overline{u}(\mathbf{x}, t_1, t)$ also satisfies the heat equation. We remember the heat equation operator from Section 2.1 (2.11):

$$L = \frac{\partial}{\partial t} - \kappa \nabla^2. \quad (3.6)$$

We can apply the operator to our smooth temperature field (3.4):

$$\begin{aligned} L(\overline{u}(\mathbf{x}, t_1, t)) = &L\left(\int_V u_S(\mathbf{x}', t_0) G(\mathbf{x}', t; \mathbf{x}, t_0) dV' \right) \\ &+ L\left(\kappa \int_{t_0}^{t_1} \int_{S(t')} G(\mathbf{x}', t; \mathbf{x}, t') [\mathbf{v}' \cdot \mathbf{n}'] ds' dt' \right). \end{aligned} \quad (3.7)$$

Our equations are evaluated at a point on the interface ($\mathbf{x}$ and t), however, $\mathbf{x}$ and t do not depend on our variables of integration in any way. Therefore, we may bring

the operator inside the integrals:

$$L\left(\overline{u}\left(\mathbf{x},t_1,t\right)\right)=\int_V u_S\left(\mathbf{x}',t_0\right)L\left(G\left(\mathbf{x}',t;\mathbf{x},t_0\right)\right)dV' \\ +\kappa\int_{t_0}^{t_1}\int_{S(t')}L\left(G\left(\mathbf{x}',t;\mathbf{x},t'\right)\right)\left[\mathbf{v}'\cdot\mathbf{n}'\right]ds'dt'. \tag{3.8}$$

We know that $G\left(\mathbf{x},t;\mathbf{x}',t'\right)$ satisfies the heat equation, so we see that the smooth temperature field $\overline{u}\left(\mathbf{x},t_1,t\right)$ does as well.

$$L\left(\overline{u}\left(\mathbf{x},t_1,t\right)\right)=\int_V u_S\left(\mathbf{x}',t_0\right)(0)\,dV'+\kappa\int_{t_0}^{t_1}\int_{S(t')}(0)\left[\mathbf{v}'\cdot\mathbf{n}'\right]ds'dt' \tag{3.9}$$

or

$$L\left(\overline{u}\left(\mathbf{x},t_1,t\right)\right)=0. \tag{3.10}$$

To find the interface position $\zeta\left(s,t\right)$, we then only need to solve the equation (3.3). If we evaluate the underlying temperature field at each point in the domain, we can interpolate its value for any possible interface position $\mathbf{x}=\zeta\left(s,t\right)$. We should also be able to approximate the integral with the singularity for any possible value of $\zeta\left(s,t\right)$.

After we have found our interface position at time t, we are interested in finding the interface position at the next time step, $t+\Delta t$. We are then trying to solve the new equation:

$$\Delta=d_0 f\left(s,t+\Delta t,\alpha\right)K\left(s,t+\Delta t\right) \\ +\overline{u}\left(\zeta\left(s,t+\Delta t\right),t-\left(N-1\right)\Delta t,t+\Delta t\right) \\ +Q\left(\mathbf{x},\zeta\left(s,t+\Delta t\right),t-\left(N-1\right)\Delta t,t+\Delta t\right). \tag{3.11}$$

To find the interface position at the new time, we again need to have values for the underlying temperature field $\overline{u}\left(\mathbf{x},t-\left(N-1\right)\Delta t,t+\Delta t\right)$ at all points in the domain.

Our new temperature field is given by

$$\begin{aligned}\overline{u}\left(\mathbf{x}, t-N\Delta t+\Delta t, t+\Delta t\right) = & \int_V u_S\left(\mathbf{x}', t_0\right) G\left(\mathbf{x}', t+\Delta t; \mathbf{x}, t_0\right) dV' \\ & + \kappa \int_{t_0}^{t-N\Delta t} \int_{S(t')} G\left(\mathbf{x}', t+\Delta t; \mathbf{x}, t'\right) \left[\mathbf{v}' \cdot \mathbf{n}'\right] ds' dt' \\ & + \kappa \int_{t-N\Delta t}^{t-(N-1)\Delta t} \int_{S(t')} G\left(\mathbf{x}', t+\Delta t; \mathbf{x}, t'\right) \left[\mathbf{v}' \cdot \mathbf{n}'\right] ds' dt'.\end{aligned} \tag{3.12}$$

This can be separated into two pieces:

$$\overline{u}\left(\mathbf{x}, t-\left(N-1\right)\Delta t, t+\Delta t\right) = A + B, \tag{3.13}$$

where

$$A = \int_V u_S\left(\mathbf{x}', t_0\right) G\left(\mathbf{x}', t+\Delta t; \mathbf{x}, t_0\right) dV' \tag{3.14}$$

and

$$B = \kappa \int_{t-N\Delta t}^{t-(N-1)\Delta t} \int_{S(t')} G\left(\mathbf{x}', t+\Delta t; \mathbf{x}, t'\right) \left[\mathbf{v}' \cdot \mathbf{n}'\right] ds' dt'. \tag{3.15}$$

Because the underlying temperature field satisfies the heat equation, we can find the piece we call A by advancing the temperature field from the previous time step using the heat equation. This allows us a straightforward method to advance the underlying heat equation without needing to evaluate the integral over the entire history from t_0 to $t - N\Delta t$ at each point. The second piece, B, must be evaluated separately at each point in the domain. However, if Δt is small, the calculation will be rapid at each point because the time range $t - N\Delta t$ to $t - (N-1)\Delta t$ will be small and the Green's function decays rapidly as $\mathbf{x}'$ moves away from the point we are looking at on the interface $\mathbf{x}$.

The numerical method can be summarized as follows:

1. Separate the problem (2.30) into a part with a singularity and a part which is smooth and satisfies the heat equation. This introduces an underlying smooth temperature field $\overline{u}\left(\mathbf{x}, t_1, t\right)$, which must be evaluated at all points throughout the domain of the problem.

2. Approximate the remaining unknown integral $Q(\mathbf{x}, t_1, t)$ with the singularity in terms of the interface position at the current time.

3. Calculate the interface position at the current time using equation (3.3).

4. Update the underlying smooth temperature field A (3.14) using the diffusion equation to advance to the next time step.

5. Compute the contribution B of the time integral to the smooth temperature distribution for the next time step (3.15).

3.1.1 Step 1: Separate Singular and Smooth Parts

The integral seen in (2.30) will be broken into a contribution with a discontinuity and a contribution without a discontinuity: ε is some small, yet positive amount of time which allows us to separate this integral into one with a singularity where t is an element of the integral $t' \in [t-\varepsilon, t]$ and one without a singularity (because t is not a part of the integral) where $t' \in [t_0, t-\varepsilon]$.

$$\begin{aligned}\Delta = {} & d_0 f(s,t,\alpha) K(s,t) + \int_V u_S(\mathbf{x}', t_0) G(\mathbf{x}', t; \zeta(s,t), t_0) \, dV' \\ & + \kappa \int_{t_0}^{t-\varepsilon} \int_{S(t')} G(\mathbf{x}', t; \zeta(s,t), t') [\mathbf{v}' \cdot \mathbf{n}'] \, ds' dt' \\ & + \kappa \int_{t-\varepsilon}^{t} \int_{S(t')} G(\mathbf{x}', t; \zeta(s,t), t') [\mathbf{v}' \cdot \mathbf{n}'] \, ds' dt'.\end{aligned} \tag{3.16}$$

We define a function which satisfies the heat equation and with finite derivatives of all orders at the interface where $t_1 < t$ as follows,

$$\overline{u}(\mathbf{x}, t_1, t) = A + B \qquad \text{for } t > t_1, \tag{3.17}$$

where

$$A = \int_V u_S(\mathbf{x}', t_0) G(\mathbf{x}', t; \mathbf{x}, t_0) \, dV' \tag{3.18}$$

and

$$B = \kappa \int_{t_0}^{t_1} \int_{S(t')} G\left(\mathbf{x}', t; \mathbf{x}, t'\right) \left[\mathbf{v}' \cdot \mathbf{n}'\right] ds' dt'. \tag{3.19}$$

In (3.18), we know the value of the function $G\left(\mathbf{x}', t; \mathbf{x}, t_0\right)$ from equation (2.14) at each point in the domain. $G\left(\mathbf{x}', t; \mathbf{x}, t_0\right)$ is a smooth function because $t > t_0$. The initial state of the system $u_S\left(\mathbf{x}, t_0\right)$ is given at time t_0 and must be smooth throughout the solid. A classical numerical integration scheme for equally spaced abscissas, such as an extended trapezoidal method, will be able to approximate A.

In (3.19), we know the function $G\left(\mathbf{x}', t; \mathbf{x}, t'\right)$ from equation (2.15) .$G\left(\mathbf{x}', t; \mathbf{x}, t'\right)$ will be a smooth function because $t > t'$. Additionally, we know the interface position at previous times $t' \in [t_0, t_1]$. A smooth function for the normal velocity can be found using interpolation over the previous time steps. Again an extended trapezoidal method may be used to approximate B.

We can then calculate $\overline{u}\left(\mathbf{x}, t_1, t\right)$ for all points in the domain. Therefore, we have reduced the problem to one with only one unknown integral.

$$\begin{aligned} \Delta = {} & d_0 f\left(s, t, \alpha\right) K\left(s, t\right) + \overline{u}\left(\zeta\left(s, t\right), t - \varepsilon, t\right) \\ & + \kappa \int_{t_1}^{t} \int_{S(t')} G\left(\mathbf{x}', t; \zeta\left(s, t\right), t'\right) \left[\mathbf{v}' \cdot \mathbf{n}'\right] ds' dt'. \end{aligned} \tag{3.20}$$

The remaining integral which we define separately here,

$$Q\left(\mathbf{x}, t_1, t\right) = \kappa \int_{t_1}^{t} \int_{S(t')} G\left(\mathbf{x}', t; \mathbf{x}, t'\right) \left[\mathbf{v}' \cdot \mathbf{n}'\right] ds' dt', \tag{3.21}$$

is much more difficult to evaluate because of the singularity as $t' \to t$. We will explore its evaluation in more detail in the next section.

Although $\overline{u}\left(\mathbf{x}, t - \varepsilon, t\right)$ has derivatives of all orders, if ε is too small, the numerical scheme will not be able to distinguish it from one with a discontinuity. Therefore, N steps of the integral will be held out of the formation of $\overline{u}\left(\mathbf{x}, t - N\Delta t, t\right)$. It will be necessary to calculate $\overline{u}\left(\mathbf{x}, t_1, t\right)$ at each point in the domain. However, $\overline{u}\left(\mathbf{x}, t - N\Delta t, t\right)$ is a rapidly decaying function as the distance between a point $\mathbf{x}$ in the domain and the interface increases. In fact, with a fixed number of time steps

held in memory, N, the contribution from the interface becomes negligible [4] when the distance exceeds several diffusion lengths:

$$\max_{s} \; |\mathbf{x} - \zeta(s,t)| > \sqrt{\kappa N \Delta t}. \tag{3.22}$$

On the other hand, the grid points need to be sufficiently fine to allow accurate advancement of the temperature field $\overline{u}(\mathbf{x}, t - N\Delta t, t)$ between time steps. This will require a maximum spacing of grid points based on a fixed number of time steps held in memory, N [4]:

$$\Delta \mathbf{x} < \sqrt{\kappa N \Delta t}. \tag{3.23}$$

These two equations, (3.22) and (3.23), balance the choices of N and Δt. Decreasing N gives a finer grid, i.e. reduces the size $\Delta \mathbf{x}$ which would correspond to reducing Δx and Δy in a two-dimensional Cartesian coordinate system, while it increases the amount of work needed for the diffusion equation calculation. However, it does reduce the number of calculations needed to determine the underlying temperature field. Increasing N allows a coarser grid to speed to diffusion calculations, but increases the number of points which are necessary for the temperature field determination.

By having $\overline{u}(\mathbf{x}, t_1, t)$ at each point, we will be able to find any $\overline{u}(\zeta(s,t), t_1, t)$ by interpolation. The system that we are interested in solving has been reduced to

$$\Delta = d_0 f(s,t,\alpha) K(s,t) + \overline{u}(\zeta(s,t), t - N\Delta t, t) + Q(\zeta(s,t), t - N\Delta t, t). \tag{3.24}$$

For each time step, we can evaluate each piece of this equation (3.24) at any estimated new interface position. We should then be able to solve for the new interface position (step 3). Because the approximation required is quite complicated (step 2), we will use an iterative method to find the new interface position.

3.1.2 Step 2: Approximate the Singular Integral

In order to find the interface position from our integral equation, we need to be able to numerically compute the remaining portion of the memory integral. Given an

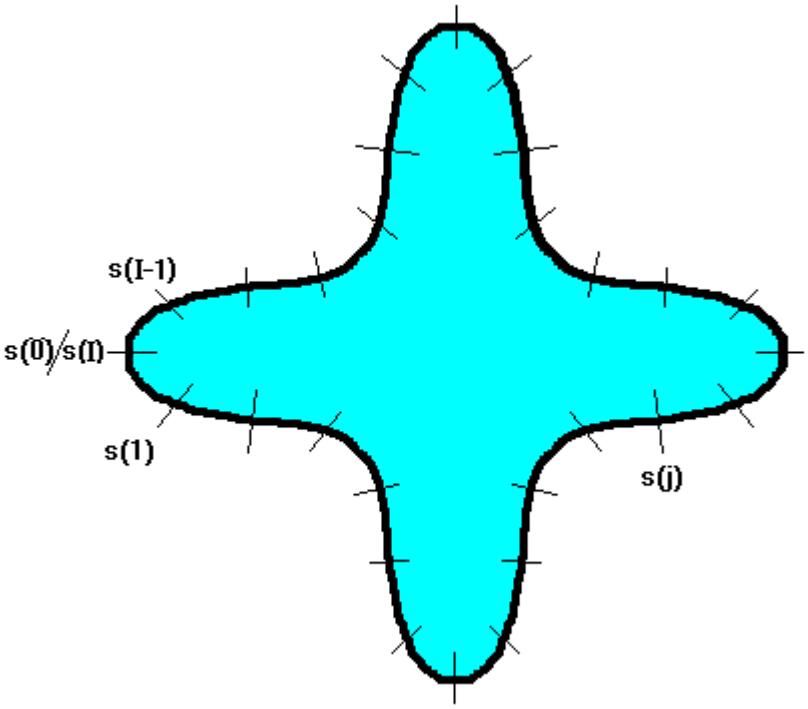

Figure 3.1: Segmentation of the interface into I segments of equal length starting at the negative real axis (angle $= -\pi$).

approximation of the interface position at recent times, we can find

$$Q\left(\zeta\left(s,t\right),t_1,t\right)=\kappa\int_{t_1}^{t}\int_{S(t')}G\left(\mathbf{x}',t;\zeta\left(s,t\right),t'\right)\left[\mathbf{v}'\cdot\mathbf{n}'\right]ds'dt'. \tag{3.25}$$

In two dimensions, the interface can be split into $I+1$ finite segments of equal length Δs, where $s_j=-\pi+j\Delta s$ (see Figure 3.1).

$$Q\left(\zeta\left(s,t\right),t_1,t\right)=\int_{t_1}^{t}\sum_{j=0}^{I-1}\int_{s_j}^{s_{j+1}}\mathbf{v}'\cdot\mathbf{n}'G\left(\mathbf{x}',t;\zeta\left(s,t\right),t'\right)ds'dt' \tag{3.26}$$

or equivalently

$$Q\left(\zeta\left(s,t\right),t_1,t\right)=\int_{t_1}^{t}\sum_{j=0}^{I-1}\int_{s_j}^{s_{j+1}}\frac{\mathbf{v}'\cdot\mathbf{n}'}{4\pi\kappa\left(t-t'\right)}\exp\left(-\frac{\left(X'-X_\zeta\right)^2+\left(Y'-Y_\zeta\right)^2}{4\kappa\left(t-t'\right)}\right)ds'dt', \tag{3.27}$$

where

$$\zeta(s,t) = X_\zeta \mathbf{i} + Y_\zeta \mathbf{j} \tag{3.28}$$

$$\zeta(s',t') = X' \mathbf{i} + Y' \mathbf{j} \tag{3.29}$$

$$\zeta(s_j,t') = X_j \mathbf{i} + Y_j \mathbf{j}. \tag{3.30}$$

If we have enough points on the interface, we can approximate each segment as a straight line.

$$\begin{aligned} X' &\approx \frac{X_{j+1}-X_j}{s_{j+1}-s_j}(s'-s_j)+X_j \qquad s' \in [s_j, s_{j+1}] \\ Y' &\approx \frac{Y_{j+1}-Y_j}{s_{j+1}-s_j}(s'-s_j)+Y_j \qquad s' \in [s_j, s_{j+1}]. \end{aligned} \tag{3.31}$$

The integral in s does not depend strictly on the terms s_j except in its limits of integration. Making the change of variables $S' = s' - s_j$, changes our limits of integration to a fixed range.

$$Q \approx \frac{1}{4\pi\kappa} \sum_{j=0}^{I-1} \int_{t-N\Delta t}^{t} \frac{1}{t-t'} \int_0^{\Delta s} \mathbf{v}' \cdot \mathbf{n}' \exp\left(-\frac{A_j + B_j S' + C_j S'^2}{4\kappa(t-t')}\right) ds'\, dt', \tag{3.32}$$

where

$$\begin{aligned} A_j &= (X_j - X_\zeta)^2 + (Y_j - Y_\zeta)^2 \\ B_j &= 2(X_j - X_\zeta)\frac{X_{j+1}-X_j}{s_{j+1}-s_j} + 2(Y_j - Y_\zeta)\frac{Y_{j+1}-Y_j}{s_{j+1}-s_j} \\ C_j &= \left(\frac{X_{j+1}-X_j}{s_{j+1}-s_j}\right)^2 + \left(\frac{Y_{j+1}-Y_j}{s_{j+1}-s_j}\right)^2. \end{aligned} \tag{3.33}$$

We will also assume that Δs is small enough so that $\mathbf{v}' \cdot \mathbf{n}'$ can be reasonably approximated by the value of $\mathbf{v}' \cdot \mathbf{n}'$ at the central position of each segment, the position $S' = 0$ or $s' = s_{j+1/2}$. This gives us a new equation for Q:

$$Q \approx \frac{1}{4\pi\kappa} \sum_{j=0}^{I-1} \int_{t-N\Delta t}^{t} \frac{1}{t-t'} \left[\mathbf{v}' \cdot \mathbf{n}'\right]_{s'=s_{j+1/2}} \int_{0}^{\Delta s} \exp\left(-\frac{A_j + B_j S' + C_j S'^2}{4\kappa\left(t-t'\right)}\right) dS'\, dt'. \tag{3.34}$$

The surface integral may then be evaluated.

$$Q \approx \sum_{j=0}^{I-1} \int_{t-N\Delta t}^{t} \frac{\left[\mathbf{v}' \cdot \mathbf{n}'\right]_{s'=s_{j+1/2}}/4}{4\sqrt{\pi\kappa C_j\left(t-t'\right)}} \exp\left(\frac{B_j^2 - 4A_jC_j}{16\kappa C_j\left(t-t'\right)}\right) \left[\operatorname{erf}\left(\frac{B_j + 2C_j\Delta s}{4\sqrt{\kappa C_j\left(t-t'\right)}}\right) - \operatorname{erf}\left(\frac{B_j}{4\sqrt{\kappa C_j\left(t-t'\right)}}\right)\right] dt'. \tag{3.35}$$

The error function, $\operatorname{erf}(z)$, and the complementary error function, $\operatorname{erf} c(z)$, are special cases of the incomplete gamma function.

$$\operatorname{erf}(z) = \frac{2}{\sqrt{\pi}} \int_{0}^{z} e^{-t^2} dt. \tag{3.36}$$

$$\operatorname{erfc}(z) = \frac{2}{\sqrt{\pi}} \int_{z}^{\infty} e^{-t^2} dt = 1 - \operatorname{erf}(z). \tag{3.37}$$

We make a change of variables in time, $\beta^2 = t - t'$.

$$Q \approx \sum_{j=0}^{I-1} \int_{0}^{\sqrt{N\Delta t}} \frac{\left[\mathbf{v}' \cdot \mathbf{n}'\right]_{s'=s_{j+1/2}}}{2\sqrt{\pi\kappa C_j}} \exp\left(\frac{B_j^2 - 4A_jC_j}{16\kappa C_j\beta^2}\right) \left[\operatorname{erf}\left(\frac{B_j + 2C_j\Delta s}{4\beta\sqrt{\kappa C_j}}\right) - \operatorname{erf}\left(\frac{B_j}{4\beta\sqrt{\kappa C_j}}\right)\right] d\beta. \tag{3.38}$$

We will use Gaussian quadrature in time to evaluate the integral Q. Quadrature methods are concerned with choosing points x_g and weights w_g, such that the error

obtained from estimating the integral is minimized.

$$\int_{-1}^{1} P(x)\,dx = \sum_{g=1}^{G} w_g P(x_g). \tag{3.39}$$

For Gaussian quadrature, $x_1, x_2, ..., x_g, ...x_G$ are the zeroes of the Gth Legendre polynomial and the weights w_g are given by the formula

$$w_g = \int_{-1}^{1} \prod_{\substack{h=1 \\ h\neq g}}^{G} \frac{x - x_h}{x_g - x_h} dx. \tag{3.40}$$

Both of these are widely tabulated and computer programs are readily available for their evaluation. Here $\beta_g = \frac{1}{2}(1 + x_g)\sqrt{N\Delta t}$ and Q is approximated by

$$\begin{aligned} Q \approx & \sum_{j=0}^{I-1}\sum_{g=1}^{G} w_g \left[\frac{[\mathbf{v}' \cdot \mathbf{n}']_{s'=s_{j+1/2}}}{2\sqrt{\pi\kappa C_j}} \exp\left(\frac{B_j^2 - 4A_jC_j}{16\kappa C_j\beta^2}\right) \operatorname{erf}\left(\frac{B_j + 2C_j\Delta s}{4\beta\sqrt{\kappa C_j}}\right)\right]_{\beta=\beta_g} \\ & - \sum_{j=0}^{I-1}\sum_{g=1}^{G} w_g \left[\frac{[\mathbf{v}' \cdot \mathbf{n}']_{s'=s_{j+1/2}}}{2\sqrt{\pi\kappa C_j}} \exp\left(\frac{B_j^2 - 4A_jC_j}{16\kappa C_j\beta^2}\right) \operatorname{erf}\left(\frac{B_j}{4\beta\sqrt{\kappa C_j}}\right)\right]_{\beta=\beta_g}. \end{aligned} \tag{3.41}$$

We have the interface position at the previous N time steps, and an approximation for the interface position at the current time. Therefore, we have known interface positions at each position on the interface s_j. We will call the interface position at each of the time steps $\zeta(s_j, b_k) = X_j(b_k)\,\mathbf{i} + Y_j(b_k)\,\mathbf{j}$ where $b_k = \beta(t - k\Delta t) = \sqrt{k\Delta t}$. At each β_g, X_j and Y_j will be approximated by a Lagrange interpolating polynomial over the previous N time steps and the current time.

$$\begin{aligned} X_j &= X_j(b_0)\,L_{N,0}(\beta) + \cdots + X_j(b_k)\,L_{N,k}(\beta) + \cdots + X_j(b_N)\,L_{N,N}(\beta) \\ X_j &= \sum_{k=0}^{N} X_j(b_k)\,L_{N,k}(\beta). \end{aligned} \tag{3.42}$$

$$Y_j = Y_j(b_0)\, L_{N,0}(\beta) + \cdots + Y_j(b_k)\, L_{N,k}(\beta) + \cdots + Y_j(b_N)\, L_{N,N}(\beta) \tag{3.43}$$

$$Y_j = \sum_{k=0}^{N} Y_j(b_k)\, L_{N,k}(\beta).$$

$$L_{N,k}(\beta) = \frac{(\beta - b_0)\cdots(\beta - b_{k-1})(\beta - b_{k+1})\cdots(\beta - b_N)}{(b_k - b_0)\cdots(b_k - b_{k-1})(b_k - b_{k+1})\cdots(b_k - b_N)} \tag{3.44}$$

$$L_{N,k}(\beta) = \prod_{\substack{i=0 \\ i\neq k}}^{N} \frac{\beta - b_i}{b_k - b_i}.$$

Finally, we need to be able to evaluate the normal velocity of the interface at β_g,

$$\mathbf{v}' \cdot \mathbf{n}' = \frac{\partial X_j}{\partial \beta} \cdot \frac{\partial Y_j}{\partial s'} - \frac{\partial Y_j}{\partial \beta} \cdot \frac{\partial X_j}{\partial s'}, \tag{3.45}$$

which will be evaluated at $s' = s_{j+1/2}$ and $\beta = \beta_g$.

3.1.3 Step 3: Find the Interface Position

We can now use Newton's method to solve for the new interface position. We have an equation describing the position of each point on the interface:

$$\Delta - d_0 f(s_j, t, \alpha)\, K(s_j, t) - \overline{u}(\zeta(s_j, t), t - N\Delta t, t) - Q(\zeta(s_j, t), t - N\Delta t, t) = 0. \tag{3.46}$$

There will be an equation for each $j = 0, \ldots, I-1$. Each equation depends only on known quantities such as the position of the interface at previous times and the physical parameters of the system and the unknown values of the current interface position $(X_0, X_1, \ldots, X_j, \ldots, X_{I-1}, Y_0, Y_1, \ldots, Y_j, \ldots, Y_{I-1})$. We can rewrite the left-hand side of (3.46) and call it g_j. We can write equation (3.46) as a sum of known coefficients multiplied by our unknown quantities.

$$g_j = \sum_{i=0}^{I-1} \alpha_{ij} X_i + \beta_{ij} Y_i. \tag{3.47}$$

These coefficients are quite complex, but can be found using the methods in the previous section.

In addition, we need a prescription for point motion on the interface. There are many possible choices here. We will set the tangential velocity of the first point to zero.

$$[\mathbf{v} \cdot \mathbf{t}]_{s=-\pi} = 0. \tag{3.48}$$

This equation (3.48) also depends only on the unknown values of the current interface position $(X_0, X_1, \ldots, X_j, \ldots, X_{I-1}, Y_0, Y_1, \ldots, Y_j, \ldots, Y_{I-1})$ and known quantities, such as the position of the interface at previous times and the physical parameters of the system. Similarly, we can write equation (3.48) as a sum of known coefficients multiplied by our unknown quantities. We will call this new value h_0.

$$h_0 = \sum_{i=0}^{I-1} \mu_{i0} X_i + \nu_{i0} Y_i. \tag{3.49}$$

These coefficients are determined by finding the tangential velocity of point t in terms of the current and previous interface positions.

The remaining equations are found by assuming that the points are equally spaced along the interface.

$$\text{arclen}(\zeta(s_j, t), \zeta(s_{j+1}, t)) - \text{arclen}(\zeta(s_0, t), \zeta(s_1, t)) = 0. \tag{3.50}$$

We are comparing the arc length between point s_j and its next neighbor with the arc length between the first two points on the interface. There is an equation for each $j = 1, \ldots, I-1$. And each of these equations depend only on the unknown values of the current interface position $(X_0, X_1, \ldots, X_j, \ldots, X_{I-1}, Y_0, Y_1, \ldots, Y_j, \ldots, Y_{I-1})$ and known quantities, such as the position of the interface at previous times and the physical parameters of the system. We write the quantity on the left-hand side of equation (3.50) as h_j. Only the position of the current and previous interface should

be necessary to evaluate this expression.

$$h_j = \sum_{i=0}^{I-1} \mu_{ij} X_i + \nu_{ij} Y_i. \tag{3.51}$$

Our series of equations may be approximated by a matrix equation.

$$\mathbf{F}\mathbf{x} = \mathbf{0}, \tag{3.52}$$

where

$$\mathbf{F} = \begin{bmatrix}
\alpha_{00} & \alpha_{10} & & & & \beta_{00} & \beta_{10} & & & \\
 & \ddots & \ddots & & & & \ddots & \ddots & & \\
 & & \alpha_{ij} & \alpha_{i+1,j} & & & & \beta_{ij} & \beta_{i+1,j} & \\
 & & & \ddots & \ddots & & & & \ddots & \ddots \\
 & & & & \alpha_{I-1,I-1} & & & & & \beta_{I-1,I-1} \\
\mu_{00} & \mu_{10} & & & & \nu_{00} & \nu_{10} & & & \\
 & \ddots & \ddots & & & & \ddots & \ddots & & \\
 & & \mu_{ij} & \mu_{i+1,j} & & & & \nu_{ij} & \nu_{i+1,j} & \\
 & & & \ddots & \ddots & & & & \ddots & \ddots \\
 & & & & \mu_{I-1,I-1} & & & & & \nu_{I-1,I-1}
\end{bmatrix} \tag{3.53}$$

and

$$\mathbf{x} = \left[X_0, X_1, \ldots, X_j, \ldots, X_{I-1}, Y_0, Y_1, \ldots, Y_j, \ldots, Y_{I-1}\right]^T. \tag{3.54}$$

Given a system $\mathbf{F}\mathbf{x} = \mathbf{0}$, an initial approximation to the interface position $\mathbf{x}_0$, and the Jacobian of the system, we can use Newton's method for nonlinear systems to find a new estimate for the vector containing $\mathbf{x}$, the new interface position. The method is expected to give quadratic convergence, provided that a sufficiently accurate starting value is given and that the inverse of the Jacobian exists. The method uses an iterative procedure, where

$$\mathbf{x}^{(k)} = \mathbf{x}^{(k-1)} - \left(\mathbf{J}^{(k-1)}\right)^{-1} \mathbf{F}^{(k-1)} \mathbf{x}^{(k-1)}. \tag{3.55}$$

A weakness in applying this method directly is the need to calculate the inverse of the Jacobian at every step. In practice, the computation can be avoided by splitting the method into two steps. First, a vector $\mathbf{y}$ is found such that

$$\mathbf{J}^{(k-1)}\mathbf{y} = -\mathbf{F}^{(k-1)}\mathbf{x}^{(k-1)}. \tag{3.56}$$

Then the new approximation $\mathbf{x}$ is found by adding $\mathbf{y}$.

$$\mathbf{x}^{(k)} = \mathbf{x}^{(k-1)} + \mathbf{y}. \tag{3.57}$$

This does, of course, still require us to solve a linear system. However, we are able to avoid the explicit computation of the inverse of the Jacobian at each time step by using this two-step procedure.

The Jacobian for the system is given by a matrix with four distinct sections.

$$\mathbf{J} = \begin{bmatrix} \mathbf{A} & \mathbf{B} \\ \mathbf{C} & \mathbf{D} \end{bmatrix}, \tag{3.58}$$

where

$$\mathbf{A} = \begin{bmatrix} \frac{\partial \alpha_{00}}{\partial X_0} & \cdots & \frac{\partial \alpha_{i0}}{\partial X_i} & \cdots & \frac{\partial \alpha_{I-1,0}}{\partial X_{I-1}} \\ \vdots & \ddots & \vdots & \ddots & \vdots \\ \frac{\partial \alpha_{0j}}{\partial X_0} & \cdots & \frac{\partial \alpha_{ij}}{\partial X_i} & \cdots & \frac{\partial \alpha_{I-1,j}}{\partial X_{I-1}} \\ \vdots & \ddots & \vdots & \ddots & \vdots \\ \frac{\partial \alpha_{0,I-1}}{\partial X_0} & \cdots & \frac{\partial \alpha_{i,I-1}}{\partial X_i} & \cdots & \frac{\partial \alpha_{I-1,I-1}}{\partial X_{I-1}} \end{bmatrix}, \tag{3.59}$$

$$\mathbf{B} = \begin{bmatrix} \frac{\partial \beta_{00}}{\partial X_0} & \cdots & \frac{\partial \beta_{i0}}{\partial X_i} & \cdots & \frac{\partial \beta_{I-1,0}}{\partial X_{I-1}} \\ \vdots & \ddots & \vdots & \ddots & \vdots \\ \frac{\partial \beta_{0j}}{\partial X_0} & \cdots & \frac{\partial \beta_{ij}}{\partial X_i} & \cdots & \frac{\partial \beta_{I-1,j}}{\partial X_{I-1}} \\ \vdots & \ddots & \vdots & \ddots & \vdots \\ \frac{\partial \beta_{0,I-1}}{\partial X_0} & \cdots & \frac{\partial \beta_{i,I-1}}{\partial X_i} & \cdots & \frac{\partial \beta_{I-1,I-1}}{\partial X_{I-1}} \end{bmatrix}, \tag{3.60}$$

$$\mathbf{C} = \begin{bmatrix} \frac{\partial \mu_{00}}{\partial X_0} & \cdots & \frac{\partial \mu_{i0}}{\partial X_i} & \cdots & \frac{\partial \mu_{I-1,0}}{\partial X_{I-1}} \\ \vdots & \ddots & \vdots & \ddots & \vdots \\ \frac{\partial \mu_{0j}}{\partial X_0} & \cdots & \frac{\partial \mu_{ij}}{\partial X_i} & \cdots & \frac{\partial \mu_{I-1,j}}{\partial X_{I-1}} \\ \vdots & \ddots & \vdots & \ddots & \vdots \\ \frac{\partial \mu_{0,I-1}}{\partial X_0} & \cdots & \frac{\partial \mu_{i,I-1}}{\partial X_i} & \cdots & \frac{\partial \mu_{I-1,I-1}}{\partial X_{I-1}} \end{bmatrix}, \tag{3.61}$$

$$\mathbf{D} = \begin{bmatrix} \frac{\partial \nu_{00}}{\partial X_0} & \cdots & \frac{\partial \nu_{i0}}{\partial X_i} & \cdots & \frac{\partial \nu_{I-1,0}}{\partial X_{I-1}} \\ \vdots & \ddots & \vdots & \ddots & \vdots \\ \frac{\partial \nu_{0j}}{\partial X_0} & \cdots & \frac{\partial \nu_{ij}}{\partial X_i} & \cdots & \frac{\partial \nu_{I-1,j}}{\partial X_{I-1}} \\ \vdots & \ddots & \vdots & \ddots & \vdots \\ \frac{\partial \nu_{0,I-1}}{\partial X_0} & \cdots & \frac{\partial \nu_{i,I-1}}{\partial X_i} & \cdots & \frac{\partial \nu_{I-1,I-1}}{\partial X_{I-1}} \end{bmatrix}. \tag{3.62}$$

3.1.4 Step 4: Diffuse the Smooth Temperature Field

Now that we have solved for the new interface position at time t, we need to prepare to step forward to time $t + \Delta t$. In order to proceed to the next time step, we need to advance the smooth temperature field $\overline{u}(\mathbf{x}, t - N\Delta t, t)$. Because $\overline{u}(\mathbf{x}, t - N\Delta t, t)$ satisfies the heat equation, we may advance the information that it contains using any standard finite difference, finite element or spectral method. We have a diffusion equation solver easily available that operates in radial coordinates. In fact, $\overline{u}(\mathbf{x}, t - N\Delta t, t)$ may be held in either radial or Cartesian coordinates. We merely need to be able to interpolate $\overline{u}(\mathbf{x}, t - N\Delta t, t)$ for any possible interface position. As long as our coordinate system covers any possible interface position, it does not matter in which coordinate system we hold the underlying temperature field. Our interface positions $\zeta(s_j, t)$ can also easily be converted between the two coordinate systems.

The underlying temperature field $\overline{u}(\mathbf{x}, t - N\Delta t, t)$ satisfies the following equation in radial coordinates:

$$\frac{\partial \overline{u}}{\partial t} = \frac{\kappa}{r}\frac{\partial}{\partial r}\left(r\frac{\partial \overline{u}}{\partial r}\right) + \frac{\kappa}{r^2}\frac{\partial^2 \overline{u}}{\partial \theta^2}, \tag{3.63}$$

with boundary conditions

$$\lim_{r\to 0} \frac{1}{r}\frac{\partial \overline{u}}{\partial r} = 0, \tag{3.64}$$

$$\lim_{r\to \infty} \overline{u} = 0, \tag{3.65}$$

and initial conditions

$$\overline{u} = g(r,\theta) = \overline{u}\,(r,\theta,t-N\Delta t,t) \qquad t=0.$$

We will take a finite Fourier transform in the θ-direction. For any point, where $\overline{u}_{i,j,k} = \overline{u}\,(t_i, r_j, \theta_k)$, we have

$$U_{i,j,n} = \sum_{k=0}^{N_\theta - 1} \overline{u}_{i,j,k}\, \mathrm{e}^{2\pi i k n/N}\,. \tag{3.66}$$

$$\overline{u}_{i,j,k} = \frac{1}{N_\theta}\sum_{n=0}^{N_\theta - 1} U_{i,j,n}\, \mathrm{e}^{-2\pi i k n/N}\,.$$

Substituting into our original differential equation gives us

$$\frac{\partial U_{i,j,n}}{\partial t} = \frac{\kappa}{r_j}\frac{\partial}{\partial r}\left(r_j \frac{\partial U_{i,j,n}}{\partial r}\right) - \frac{\kappa}{r_j^2} n^2 U_{i,j,n} \qquad r \neq 0, \tag{3.67}$$

$$U_{i,0,n} = 0 \qquad r = 0, n \neq 0,$$

$$\frac{\partial U_{i,0,0}}{\partial t} = \kappa \frac{\partial^2 U_{i,0,0}}{\partial r^2} \qquad r = n = 0.$$

We are interested in discretizing the time derivative in (3.67). We could choose a Forward-Difference method in time for our function at time t_i:

$$\frac{U_{i+1,j,n} - U_{i,j,n}}{\Delta t} = \kappa \nabla^2 U_{i,j,n}. \tag{3.68}$$

Alternatively, we could choose a Backward-Difference method in time for our function at the time t_{i+1}:

$$\frac{U_{i+1,j,n} - U_{i,j,n}}{\Delta t} = \kappa \nabla^2 U_{i+1,j,n}. \tag{3.69}$$

Though averaging these two methods gives us the Crank-Nicolson scheme:

$$2\frac{U_{i+1,j,n}-U_{i,j,n}}{\Delta t}=\kappa\nabla^2U_{i,j,n}+\kappa\nabla^2U_{i+1,j,n} \tag{3.70}$$

or

$$\frac{U_{i+1,j,n}-U_{i,j,n}}{\Delta t}=\frac{\kappa}{2}\left[\nabla^2U_{i+1,j,n}+\nabla^2U_{i,j,n}\right]. \tag{3.71}$$

Applying the Crank-Nicolson scheme to (3.67) gives us

$$\begin{aligned}\frac{U_{i+1,j,n}-U_{i,j,n}}{\Delta t}&=\frac{1}{2}\left[\frac{\kappa}{r_j}\frac{\partial}{\partial r}\left(r_j\frac{\partial U_{i+1,j,n}}{\partial r}\right)-\frac{\kappa}{r_j^2}n^2U_{i+1,j,n}\right] \\ &\quad+\frac{1}{2}\left[\frac{\kappa}{r_j}\frac{\partial}{\partial r}\left(r_j\frac{\partial U_{i,j,n}}{\partial r}\right)-\frac{\kappa}{r_j^2}n^2U_{i,j,n}\right] \qquad r\neq 0, \\ U_{i+1,0,n}&=0 \qquad\qquad r=0,\, n\neq 0, \\ \frac{U_{i+1,0,0}-U_{i,0,0}}{\Delta t}&=\frac{1}{2}\left[\kappa\frac{\partial^2U_{i+1,0,0}}{\partial r^2}\right]+\frac{1}{2}\left[\kappa\frac{\partial^2U_{i,0,0}}{\partial r^2}\right] \qquad r=n=0.\end{aligned} \tag{3.72}$$

We will use a finite difference approximation for the spatial derivatives.

$$\frac{1}{r_j}\frac{\partial}{\partial r}\left(r_j\frac{\partial U_{i+1,j,n}}{\partial r}\right). \tag{3.73}$$

First, we use a Centered-Difference scheme with width Δr centered at r_j to evaluate the interior spatial derivative:

$$\frac{1}{r_j}\frac{\partial}{\partial r}\left(r_j\frac{\partial U_{i+1,j,n}}{\partial r}\right)\approx\frac{1}{r_j}\frac{\partial}{\partial r}\left(r_j\frac{U_{i+1,j+1/2,n}-U_{i+1,j-1/2,n}}{\Delta r}\right). \tag{3.74}$$

Now we will repeat the application of the Centered-Difference method to evaluate the remaining spatial derivative in (3.74) with width Δr centered at r_j :

$$\begin{aligned}\frac{1}{r_j}\frac{\partial}{\partial r}\left(r_j\frac{\partial U_{i+1,j,n}}{\partial r}\right)&\approx\frac{1}{r_j}\frac{1}{\Delta r}\left(r_j\frac{U_{i+1,j+1/2,n}-U_{i+1,j-1/2,n}}{\Delta r}\right)_{j=J+1/2} \\ &\quad-\frac{1}{r_j}\frac{1}{\Delta r}\left(r_j\frac{U_{i+1,j+1/2,n}-U_{i+1,j-1/2,n}}{\Delta r}\right)_{j=J-1/2}.\end{aligned} \tag{3.75}$$

The method (3.75) can be simplified to yield

$$\frac{1}{r_j}\frac{\partial}{\partial r}\left(r_j\frac{\partial U_{i+1,j,n}}{\partial r}\right) \approx \frac{1}{r_j}\left[\frac{r_{j+\frac{1}{2}}U_{i+1,j+1,n} - 2r_jU_{i+1,j,n} + r_{j-\frac{1}{2}}U_{i+1,j-1,n}}{r_j\left(\Delta r\right)^2}\right] \tag{3.76}$$

A finite difference scheme for the simple second derivative needed for $r = 0$ can be derived in a similar fashion. Finally, these finite difference schemes can be applied to our equation (3.72):

$$\begin{aligned}
\frac{U_{i+1,j,n} - U_{i,j,n}}{\Delta t} &= \frac{\kappa}{2}\left[\frac{r_{j+\frac{1}{2}}U_{i+1,j+1,n} - 2r_jU_{i+1,j,n} + r_{j-\frac{1}{2}}U_{i+1,j-1,n}}{r_j\left(\Delta r\right)^2}\right] \qquad r \neq 0, \quad (3.77)\\
&+ \frac{\kappa}{2}\left[\frac{r_{j+\frac{1}{2}}U_{i,j+1,n} - 2r_jU_{i,j,n} + r_{j-\frac{1}{2}}U_{i,j-1,n}}{r_j\left(\Delta r\right)^2}\right]\\
&- \frac{\kappa}{2}\left[\frac{n^2}{r_j^2}U_{i+1,j,n} + \frac{n^2}{r_j^2}U_{i,j,n}\right]\\
U_{i+1,0,n} &= 0 \qquad\qquad r = 0, n \neq 0,\\
\frac{U_{i+1,0,0} - U_{i,0,0}}{\Delta t} &= \frac{\kappa}{2}\left[\frac{U_{i+1,1,0} - 2U_{i+1,0,0} + U_{i+1,-1,0}}{\left(\Delta r\right)^2}\right] \qquad r = n = 0.\\
&+ \frac{\kappa}{2}\left[\frac{U_{i,1,0} - 2U_{i,0,0} + U_{i,-1,0}}{\left(\Delta r\right)^2}\right]
\end{aligned}$$

Because we are eventually interested in forming a matrix equation describing this system, we will try to group all of the terms at time $i+1$ on one side of the equations and all of the terms at time i on the other side of the equations. For $r \neq 0$,

$$-c_jU_{i+1,j+1,n} + \left(b + d_{j_n}\right)U_{i+1,j,n} - a_jU_{i+1,j-1,n} = c_jU_{i,j+1,n} + \left(b - d_{jn}\right)U_{i,j,n} + a_jU_{i,j-1,n}. \tag{3.78}$$

For $r = 0, n \neq 0$,

$$U_{i+1,0,n} = 0. \tag{3.79}$$

We assume a Neumann condition at $r = 0$, which gives us $U_{i,-1,0} = U_{i,1,0}$ and $U_{i+1,-1,0} = U_{i+1,1,0}$. For $r = n = 0$,

$$-2U_{i+1,1,0} + \left(b + 2\right)U_{i+1,0,0} = 2U_{i+1,1,0} + \left(b - 2\right)U_{i+1,0,0}, \tag{3.80}$$

where $a_j = r_{j-\frac{1}{2}}/r_j$, $b = 2\left(\Delta r\right)^2/\left(\kappa \Delta t\right)$, $c_j = r_{j+\frac{1}{2}}/r_j$, and $d_{jn} = 2 + \left(\Delta r\right)^2 n^2/\left(r_j\right)^2$.

We now have a tridiagonal matrix system $\mathbf{A}_n\,\mathbf{x} = \mathbf{b}_n$ for each value of n:

$$\mathbf{x} = \left[U_{i+1,0,n}, U_{i+1,1,n}, \ldots, U_{i+1,j,n}, \ldots, U_{i+1,N_r,n}\right]^T. \tag{3.81}$$

$$\mathbf{A}_{n\neq 0} = \begin{bmatrix} 1 & & & & & & \\ -a_1 & b + d_{1n} & -c_1 & & & & \\ & \ddots & \ddots & \ddots & & & \\ & & -a_i & b + d_{in} & -c_i & & \\ & & & \ddots & \ddots & \ddots & \\ & & & & -a_{N_r} & b + d_{N_r n} \end{bmatrix}. \tag{3.82}$$

$$\mathbf{b}_{n\neq 0} = \begin{bmatrix} 0 \\ c_j U_{i,2,n} + \left(b - d_{1n}\right) U_{i,1,n} + a_j U_{i,0,n} \\ \vdots \\ c_j U_{i,j+1,n} + \left(b - d_{jn}\right) U_{i,j,n} + a_j U_{i,j-1,n} \\ \vdots \\ \left(b - d_{N_r n}\right) U_{i,N_r,n} + a_{N_r} U_{i,N_r-1,n} \end{bmatrix}. \tag{3.83}$$

$$\mathbf{A}_0 = \begin{bmatrix} b + 2 & -2 & & & & & \\ -a_1 & b + d_{1n} & -c_1 & & & & \\ & \ddots & \ddots & \ddots & & & \\ & & -a_i & b + d_{in} & -c_i & & \\ & & & \ddots & \ddots & \ddots & \\ & & & & -a_{N_r} & b + d_{N_r n} \end{bmatrix}. \tag{3.84}$$

$$\mathbf{b}_0 = \begin{bmatrix} 2U_{i+1,1,0} + (b-2)\,U_{i+1,0,0} \\ c_j U_{i,2,n} + (b-d_{1n})\,U_{i,1,n} + a_j U_{i,0,n} \\ \vdots \\ c_j U_{i,j+1,n} + (b-d_{jn})\,U_{i,j,n} + a_j U_{i,j-1,n} \\ \vdots \\ (b-d_{N_r n})\,U_{i,N_r,n} + a_{N_r} U_{i,N_r-1,n} \end{bmatrix}. \tag{3.85}$$

It is then possible to find $\overline{u}_{i,j,k}$ when all of the $U_{i,j,n}$ are known through equation (3.66).

3.1.5 Step 5: Find the New Contribution

We return to the equation (3.12) for the temperature field at the next time step:

$$\begin{aligned} \overline{u}\,(\mathbf{x}, t - N\Delta t + \Delta t, t + \Delta t) = & \int_V u_S\,(\mathbf{x}', t_0)\,G\,(\mathbf{x}', t + \Delta t; \mathbf{x}, t_0)\,dV' \\ & + \kappa \int_{t_0}^{t-N\Delta t} \int_{S(t')} G\,(\mathbf{x}', t + \Delta t; \mathbf{x}, t')\,[\mathbf{v}\,' \cdot \mathbf{n}']\,dS'dt' \\ & + \kappa \int_{t-N\Delta t}^{t-(N-1)\Delta t} \int_{S(t')} G\,(\mathbf{x}', t + \Delta t; \mathbf{x}, t')\,[\mathbf{v}\,' \cdot \mathbf{n}']\,dS'dt'. \end{aligned} \tag{3.86}$$

The value of the underlying temperature field from time t diffused one time step to $t + \Delta t$ was found in the previous section and corresponds to the first two integrals in equation (3.86).

Next we need to find the new contribution to the underlying temperature field which will be needed for the next time step. This is the third integral in equation (3.86). To complete $\overline{u}\,(\mathbf{x}, t - N\Delta t + \Delta t, t + \Delta t)$ over the entire domain, the integral needs to be evaluated at each point. This additional integral is actually our function $Q\,(\mathbf{x}, t - (N-1)\,\Delta t, t - N\Delta t)$ from Section 3.1.2. We have shown in great detail the evaluation of Q previously and that evaluation can now conveniently be used again to find the newest piece of $\overline{u}\,(\mathbf{x}, t - (N-1)\,\Delta t, t + \Delta t)$. However, Q is a very complicated and computationally intensive function to evaluate. And because it must be evaluated at every point in the domain, this becomes the most costly step in the

procedure. However, it does maintain a constant operation count for each step in the Newton iteration between time steps and does not grow as time progresses as a direct integral equation solver would.

Because each step also satisfies the heat equation, we can continue to step the method forward in this manner.

3.2 Analytic Solutions

3.2.1 Advancing Planar Front

We will look at the case where there is no anisotropy, and growth occurs only in one spatial dimension. In this case, the interface between solid and liquid becomes a line advancing into a liquid. This simplified version of the system is given by

$$\frac{\partial u_L}{\partial t} = \kappa \frac{\partial^2 u_L}{\partial x^2} \qquad \zeta(t) < x < \infty. \tag{3.87}$$

$$\frac{\partial u_S}{\partial t} = \kappa \frac{\partial^2 u_S}{\partial x^2} \qquad -\infty < x < \zeta(t). \tag{3.88}$$

The Stefan condition (2.3) becomes

$$\frac{d\zeta}{dt} = \kappa \left[\frac{\partial u_S}{\partial x} - \frac{\partial u_L}{\partial x} \right] \qquad x = \zeta(t). \tag{3.89}$$

A line has zero curvature and there is no anisotropy in the system, so our boundary condition is simply that the temperature is equal to the melting temperature at the interface.

$$u_L = u_S = \Delta \qquad x = \zeta(t). \tag{3.90}$$

As we move far from the interface, the temperature of the system should be equal to the undercooled temperature of the system. When scaled, this gives us a condition

as $x \to \pm\infty$,

$$u_L \to 0 \qquad x \to \infty. \tag{3.91}$$
$$u_S \to 0 \qquad x \to \infty.$$

Following the method outlined by Carslaw and Jaeger [10], we seek an interface position of the form

$$\zeta(t) = 2\lambda\sqrt{\kappa t}. \tag{3.92}$$

We know that $u_S = c_1 + c_2 \operatorname{erf}\left(x/\left(2\sqrt{\kappa t}\right)\right)$ is a solution to equation (3.88). Applying the boundary condition (3.91) gives us a solution for u_S.

$$u_S = c_2\left[1 + \operatorname{erf}\left(x/\left(2\sqrt{\kappa t}\right)\right)\right] \qquad -\infty < x < \zeta(t). \tag{3.93}$$

We can also apply the boundary condition (3.90) to the question of u_S.

$$\Delta = c_2\left[1 + \operatorname{erf}(\lambda)\right]. \tag{3.94}$$
$$c_2 = \Delta/\left[1 + \operatorname{erf}(\lambda)\right].$$

$$u_S = \Delta\left[1 + \operatorname{erf}\left(x/\left(2\sqrt{\kappa t}\right)\right)\right]/\left[1 + \operatorname{erf}(\lambda)\right] \qquad -\infty < x < \zeta(t).$$

We also know that $u_L = k_1 + k_2 \operatorname{erfc}\left(x/\left(2\sqrt{\kappa t}\right)\right)$ is a solution to equation (3.87). Applying the boundary condition (3.91) gives us a solution for u_L.

$$u_L = k_2 \operatorname{erfc}\left(x/\left(2\sqrt{\kappa t}\right)\right) \qquad \zeta(t) < x < \infty. \tag{3.95}$$

We can also apply the boundary condition (3.90) to the question of u_L.

$$\Delta = k_2 \operatorname{erfc}(\lambda). \tag{3.96}$$
$$k_2 = \Delta/\operatorname{erfc}(\lambda).$$

$$u_L = \Delta \operatorname{erfc}\left(x/\left(2\sqrt{\kappa t}\right)\right)/\operatorname{erfc}(\lambda) \qquad \zeta(t) < x < \infty. \tag{3.97}$$

Finally, we look at the Stefan condition (3.89).

$$\lambda\sqrt{\kappa/t} = \kappa\frac{\Delta}{\sqrt{\pi\kappa t}}\exp\left(-\frac{1}{4}x^2/(\kappa t)\right)\left[\frac{1}{1+\operatorname{erf}(\lambda)}+\frac{1}{\operatorname{erfc}(\lambda)}\right] \qquad x=\zeta(t). \quad (3.98)$$

$$\lambda = \frac{\Delta}{\sqrt{\pi}}\exp\left(-\lambda^2\right)\left[\frac{2}{(1+\operatorname{erf}(\lambda))\operatorname{erfc}(\lambda)}\right].$$

$$\Delta = \frac{\sqrt{\pi}}{2}\lambda\exp\left(\lambda^2\right)\operatorname{erfc}(\lambda)(1+\operatorname{erf}(\lambda)).$$

So we have a class of exact similarity solutions which can be written in closed form for the advancing planar front case.

$$u_S = \frac{\sqrt{\pi}}{2}\lambda\exp\left(\lambda^2\right)\operatorname{erfc}(\lambda)[1+\operatorname{erf}(\lambda x/\zeta(t))] \qquad -\infty < x < \zeta(t). \quad (3.99)$$

$$u_L = \frac{\sqrt{\pi}}{2}\lambda\exp\left(\lambda^2\right)(1+\operatorname{erf}(\lambda))\operatorname{erfc}(\lambda x/\zeta(t)) \qquad \zeta(t) < x < \infty. \quad (3.100)$$

$$\Delta = \frac{\sqrt{\pi}}{2}\lambda\exp\left(\lambda^2\right)\operatorname{erfc}(\lambda)(1+\operatorname{erf}(\lambda)). \quad (3.101)$$

$$\zeta(t) = 2\lambda\sqrt{\kappa t}. \quad (3.102)$$

3.2.2 Expanding Circle

We will look at the case where there is no anisotropy and the interface between solid and liquid becomes a circle advancing into the liquid. In the limit where curvature does not affect the interface temperature ($d_0 = 0$ in equation (2.8)). This simplified version of the system is given by

$$\frac{\partial u_L}{\partial t} = \frac{\kappa}{r}\frac{\partial}{\partial r}\left(r\frac{\partial u_L}{\partial r}\right) \qquad \zeta(t) < r < \infty. \quad (3.103)$$

$$\frac{\partial u_S}{\partial t} = \frac{\kappa}{r}\frac{\partial}{\partial r}\left(r\frac{\partial u_S}{\partial r}\right) \qquad 0 < r < \zeta(t). \quad (3.104)$$

The Stefan condition becomes

$$\frac{d\zeta}{dt} = \kappa\left[\frac{\partial u_S}{\partial r}-\frac{\partial u_L}{\partial r}\right] \qquad r=\zeta(t). \quad (3.105)$$

With $d_0 = 0$ boundary condition is simply that the temperature is equal to the melting temperature at the interface.

$$u_L = u_S = \Delta \qquad r = \zeta(t). \tag{3.106}$$

As we move far from the interface, the temperature of the system should be equal to the undercooled temperature of the system. When scaled, this gives us a condition as $r \to \infty$ and the temperature of the system should be smooth at the origin.

$$\begin{aligned} u_L &\to 0 \qquad r \to \infty. \\ \frac{1}{r}\frac{\partial u_S}{\partial r} &= 0 \qquad r = 0. \end{aligned} \tag{3.107}$$

Solutions for the advancing planar front were function of $xt^{-1/2}$ only. This suggests solutions in cylindrical coordinates which are function only of $rt^{-1/2}$. Following the method outlined by Carslaw and Jaeger [10], we again seek an interface position of the form

$$\zeta(t) = 2\lambda\sqrt{\kappa t}. \tag{3.108}$$

We can show that

$$u_S = c_1 + c_2 E_1\left(r^2/(4\kappa t)\right) \tag{3.109}$$

and

$$u_L = k_1 + k_2 E_1\left(r^2/(4\kappa t)\right) \tag{3.110}$$

are solutions to equations (3.103) and (3.104) where $E_1(z)$ is the exponential integral defined by

$$E_1(z) = \int_z^\infty \frac{e^{-t}}{t} dt. \tag{3.111}$$

In fact, it can be shown that these are the only solutions which are of the form $rt^{-1/2}$ for these equations. If we apply the boundary conditions (3.107), we find that $k_1 = 0$ and $c_2 = 0$. Our solutions are then reduced to

$$u_L = k_2 E_1\left(r^2/(4\kappa t)\right) \qquad \zeta(t) < r < \infty \tag{3.112}$$

and

$$u_S = c_1 \qquad 0 < r < \zeta(t). \tag{3.113}$$

If we apply the condition at the interface (3.106), we find that $k_2 = \Delta / E_1(\lambda^2)$ and $c_1 = \Delta$. Which reduces our solutions to

$$u_L = \Delta E_1\left(r^2/(4\kappa t)\right)/E_1\left(\lambda^2\right) \qquad \zeta(t) < r < \infty \tag{3.114}$$

$$u_S = \Delta \qquad 0 < r < \zeta(t). \tag{3.115}$$

Finally, we look at the Stefan condition (3.105).

$$\begin{aligned} \lambda\sqrt{\kappa/t} &= \kappa\left[0 + \frac{\Delta}{E_1(\lambda^2)}\frac{2}{r}\exp\left(-r^2/(4\kappa t)\right)\right] \qquad r = \zeta(t). \\ \frac{\lambda}{\sqrt{\kappa t}} &= \frac{\Delta}{E_1(\lambda^2)}\frac{2}{2\lambda\sqrt{\kappa t}}\exp\left(-\lambda^2\right). \\ \Delta &= \lambda\exp\left(\lambda^2\right)E_1\left(\lambda^2\right). \end{aligned} \tag{3.116}$$

So we have a class of exact similarity solutions which can be written in closed form for the expanding circle case.

$$\begin{aligned} u_S &= \lambda\exp\left(\lambda^2\right)E_1\left(\lambda^2\right) \qquad 0 < r < \zeta(t). \\ u_L &= \lambda\exp\left(\lambda^2\right)E_1\left(r^2/(4\kappa t)\right) \qquad \zeta(t) < r < \infty. \\ \Delta &= \lambda\exp\left(\lambda^2\right)E_1\left(\lambda^2\right). \\ \zeta(t) &= 2\lambda\sqrt{\kappa t}. \end{aligned} \tag{3.117}$$

In Chapter 4, this solution will provide a valuable check for our numerics.

Chapter 4 Numerical Stability Analysis of the Ivantsov Solution

The material in this chapter was prepared in conjunction with C. Yang and D. C. Sorenson from the department of Computational and Applied Mathematics at Rice University [45].

The Ivantsov solution describes the advancement of a simple, parabolic figure representing a dendrite tip into the undercooled melt. A family of solutions is determined by the Ivantsov solution such that the product of the tip velocity v and tip radius ρ is uniquely determined. However, a solution exists for any tip velocity v, which will fix the value of the tip radius ρ. We can, however, use the Ivantsov solution as a starting point for the analysis of the behavior of needles to predict the behavior of the solution in terms. We are interested in theoretical relationships between the tip velocity v, the tip radius ρ, the undercooling in the system Δ, and the anisotropy in the system α. In Chapter 5, we will derive the theoretical relationships between these quantities in the symmetric model based on the Ivanstov solution which we will derive here.

4.1 Introduction

There has been a great deal of interest in the simulation and modelling of crystal growth and dendritic solidification [4], [40]. It is well known that the physical behavior of a needle crystal solidifying into some undercooled liquid can be described by the

dual diffusion equations

$$\frac{\partial U_L}{\partial t} = \alpha \nabla^2 U_L \tag{4.1}$$

$$\frac{\partial U_S}{\partial t} = \alpha \nabla^2 U_S. \tag{4.2}$$

Here U_L and U_S denote the temperature of the liquid and solid respectively. They are functions of the time t and the spatial coordinates x and z. The parameter α represents the thermal diffusivity. At the solid-liquid interface, $U_L = U_S$, and the motion of the interface denoted by $\overrightarrow{r}$ and the temperature field are related by the conservation relation, where $\mathbf{n}$ is the unit outward pointing normal to the interface.

$$\frac{d\overrightarrow{r}}{dt} \cdot \mathbf{n} = \alpha \left(\nabla U_S \cdot \mathbf{n} - \nabla U_L \cdot \mathbf{n} \right) \tag{4.3}$$

It is also natural to impose the boundary condition

$$U_L \to 0 \qquad \text{as } z \to \infty. \tag{4.4}$$

Both analytical and numerical solutions are difficult to obtain because of the moving boundary. We are interested in analyzing the stability of a well known stationary solution that corresponds to a simple parabolic shaped moving front. In the following, we give a brief description of the Ivantsov solution and a standard linear stability analysis that gives rise to an eigenvalue problem. Numerical discretization of the continuous model and the solution of the large scale algebraic eigenvalue problem derived from the discretization are also discussed. It is observed from our numerical computation that the solidification is unstable.

4.2 Ivantsov Solution

A stationary solution that corresponds to a parabolically shaped moving front can be obtained by the method of Ivantsov [17]. Suppose the front is moving in the z direction with a constant velocity v. We first rewrite the equation (4.1) in a moving

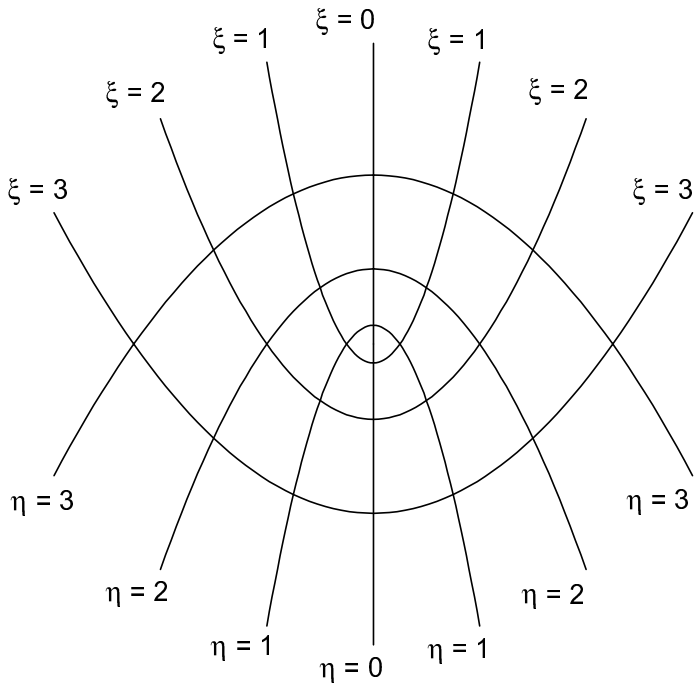

Figure 4.1: $\eta - \xi$ orthogonal coordinate system

frame.

$$z \leftarrow z - vt \tag{4.5}$$

$$x \leftarrow x \tag{4.6}$$

After this change of variables, we have a new equation in both the liquid and solid phases.

$$\nabla^2 U + \frac{2}{l}\frac{\partial U}{\partial z} = \frac{1}{\alpha}\frac{\partial U}{\partial t} \tag{4.7}$$

The boundary conditions remain the same. To simplify the geometry, we introduce a transformation to map the parabolic interface in (x, z) coordinates to the horizontal line $\eta = 1$ in (ξ, η) coordinates (see Figure 4.1).

$$x = \rho\eta\xi \tag{4.8}$$

$$z = \rho\frac{\eta^2 - \xi^2}{2} \tag{4.9}$$

In these new coordinates, the convection diffusion equation (4.7) can be rewritten where $P \equiv \rho/l$ is the Peclet number, and τ is defined to be $\tau \equiv (v/2\rho)\, t$.

$$\frac{\partial^2 U}{\partial \xi^2} + \frac{\partial^2 U}{\partial \eta^2} + 2P\left(\eta\frac{\partial U}{\partial \eta} - \xi\frac{\partial U}{\partial \xi}\right) = \left(\eta^2 + \xi^2\right) P\frac{\partial U}{\partial \tau} \tag{4.10}$$

The boundary condition imposed at the moving front $N = 1$ satisfies

$$P\left[\frac{\partial N}{\partial t}\left(N^2 + \xi^2\right) + 2\left(N + \xi\frac{\partial N}{\partial \xi}\right)\right] = \left(\frac{\partial U_S}{\partial \eta} - \frac{\partial U_L}{\partial \eta}\right) - \frac{\partial N}{\partial \xi}\left(\frac{\partial U_S}{\partial \xi} - \frac{\partial U_L}{\partial \xi}\right). \tag{4.11}$$

The known Ivantsov solution corresponds to the solution $N(\xi, \eta) = 1$. It is not difficult to verify that there is a stationary solution of the form

$$\overline{N} = 1 \tag{4.12}$$

$$\overline{U}_S = \sqrt{\pi P}\exp(P)\operatorname{erfc}\left(\sqrt{P}\right) \tag{4.13}$$

$$\overline{U}_L = \sqrt{\pi P}\exp(P)\operatorname{erfc}\left(\sqrt{P}\eta\right). \tag{4.14}$$

This is the Ivantsov solution which will be the basis for the examination of the relationships between tip radius, tip velocity, anisotropy, and undercooling in Chapter 5.

4.3 Linear Stability Analysis

Our objective is to determine the linear stability of the Ivantsov solution under a small disturbance. This is done by assuming that there exists a solution to equations

(4.10) and (4.11) of the form.

$$N = \overline{N} + \widetilde{N} \exp(\sigma\tau) \tag{4.15}$$

$$U_S = \overline{U}_S + \widetilde{U}_S \exp(\sigma\tau) \tag{4.16}$$

$$U_L = \overline{U}_L + \widetilde{U}_L \exp(\sigma\tau), \tag{4.17}$$

where $\overline{N}$, $\overline{U}_S$, and $\overline{U}_L$ are stationary solutions derived by Ivantsov's method and σ is the growth rate. The substitution of the above equation (4.15) into equation (4.10) leads to the disturbance equation

$$\left(\frac{\partial^2\widetilde{U}}{\partial\xi^2} + \frac{\partial^2\widetilde{U}}{\partial\eta^2}\right) + 2P\left(\eta\frac{\partial\widetilde{U}}{\partial\eta} - \xi\frac{\partial\widetilde{U}}{\partial\xi}\right) = \left(\eta^2+\xi^2\right)P\sigma\widetilde{U} \tag{4.18}$$

in both phases with boundary conditions

$$\widetilde{U}_S = 0 \qquad \text{everywhere} \tag{4.19}$$

$$\widetilde{U}_L = -\frac{\partial\overline{U}_L}{\partial\eta}\widetilde{N} \qquad \text{at } \eta = 1 \tag{4.20}$$

$$P\left[\sigma\widetilde{N}\left(1+\xi^2\right) + 2\left(\widetilde{N} + \xi\frac{\partial\widetilde{N}}{\partial\xi}\right)\right] = \left(-\frac{\partial\widetilde{U}_L}{\partial\eta} - 4P^2\widetilde{N}\right) \qquad \text{at } \eta = 1. \tag{4.21}$$

To simplify the notation, we rename variables $\widetilde{N}$ and $\widetilde{U}$ to N and U, respectively, and let $\lambda = \sigma P$. Equations (4.19) and (4.20) the boundary condition (4.21) can be written as the following eigenvalue problem:

$$\frac{1}{\eta^2+\xi^2}\left[\frac{\partial^2 U}{\partial\xi^2} + \frac{\partial^2 U}{\partial\eta^2} + 2P\left(\eta\frac{\partial U}{\partial\eta} - \xi\frac{\partial U}{\partial\xi}\right)\right] = \lambda U \tag{4.22}$$

$$-\frac{1}{1+\xi^2}\left[\frac{\partial U}{\partial\eta} + 4P^2N + 2P\left(N + \xi\frac{\partial N}{\partial\xi}\right)\right] = \lambda N \qquad \text{at } \eta = 1, \tag{4.23}$$

where N and U are coupled by

$$U = 2PN \qquad \text{at } \eta = 1. \tag{4.24}$$

On an infinite domain, the boundary conditions at infinity are

$$\frac{\partial U}{\partial \eta} \to 0 \text{ as } \eta \to \infty \tag{4.25}$$

$$\frac{\partial U}{\partial \xi} \to 0 \text{ as } \xi \to \infty. \tag{4.26}$$

4.4 Discretization

In our numerical approximation, the infinite domain problem is first transformed into a finite domain problem by using the following change of variables.

$$\widetilde{s} = \frac{\xi}{1+\xi} \tag{4.27}$$

$$\widetilde{t} = \frac{2\eta}{1+\eta} \tag{4.28}$$

In these new variables, equation (4.22) and boundary condition (4.23) become

$$C\left(\widetilde{s},\widetilde{t}\right)\left[\left(1-\widetilde{s}\right)^4 \frac{\partial^2 U}{\partial \widetilde{s}^2} + \frac{1}{4}\left(2-\widetilde{t}\right)^4 \frac{\partial^2 U}{\partial \widetilde{t}^2} - E\left(\widetilde{s}\right)\frac{\partial U}{\partial \widetilde{s}} + F\left(\widetilde{t}\right)\frac{\partial U}{\partial \widetilde{t}}\right] = \lambda U \tag{4.29}$$

$$D\left(\widetilde{s},\widetilde{t}\right)\left\{P\frac{\partial U}{\partial \widetilde{t}} + 4P^2 N + 2P\left[N + \left(1-\widetilde{s}\right)^2 \frac{\partial N}{\partial \widetilde{s}}\right]\right\} = -\lambda N, \tag{4.30}$$

where

$$C\left(\widetilde{s},\widetilde{t}\right) = \left[\left(\frac{\widetilde{s}}{1-\widetilde{s}}\right)^2 + \left(\frac{\widetilde{t}}{2-\widetilde{t}}\right)^2\right]^{-1} \tag{4.31}$$

$$D\left(\widetilde{s},\widetilde{t}\right) = \left[\left(\frac{\widetilde{s}}{1-\widetilde{s}}\right)^2 + 1\right]^{-1} \tag{4.32}$$

$$E\left(\widetilde{s}\right) = 2\left(1-\widetilde{s}\right)^3 + 2P\widetilde{s}\left(1-\widetilde{s}\right) \tag{4.33}$$

$$F\left(\widetilde{t}\right) = -\frac{1}{2}\left(2-\widetilde{t}\right)^3 + P\widetilde{t}\left(2-\widetilde{t}\right). \tag{4.34}$$

Let $\widetilde{s}_i = i\Delta\widetilde{s}$, $\widetilde{t}_j = j\Delta\widetilde{t}$, $U_{ij} = U\left(\widetilde{s}_i,\widetilde{t}_j\right)$, and $N_i = N\left(\widetilde{s}_i\right)$. The standard centered difference formula is used to discretize the equation (4.29). At the boundaries $\widetilde{s} = 0$

and $\widetilde{s} = 1$, we use ghost values $U_{-1,j} = U_{1,j}$ and $U_{n+1,j} = U_{n-1,j}$ and a centered difference formula to discretize $\partial U/\partial \widetilde{s}$. A similar scheme is used to discretize $\partial U/\partial \widetilde{t}$ at $\widetilde{t} = 2$. At the interface boundary $\widetilde{t} = 1$, the temperature $U_{i,0}$ and the displacement of the moving from N_i satisfies $U_{i,0} = 2PN_i$. To avoid mixing U and N values, an upwind difference scheme is used to discretize the term $\partial U/\partial \widetilde{t}$ in (4.30). The term $\partial N/\partial \widetilde{s}$ is approximated by a centered difference formula.

The above discretization scheme gives rise to an algebraic eigenvalue problem.

$$\mathbf{A}\mathbf{x} = \lambda \mathbf{x} \tag{4.35}$$

$$\mathbf{x} = \begin{bmatrix} U_1 \\ \vdots \\ U_m \\ N \end{bmatrix} \tag{4.36}$$

$$\mathbf{U}_j = \begin{bmatrix} U_{0,j} \\ \vdots \\ \vdots \\ U_{n,j} \end{bmatrix} \tag{4.37}$$

$$\mathbf{N} = \begin{bmatrix} N_0 \\ \vdots \\ \vdots \\ N_n \end{bmatrix} \tag{4.38}$$

Eigenvalues of positive real parts are sought to determine interesting unstable modes that involve excitation of the interface. Analysis suggests [34] that at least part of the spectrum corresponding to this eigenvalue problem is continuous and unbounded. The conventional QR method becomes expensive as the mesh size of the discretization becomes small. A fast iterative scheme, such as the Arnoldi method, is attractive in this setting.

4.5 Implicitly Restarted Arnoldi Method

The standard Arnoldi method computes a factorization of the form

$$AV_k = V_k H_k + f e_k^T \tag{4.39}$$

$$V_k^H V_k = I \tag{4.40}$$

$$V_k^H f = 0, \tag{4.41}$$

where H_k is a $k \times k$ upper Hessenberg matrix. The first column of V_k is arbitrarily chosen and normalized such that $\|v_1\| = 1$. Subsequent columns of V_k, the matrix H_k, and the vector f are generated from the Arnoldi process illustrated below.

Input : (A, v_1)

Output : (V_k, H_k, f)

Set : $w \leftarrow Av$

Set : $\alpha_1 = v_1^H w$

Set : $H_1 = (\alpha_1)$

Set : $V_1 = (v_1)$

Set : $f \leftarrow w - v_1 \alpha_1$

$$\textbf{For} : j = 1, 2, 3, \ldots, k-1$$

$$\beta_j = \|f\|$$

$$v_{j+1} \leftarrow \frac{f}{\beta_j}$$

$$V_{j+1} = (V_j, v_{j+1})$$

$$\begin{pmatrix} H_j \\ \beta_j e_j^T \end{pmatrix}$$

$$z \leftarrow A v_{j+1}$$

$$h \leftarrow V_j^H z$$

$$H_{j+1} = (H_{j-1}, h)$$

$$f \leftarrow z - V_{j+1} h$$

It can be verified that the columns of V form an orthonormal basis for the Krylov subspace $K = \left\{v_1, Av_1, A^2v_1, \ldots, A^{k-1}v_1\right\}$. Eigenvalues of H provide approximations to the eigenvalues of A. They are often referred to as the Ritz values. If y is the eigenvector of H corresponding to an eigenvalue θ, the Ritz vector $z = Vy$ is an approximation to the eigenvector of A. It is well known that Ritz values converge very fast to well-separated extreme eigenvalues. However, in our problem these eigenvalues correspond to the ones on the left half of the real axis, and are not interesting. To overcome this difficulty, one must carefully choose a starting vector v_1 such that the subspace spanned by the columns of V contains the desired eigencomponents. The choice of v_1 is not trivial. An elegant way to identify this vector is to use Sorensen's implicit restarting scheme discussed in [41] to repeatedly modify an arbitrary starting vector v_1 so that the unwanted eigencomponents v_1 are annihilated by a polynomial in A. The analysis and some of the implementation issues of the Implicitly Restarted Arnoldi method (IRAM) are also contained in [32].

Given a $(k+p)$-step Arnoldi factorization.

$$AV_{k+p} = V_{k+p}H_{k+p} + fe_{k+p}^T \tag{4.42}$$

$$V_{k+p}^H V_{k+p} = I \tag{4.43}$$

$$V_{k+p}^H f = 0 \tag{4.44}$$

A sequence of QR updates corresponding to the shifts $\mu_1,\mu_2,\ldots,\mu_p$ may be applied as follows. Let $H_{k+p} - \mu_1 I = Q_1 R_1$ be the QR decomposition of $H_{k+p} - \mu_1 I$, it follow from equations (4.42) that

$$(A - \mu_1 I)\, V_{k+p} = V_{k+p}\,(H_{k+p} - \mu_1 I) + fe_{k+p}^T = (V_{k+p}Q_1)\, R_1 + fe_{k+p}^T. \tag{4.45}$$

Multiplying the above equation on the right-hand side by Q_1 yields

$$(A - \mu_1 I)\,(V_{k+p}Q_1) = (V_{k+p}Q_1)\left(Q_1^H H_{k+p} Q_1\right) + fe_{k+p}^T Q_1 \tag{4.46}$$

It is easily seen that the first column of the update $V_{k+p}^+ = V_{k+p}Q_1$ is related to the first column of V_{k+p} through $(A - \mu_1 I)\, v_1 = v_1^+ \rho_{11}$. Let $H_{k+p}^+ = Q_{j-1}^H H Q_{j-1}$. The next step starts with the factorization of $H_{k+p}^+ - \mu_2 I$ followed by the update of V_{k+p}^+ and H_{k+p}^+ and performing p more steps of Arnoldi iteration to give

$$AV_{k+p}^+ = V_{k+p}^+ H_{k+p}^+ + f^+ e_{k+p}^T. \tag{4.47}$$

This is equivalent to a new Arnoldi factorization with v_1 replaced by $v_1^+ = P_p\,(A)\, v_1$, where $P_p\,(\lambda)$ is a polynomial with roots at $\mu_1,\mu_2,\ldots,\mu_p$. This polynomial is designed to filter out the unwanted eigencomponents in the original starting vector v_1. Thus the shifts $\mu_1,\mu_2,\ldots,\mu_p$ are chosen to be approximations to the unwanted eigenvalues of A.

A software package based on this algorithm, ARPACK, is used successfully in our computation. Table 1 lists the leading eigenvalues that correspond to different levels of discretization and the number of matrix vector multiplications (MATVECs) and

CPU time used to obtain them. The Peclet number is set to be 0.1 in our computation. The experiment is performed on a SUN-SPARC 20. For coarse discretization up to about $\Delta\widetilde{s} = \Delta\widetilde{t} = 1/29$, the results compared favorably to those obtained from LAPACK [3]. As the matrix size increases, the computation becomes more expensive as indicated by a large number of matrix vector multiplications used. In the case $\Delta\widetilde{s} = \Delta\widetilde{t} = 1/99$, IRAM did not converge in 300 iterations.

Matrix Size	Eigenvalue	MATVECs	CPU(seconds)
2500	6.39	4831	876.68
3600	7.78	6408	1547.68
4900	9.17	10905	3656.83
6400	10.6	11086	3897.88

Table 1. The Performance of ARPACK in direct mode

An alternative to compute the eigenvalues of A directly is to work with $(A - \sigma I)^{-1}$, where σ is defined as an estimated location of a desired eigenvalue. Since eigenvalues of $(A - \sigma I)^{-1}$ are often large and well separated, the Arnoldi approximation converges extremely fast. However, the fast convergence is obtained at the cost of factoring the matrix $A - \sigma I$ and solving the linear system $(A - \sigma I)\, w = v$ at each iteration. In our application, the matrix can be easily factored using a block Gauss elimination. The initial shift can be predicted from the runs of smaller size problems. In Table 2, we list the number of linear system solved (LSs) and the CPU time used form problems of various size. It is observed that using ARPACK in shift-invert mode is considerably faster in this application.

Matrix Size	Shift σ	LSs	CPU(seconds)
2500	10.0	87	21.35
3600	10.0	81	31.86
4900	14.0	87	48.78
6400	14.0	86	104.21
8100	15.0	86	115.83
10000	15.0	87	189.46

Table 2. The Performance of ARPACK in Shift-Invert Mode

4.6 Numerical Results

Our computation shows that there are many eigenvalues of A with positive real parts. This implies that the solidification of the needle crystal is unstable. As expected, it is observed in our computation that the leading eigenvalue increases as $\Delta\widetilde{s}, \Delta\widetilde{t} \to 0$. The computed interface N for the disturbance equation corresponding to three positive eigenvalues of A are plotted in Figures 4.2, 4.3, and 4.4.

The computation was done on a grid with $\Delta\widetilde{s} = \Delta\widetilde{t} = 1/99$. It is observed that as the eigenvalue increases, the interface becomes more oscillatory. This agrees with the result obtained from analysis. Finally, the temperature field U in both phases that corresponds to a typical positive eigenvalue is also plotted in Figure 4.5.

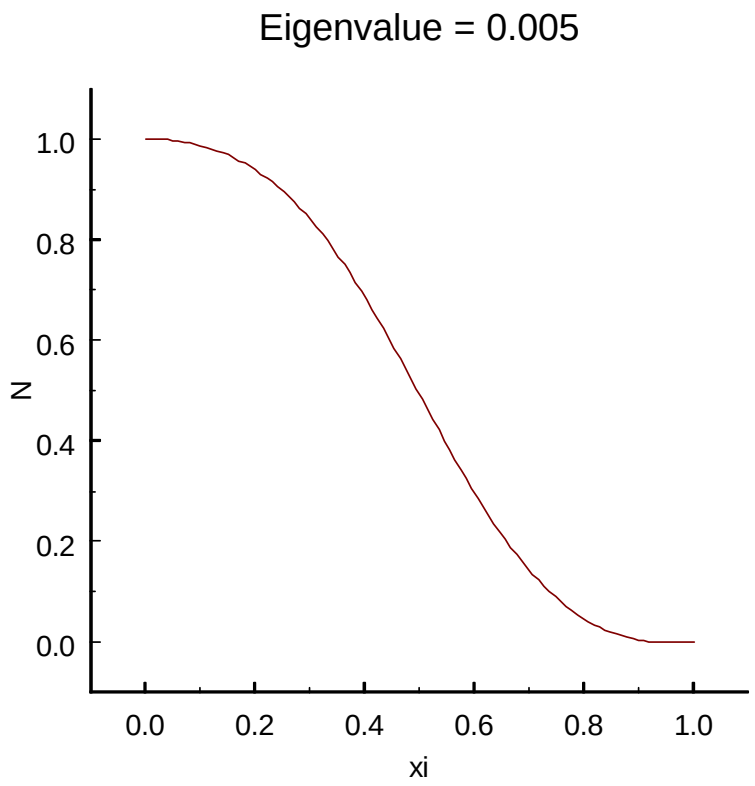

Figure 4.2: The computed interface position N associated with the positive eigenvalue $\sigma = 0.005$ of our matrix A. Positive eigenvalues imply that the solidification of the needle crystal is unstable.

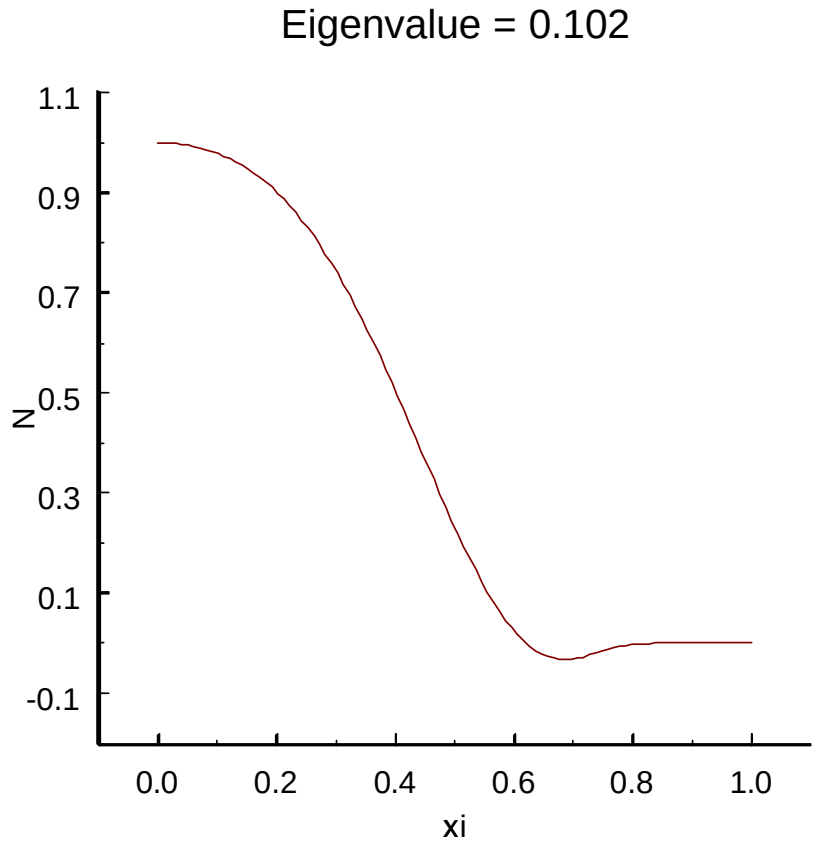

Figure 4.3: The computed interface position N associated with the positive eigenvalue $\sigma = 0.102$ of our matrix A. Positive eigenvalues imply that the solidification of the needle crystal is unstable.

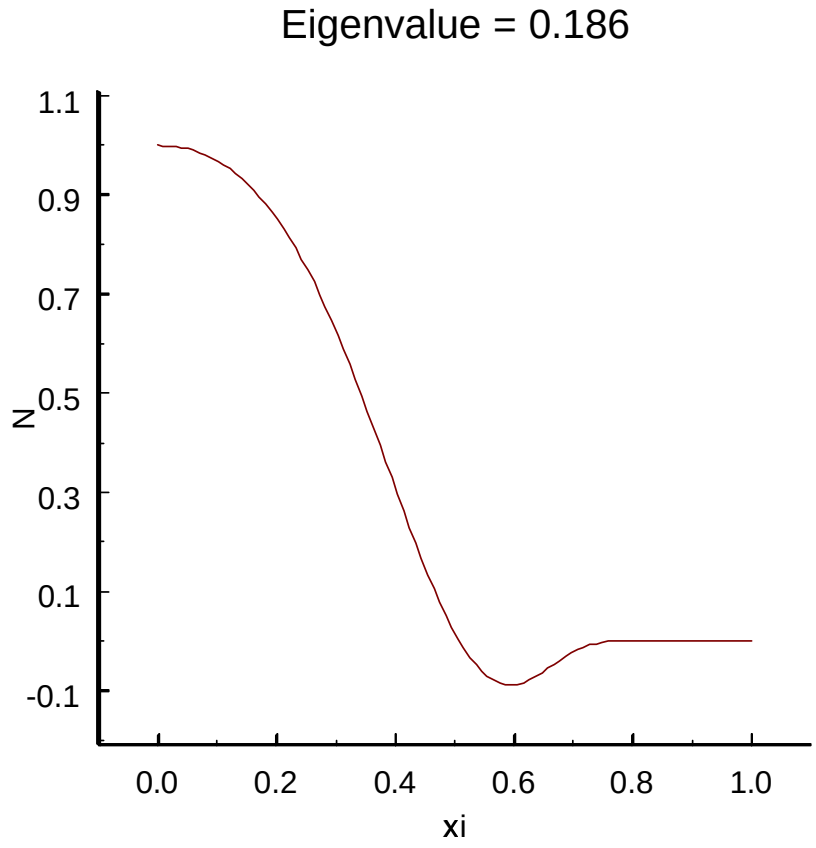

Figure 4.4: The computed interface position N associated with the positive eigenvalue $\sigma = 0.186$ of our matrix A. Positive eigenvalues imply that the solidification of the needle crystal is unstable.

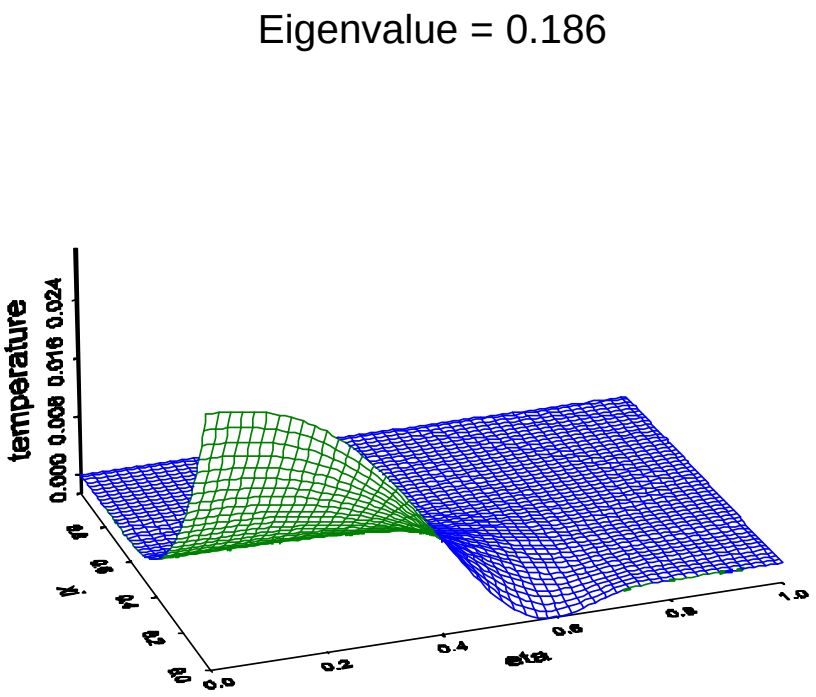

Figure 4.5: The temperature field U in both phases corresponding to the positive eigenvalue $\sigma = 0.186$.

Chapter 5 Application to 2-D Solidification

5.1 Expanding Circle Case

We will look at the expanding circle case discussed in Section 3.2.2. We have a similarity solution based on a non-dimensional parameter λ (3.117).

$$\begin{aligned} u_S &= \lambda \exp\left(\lambda^2\right) E_1\left(\lambda^2\right) \qquad 0 < r < \zeta(t). \\ u_L &= \lambda \exp\left(\lambda^2\right) E_1\left(r^2/(4\kappa t)\right) \qquad \zeta(t) < r < \infty. \\ \Delta &= \lambda \exp\left(\lambda^2\right) E_1\left(\lambda^2\right). \\ \zeta(t) &= 2\lambda\sqrt{\kappa t}. \end{aligned} \tag{5.1}$$

The code was first run with a variety of coefficients for the Gibbs-Thomson condition (d_0). Figure 5.1 shows that as d_0 decreases, we are approaching the exact solution that we have derived for $d_0 = 0$. At a given time, we are interested in finding the rate of difference from the $d_0 = 0$ similarity solution as d_0 increases. We expect that the difference from the similarity solution will increase as a factor of d_0:

$$|r_{similarity} - r_{d_0}| = \beta (d_0)^{\alpha}. \tag{5.2}$$

We can multiply by a constant without affecting the slope α.

$$1000\,|r_{similarity} - r_{d_0}| = 1000^{1-\alpha}\beta\,(1000 d_0)^{\alpha}.$$

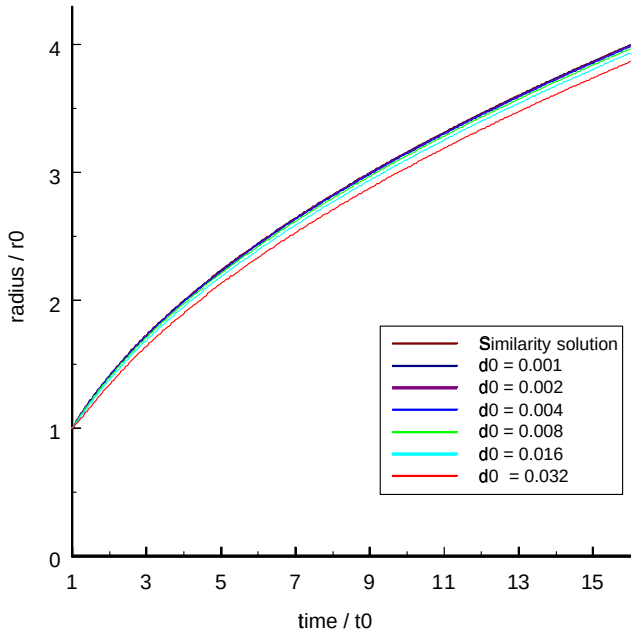

Figure 5.1: The similarity solution is used to test our code with a similarity constant $\lambda = 0.5$, a constant for diffusion $\kappa = 1$, the number of steps held in memory $N = 2$, and the outer radius of the system $r_{\max}/r_0 = 60$.

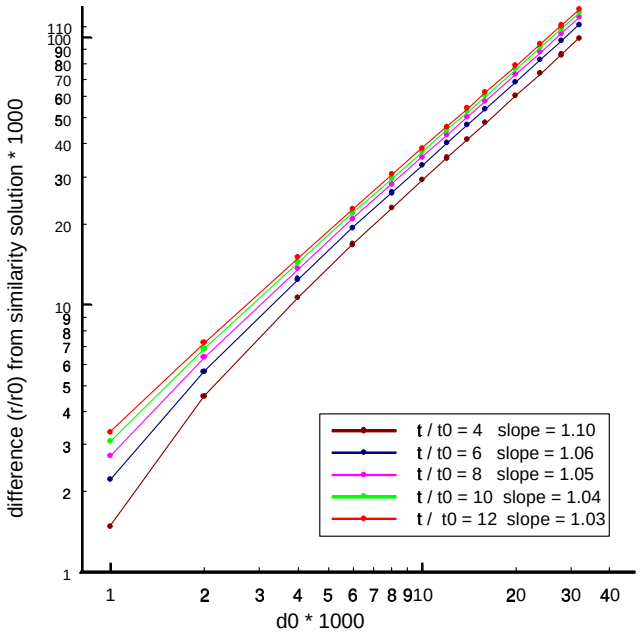

Figure 5.2: The similarity solution is used to test our code with a similarity constant $\lambda = 0.5$, a constant for diffusion $\kappa = 1$, the number of steps held in memory $N = 2$, and the outer radius of the system $r_{\max} = 60$.

If we take the logarithm of both sides, we can try to find the slope of a linear plot:

$$\log\left(1000\left|r_{similarity} - r_{d_0}\right|\right) = \alpha \log\left(1000 d_0\right) + \log\left(1000^{1-\alpha}\beta\right). \tag{5.3}$$

Figure 5.2 shows the log-log plot at several different times. The average slope of our lines α is equal to 1.06. This tells us that the difference between the similarity solution and our solution for a given d_0 grows linearly as d_0 increases.

Our code was run with a variety number of points on the interface. We cannot easily distinguish the solutions for different values of Δs from each other in Figure 5.3. However, we are interested in finding the rate at which our code converges to this solution as the number of points on the interface increases. If we assume that the solution found for $pts = 800$ is the converged solution, we will look at the difference between the converged solution and our solution at other values of pts. We expect

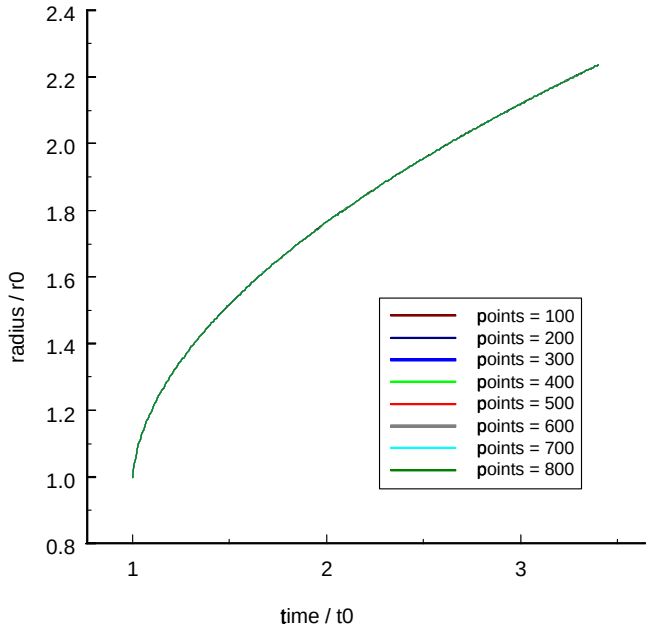

Figure 5.3: The similarity solution is used to test our code with a similarity constant $\lambda = 0.5$, a constant for diffusion $\kappa = 1$, and the number of steps held in memory $N = 2$.

that the difference from the converged solution will decrease as a factor of the number of points on the interface:

$$|r_{pts=800} - r_{pts}| = \beta\,(pts)^{\alpha}\,. \tag{5.4}$$

If we take the logarithm of both sides, we can try to find the slope of a linear plot:

$$\log\left(|r_{pts=800} - r_{pts}|\right) = \alpha \log\left(pts\right) + \log\left(\beta\right). \tag{5.5}$$

Figure 5.4 shows the log-log plot at several different times. The average slope of our lines α is equal to -2.35. This shows that we are getting better than second-order convergence as the number of points on the interface increases.

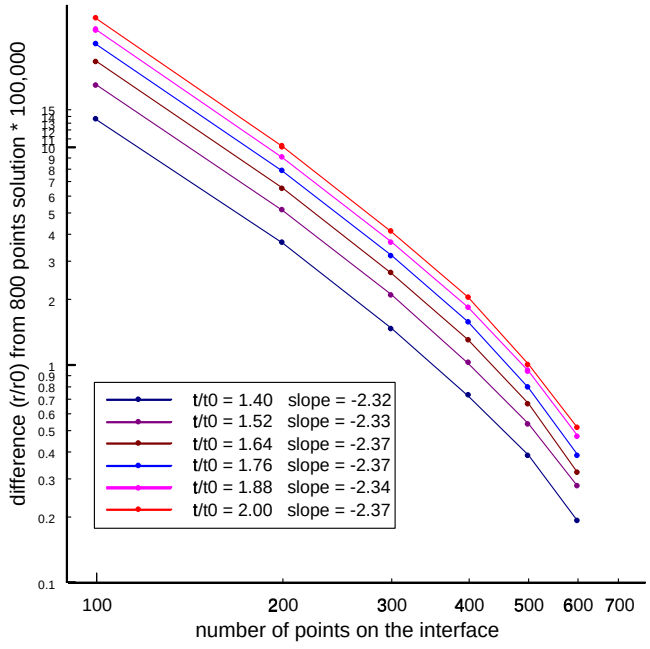

Figure 5.4: The similarity solution is used to test our code with a similarity constant $\lambda = 0.5$, a constant for diffusion $\kappa = 1$, the number of steps held in memory $N = 2$, and the outer radius of the system $r_{\max} = 60$.

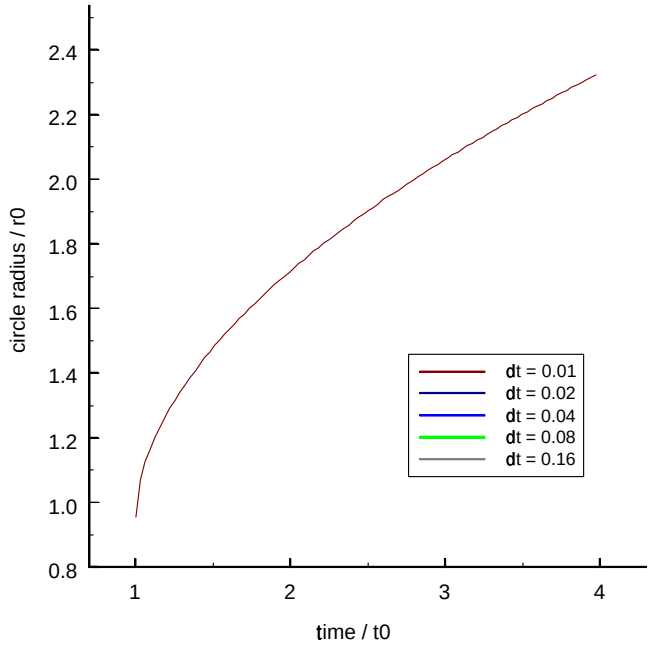

Figure 5.5: Runs for different time step sizes with similarity constant $\lambda = 0.5$, constant for diffusion $\kappa = 1$, the number of steps held in memory $N = 2$, and $d_0 = 0.04$.

Our code was run with a variety of time step sizes. We cannot easily distinguish the solutions for different values of Δt from each other in Figure 5.5. However, we are interested in finding the rate at which our code converges to this solution as Δt decreases. If we assume that the solution found for $\Delta t = 0.02$ is the converged solution, we will look at the difference between the converged solution and our solution at other values of Δt. We expect that the difference from the converged solution will increase as a factor of Δt:

$$|r_{\Delta t=0.02} - r_{\Delta t}| = \beta \, (\Delta t)^{\alpha} \, . \tag{5.6}$$

We can multiply by a constant without affecting the slope α.

$$100 \, |r_{\Delta t=0.02} - r_{\Delta t}| = 100^{1-\alpha} \beta \, (100 \Delta t)^{\alpha} \, .$$

If we take the logarithm of both sides, we can try to find the slope of a linear plot:

$$\log\left(100\left|r_{\Delta t=0.02}-r_{\Delta t}\right|\right)=\alpha\log\left(100\Delta t\right)+\log\left(100^{1-\alpha}\beta\right). \tag{5.7}$$

Figure 5.6 shows the log-log plot at several different times. The average slope of our lines α is equal to 2.22. This is consistent with our expectation of second-order convergence in Δt.

5.2 Convergence in the 2-D Symmetric Case

Since the tip radius is expected to be small compared to d_0, we take a length scale of $d_0 * 25$.

Figures 5.7, 5.8, and 5.9 show the progression of the solidification front starting

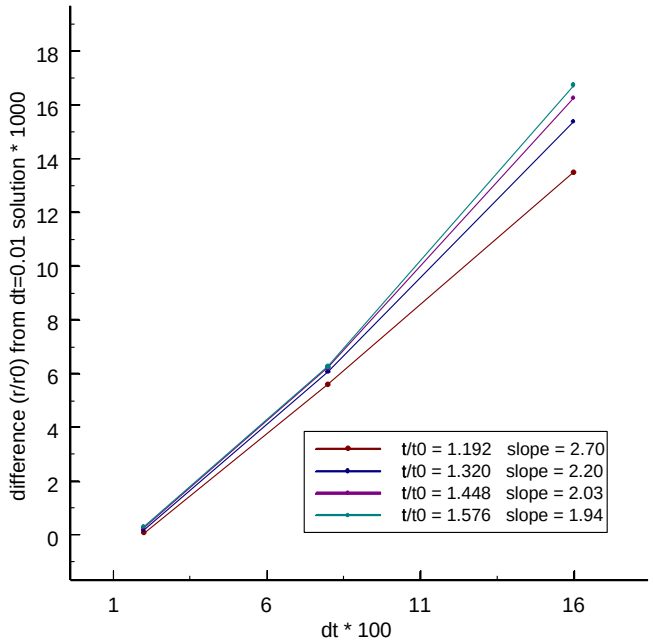

Figure 5.6: Runs for different time step sizes with similarity constant $\lambda = 0.5$, constant for diffusion $\kappa = 1$, the number of steps held in memory $N = 2$, and $d_0 = 0.04$.

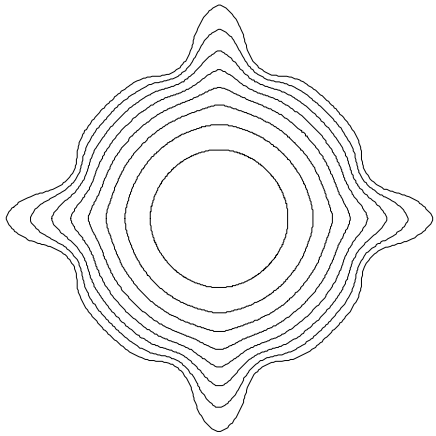

Figure 5.7: Surface position determined when starting with a circular contour with anisotropy $\alpha = 0.60$ and undercooling $\Delta = 0.56$.

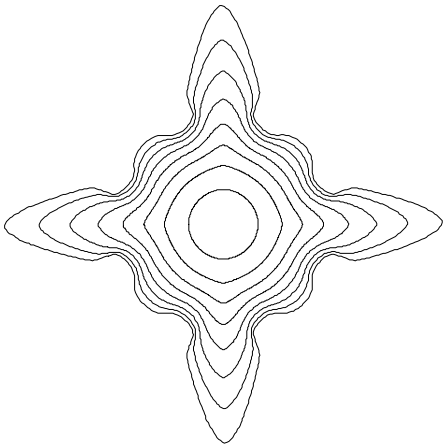

Figure 5.8: Surface position determined when starting with a circular contour with anisotropy $\alpha = 0.70$ and undercooling $\Delta = 0.56$.

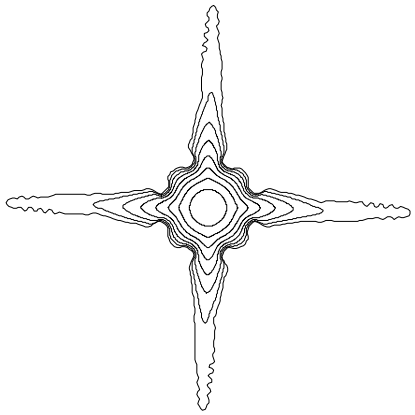

Figure 5.9: Surface position determined when starting with a circular contour with anisotropy $\alpha = 0.80$ and undercooling $\Delta = 0.56$.

with a circular surface for different values of anisotropy. You can see the formation of the dendrites due to the inclusion of anisotropy. As anisotropy increases, the dendrites become more pronounced.

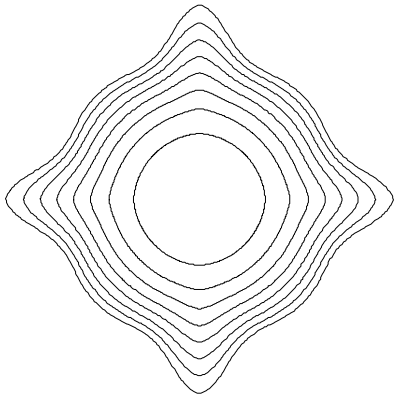

Figure 5.10: Surface position determined when starting with a circular contour with anisotropy $\alpha = 0.70$ and undercooling $\Delta = 0.48$.

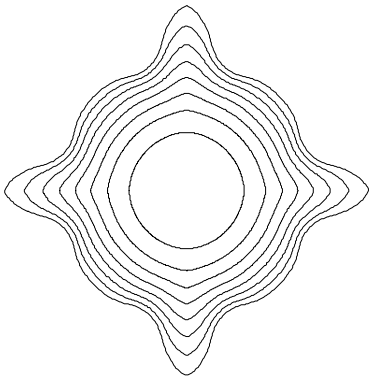

Figure 5.11: Surface position determined when starting with a circular contour with anisotropy $\alpha = 0.70$ and undercooling $\Delta = 0.52$.

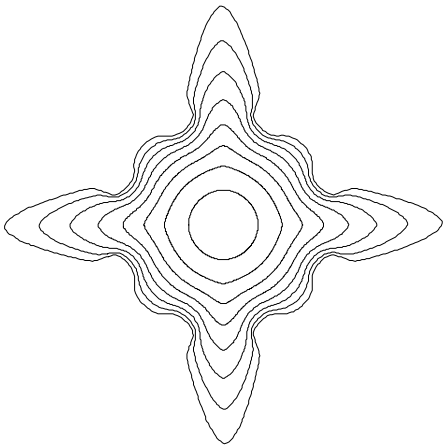

Figure 5.12: Surface position determined when starting with a circular contour with anisotropy $\alpha = 0.70$ and undercooling $\Delta = 0.56$.

Figures 5.10, 5.11, and 5.12 show the progression of the solidification front starting with a circular surface for different values of undercooling. You can see the formation of the dendrites due to the inclusion of anisotropy. As undercooling increases, the dendrites become more pronounced.

Figures 5.13 and 5.14 show the progression of the solidification front starting with a perturbed circular surface for different values of the Gibbs-Thomson coefficient in the absence of anisotropy. The initial surface is set using the following description with perturbation constant p:

$$\begin{aligned} x(s) &= p\,\cos(s)\,r_{d0=0} \\ y(s) &= p\,\sin(s)\,r_{d0=0}. \end{aligned} \tag{5.8}$$

Figure 5.15 shows an inital interface shape with $p = 0.10$.

We are interested in the convergence properties of our two-dimensional symmetric code. The code was run with a range of number of points on the interface. Figure 5.16 shows that as the number of points on the interface changes, the tip positions, r, are indistinguishable. Figure 5.17 shows that we have converged to a characteristic velocity for our range of points on the interface. If we assume that the solution found for $pts = 800$ is the converged solution, we will look at the difference between the converged solution and our solution at other number of points on the interface. We expect that the difference from the converged solution will increase as a factor of the number of points on the interface. We expect α to be negative because we expect the difference to decrease as we increase the number of points on the interface.

$$|r_{pts=800} - r_{pts}| = \beta\,(pts)^{\alpha}\,. \tag{5.9}$$

We can multiply by a constant without affecting the slope α.

$$10000\,|r_{pts=800} - r_{pts}| = 10000\beta\,(pts)^{\alpha}\,.$$

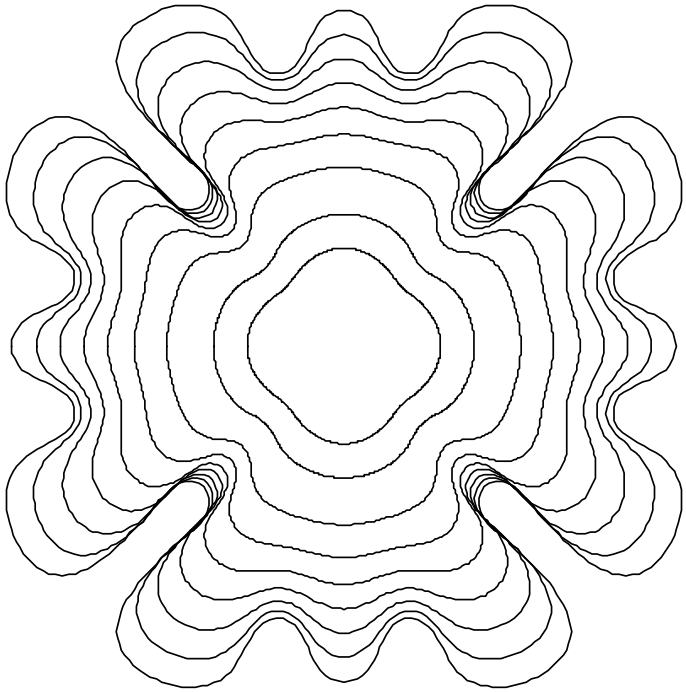

Figure 5.13: Surface position determined when starting with a perturbed circular contour with a perturbation constant of $p = 0.10$ with anisotropy $\alpha = 0.00$ and undercooling $\Delta = 0.60$ and $d_0 = 0.04$.

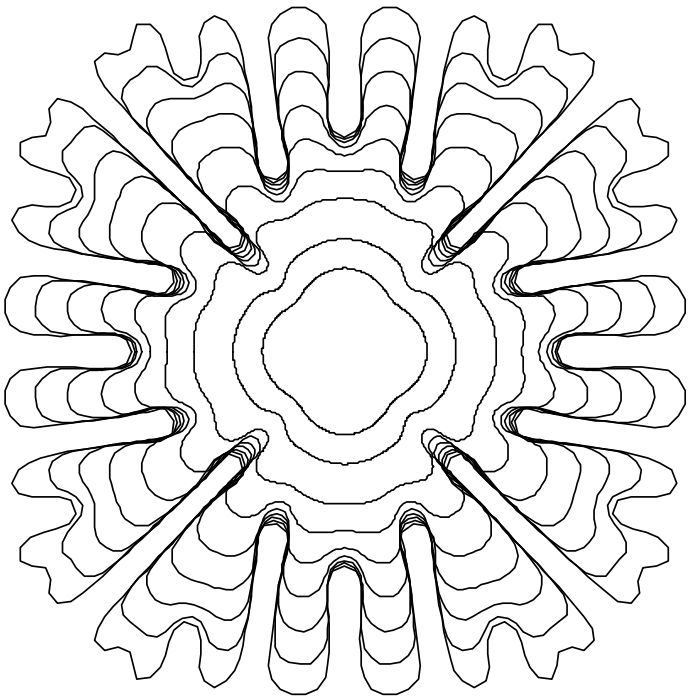

Figure 5.14: Surface position determined when starting with a perturbed circular contour with a perturbation constant of $p = 0.10$ with anisotropy $\alpha = 0.00$ and undercooling $\Delta = 0.60$ and $d_0 = 0.02$.

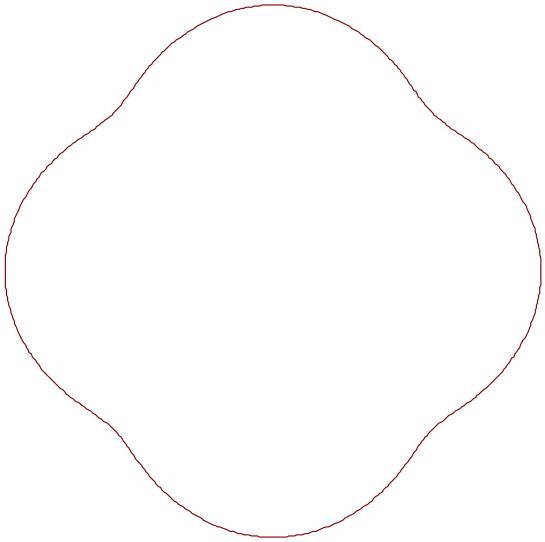

Figure 5.15: Initial perturbation of the $d_0 = 0.0$ similarity solution with a perturbation constant $p = 0.10$.

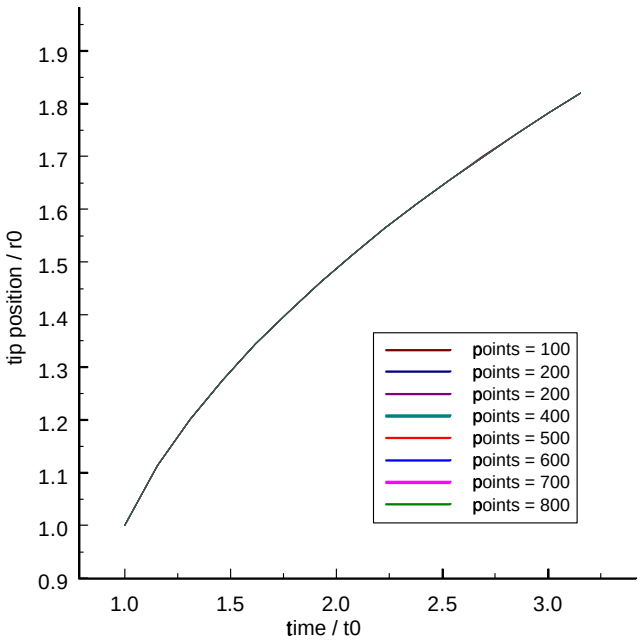

Figure 5.16: Tip position determined with anisotropy $\alpha = 0.30$ and undercooling $\Delta = 0.64$.

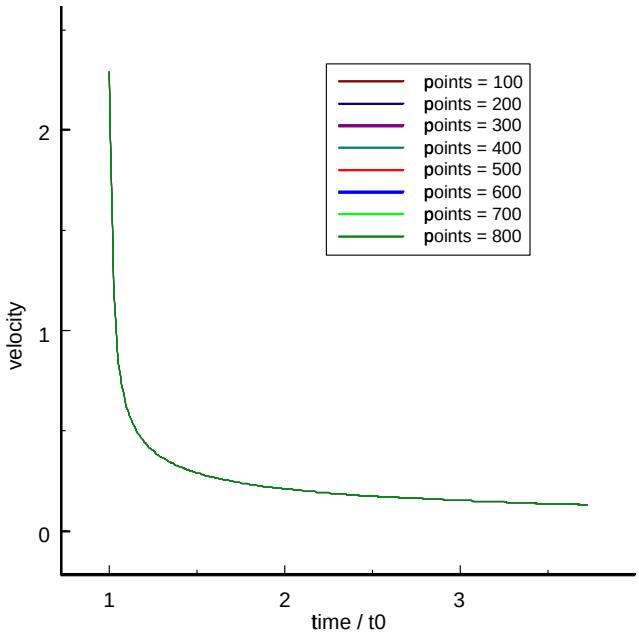

Figure 5.17: Tip velocity determined with anisotropy $\alpha = 0.30$ and undercooling $\Delta = 0.64$.

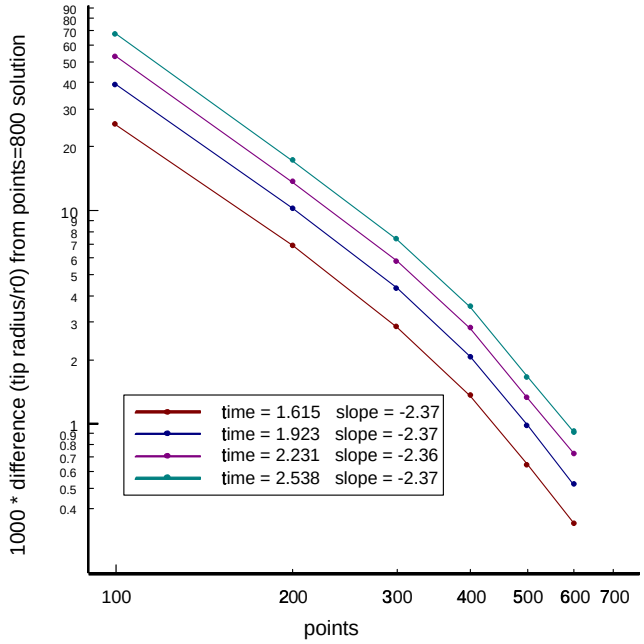

Figure 5.18: Difference from converged tip position determined with anisotropy $\alpha = 0.30$, and undercooling $\Delta = 0.64$.

If we take the logarithm of both sides, we can try to find the slope of a linear plot:

$$\log\left(10000\left|r_{pts=800} - r_{pts}\right|\right) = \alpha \log\left(pts\right) + \log\left(10000\beta\right). \tag{5.10}$$

Figure 5.18 shows the log-log plot at several different times. The average slope of our lines α is equal to -2.37. Our results are better than second-order convergence in the number of points on the interface or Δs.

The maximum radius used in the numerical simulation is the distance from the origin at which we assume that the temperature field is equal to the undercooled temperature. In other words, this is an artificially inserted value for infinity for our code. We hope that our maximum radius is large enough so that the value of the temperature field at the maximum radius is not felt at the interface. We have used a variety of values for the maximum radius in the simulation. Figure 5.19 shows

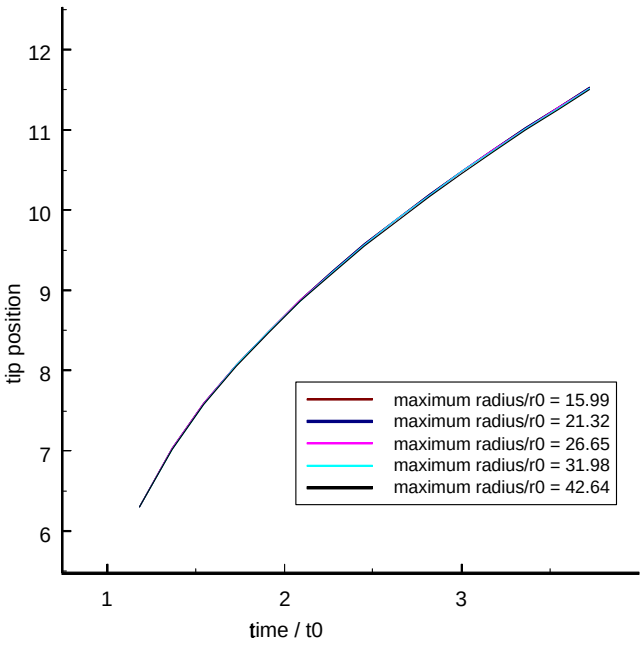

Figure 5.19: Tip position determined with anisotropy $\alpha = 0.40$ and undercooling $\Delta = 0.60$.

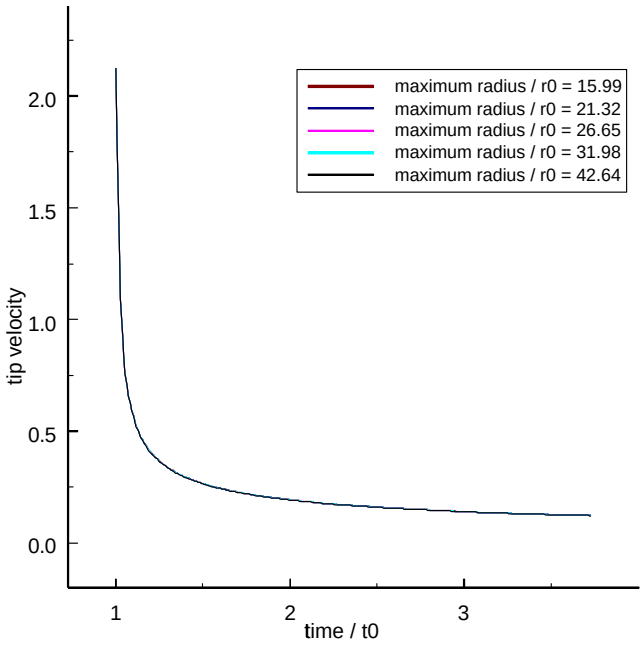

Figure 5.20: Tip velocity determined with anisotropy $\alpha = 0.40$ and undercooling $\Delta = 0.60$.

that as the maximum radius changes, there is very little noticeable difference in the calculated tip position. Figure 5.20 shows that our tip velocity also has very little noticeable difference between solutions for different values of the maximum radius. If we assume that the solution found for $r = 80$ is the converged solution, we will look at the difference between the converged solution and our solution with different values for the maximum radius. We expect that the difference from the converged solution will increase as a factor of the maximum radius. Therefore, we expect α to be negative because we expect the difference to decrease as we increase the maximum radius in the system.

$$|r_{\max=80} - r_{\max}| = \beta\,(\max)^{\alpha}\,. \tag{5.11}$$

We can multiply by a constant without affecting the slope α.

$$1000\,|r_{\max=80} - r_{\max}| = 1000\beta\,(\max)^{\alpha}\,.$$

If we take the logarithm of both sides, we can try to find the slope of a linear plot:

$$\log\left(1000\,|r_{\max=80} - r_{\max}|\right) = \alpha \log(\max) + \log(1000\beta)\,. \tag{5.12}$$

Figure 5.21 shows the log-log plot at several different times. The average slope of our lines α is equal to -0.971. Our method achieves very close to linear convergence in the maximum radius in the system.

Next, we ran the symmetric, two-dimensional code with a range of values for Δr. Figure 5.22 shows the position of the dendrite tip as a function of time for different values of Δr. However, it is very difficult to distinguish the difference between solutions for different values of Δr. Additionally, it is very difficult to distinguish the difference between tip velocities for different values of Δr in Figure 5.23.We will assume that the tip position for the smallest value of Δr for which we have calculated the position, $\Delta r = 0.075$, is the converged solution. We can then use the difference between the converged position and the calculated position at other values of Δr to

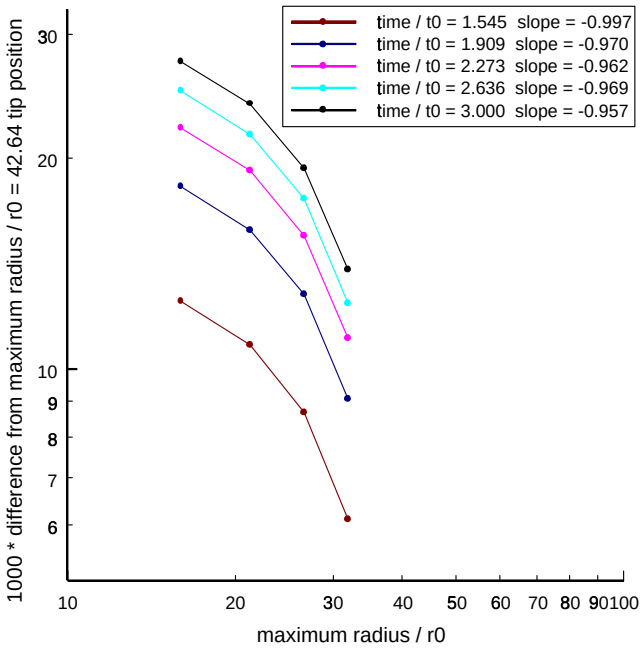

Figure 5.21: Tip position determined with anisotropy $\alpha = 0.40$ and undercooling $\Delta = 0.60$.

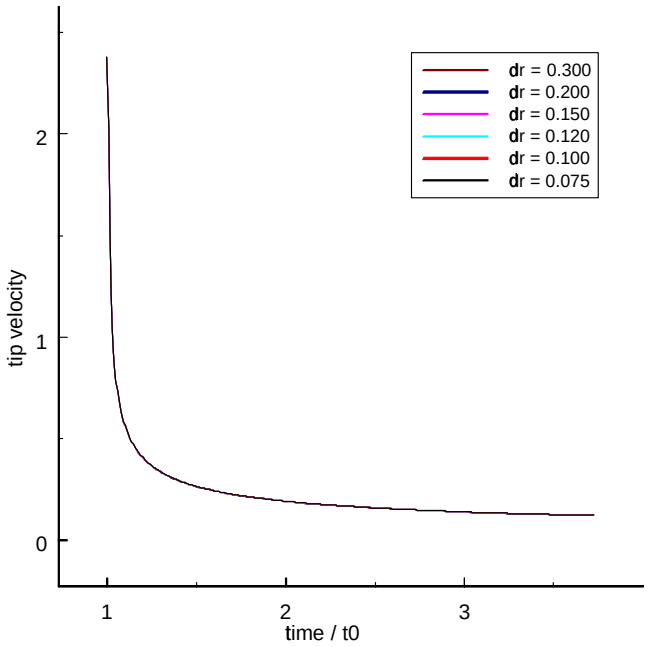

Figure 5.23: Tip velocity determined with anisotropy $\alpha = 0.40$ and undercooling $\Delta = 0.60$.

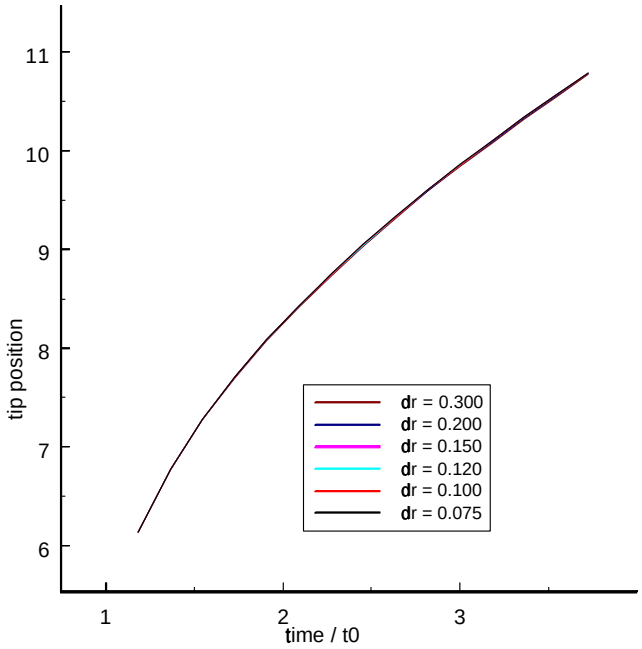

Figure 5.22: Tip position determined with anisotropy $\alpha = 0.40$ and undercooling $\Delta = 0.60$.

find the convergence rate for our code:

$$|r_{\Delta r=0.07} - r_{\Delta r}| = \beta\,(\Delta r)^{\alpha}\,. \tag{5.13}$$

We can multiply by a constant without affecting the slope α.

$$100\,|r_{\Delta r=0.07} - r_{\Delta r}| = 100^{1-\alpha}\beta\,(100\Delta r)^{\alpha}\,.$$

Again we take the logarithm of both sides, we can try to find the slope of a linear plot:

$$\log\left(100\,|r_{\Delta r=0.07} - r_{\Delta r}|\right) = \alpha \log\left(100\Delta r\right) + \log\left(100^{1-\alpha}\beta\right). \tag{5.14}$$

Figure 5.24 shows the log-log plot at several different times. The average slope of our lines α is equal to 2.633. Our code converges with greater than second-order accuracy in Δr.

Next, we ran the symmetric, two-dimensional code with a range of values for

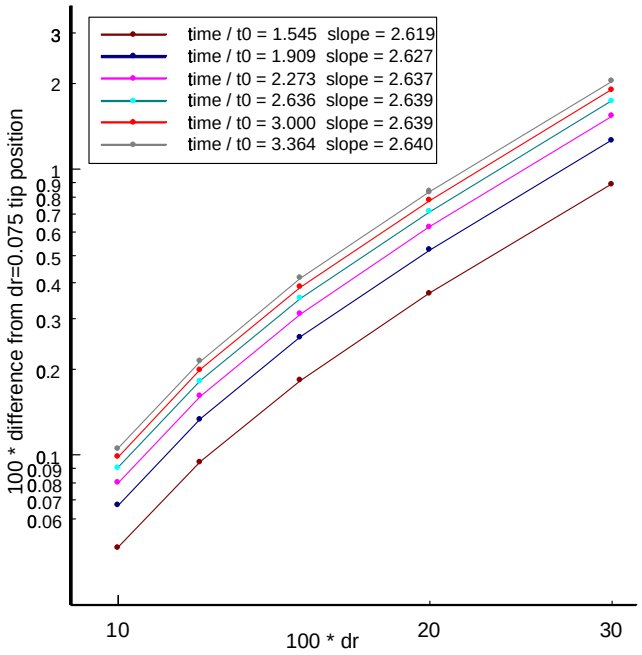

Figure 5.24: Difference in tip position from assumed converged solution with changing radial grid sizes as determined with anisotropy $\alpha = 0.40$ and undercooling $\Delta = 0.60$.

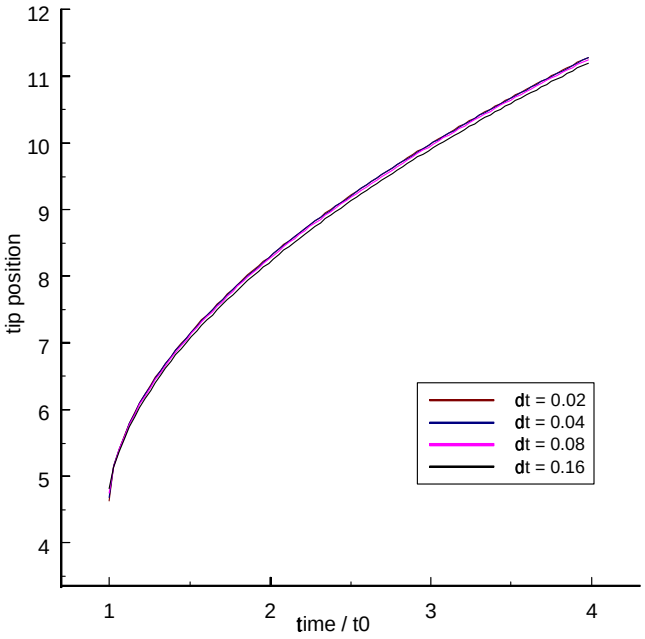

Figure 5.25: Tip position determined with anisotropy $\alpha = 0.45$ and undercooling $\Delta = 0.60$.

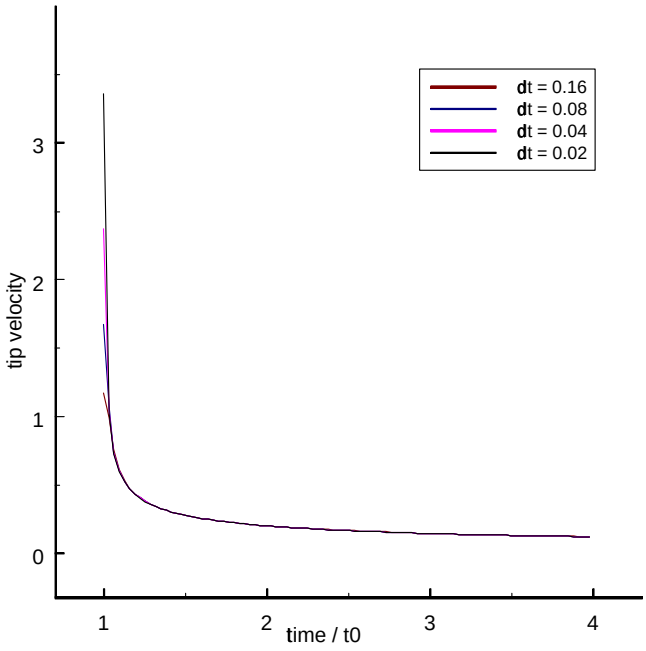

Figure 5.26: Tip velocity determined with anisotropy $\alpha = 0.45$ and undercooling $\Delta = 0.60$.

Δt. Figure 5.25 shows the position of the dendrite tip as a function of time for different values of Δt. However, it is very difficult to distinguish the difference between solutions for different values of Δt. Additionally, it is very difficult to distinguish the difference between tip velocities for different values of Δt in Figure 5.26. We will assume that the tip position for the smallest value of Δt for which we have calculated the position, $\Delta r = 0.01$, is the converged solution. We can then use the difference between the converged position and the calculated position at other values of Δr to find the convergence rate for our code:

$$|r_{\Delta t=0.01} - r_{\Delta t}| = \beta \left(\Delta t\right)^{\alpha}. \tag{5.15}$$

We can multiply by a constant without affecting the slope α.

$$100\,|r_{\Delta t=0.01} - r_{\Delta t}| = 100^{1-\alpha}\beta \left(100\Delta t\right)^{\alpha}.$$

Again we take the logarithm of both sides, we can try to find the slope of a linear plot:

$$\log\left(100\,|r_{\Delta t=0.01} - r_{\Delta t}|\right) = \alpha \log\left(100\Delta t\right) + \log\left(100^{1-\alpha}\beta\right). \tag{5.16}$$

Figure 5.27 shows the log-log plot at several different times. The average slope of our lines α is equal to 2.032. Therefore, our code converges with second-order accuracy in Δt.

5.3 Velocity Selection for a Needle Crystal

Ivantsov has shown that there is a steady-state solution to our problem where a parabolic, needle-crystal will grow steadily into an undercooled melt at a speed v in the direction of its axis of symmetry. The product of the speed v and tip radius ρ can be found by the Ivantsov relation between the undercooling and velocity:

$$\Delta = \sqrt{\pi p}\exp\left(p\right)\operatorname{erfc}\left(\sqrt{p}\right). \tag{5.17}$$

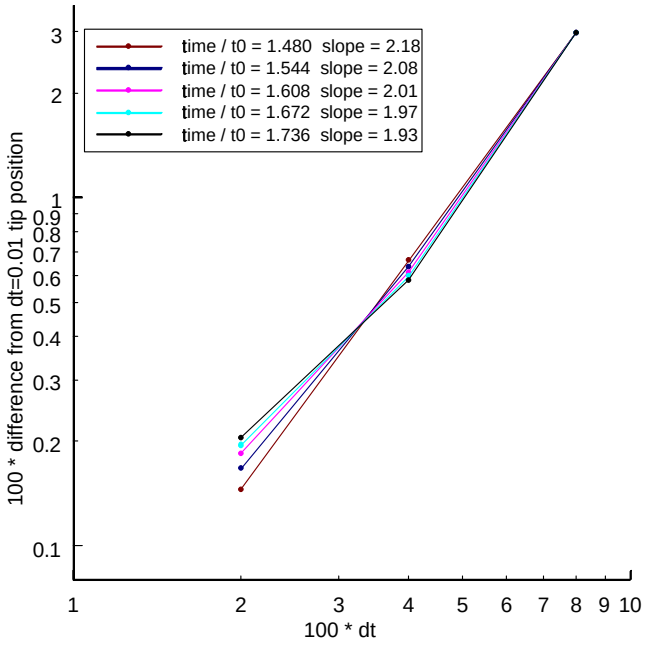

Figure 5.27: Difference from converged tip position determined with anisotropy $\alpha = 0.45$ and undercooling $\Delta = 0.60$.

The Peclet number p is defined by

$$p = \rho v / 2\kappa. \tag{5.18}$$

This presents a family of solutions. For any tip radius ρ, the Ivantsov relation predicts a unique tip velocity v. The solidification front for the Ivantsov solution is measured in units of the tip radius to be

$$\zeta_{\text{Ivantsov}}(x) = -x^2/2.$$

The derivation was summarized in Chapter 4 and is shown in greater detail by Langer in [31]. The Ivantsov solution provides a continuous family of solutions for any undercooling. In experiments, we see that a fixed velocity and tip radius are chosen for any given undercooling. Addition of a Gibbs-Thomson correction to the interface temperature based on surface tension and anisotropy seems to be necessary to select a particular velocity for a given undercooling.

One convenient feature of the symmetric model is that the equation of motion for an advancing needle crystal moving at a velocity v can be written in closed form [31]:

$$\Delta - d_0 f(\mathbf{x}, t, \alpha) K(\zeta(\mathbf{x}, t)) = \frac{\Gamma_1(\mathbf{x}, t)}{4\pi\kappa}, \tag{5.19}$$

where

$$\Gamma_1 = \int_{-\infty}^{t} \int_{-\infty}^{\infty} \frac{1}{(t-t')^{1.5}} \exp\left(-\frac{|\mathbf{x}-\mathbf{x}'|^2 + (\zeta(\mathbf{x}, t) - \zeta(\mathbf{x}', t') + v(t-t'))^2}{4\kappa(t-t')} \right) dx' dt' \tag{5.20}$$

Langer suggests a change of variables

$$\tau = v(t-t')/\rho \tag{5.21}$$

and assumes that $\mathbf{x}$ and $\zeta(\mathbf{x}, t)$ are measured in units of the tip radius ρ. This gives

us the steady-state equation of motion used by Barbieri, Hong, and Langer [2] to look at the problem of velocity selection.

$$\Delta - \frac{d_0}{\rho} f(\mathbf{x}, t, \alpha) K(\zeta(\mathbf{x})) = p\Gamma_2(p, \mathbf{x}, \zeta(\mathbf{x})), \tag{5.22}$$

where

$$\Gamma_2(p, \mathbf{x}, \zeta(\mathbf{x})) = \int_0^\infty \int_{-\infty}^\infty \frac{1}{2\pi\tau} \exp\left(-\frac{p\left((\mathbf{x}-\mathbf{x}')^2 + (\zeta(\mathbf{x}) - \zeta(\mathbf{x}') + \tau)^2\right)}{2\tau}\right) dx' d\tau. \tag{5.23}$$

Here the position of the advancing front is given by $\zeta(\mathbf{x})$ close to, but not necessarily equal to, the Ivantsov solution. We can subtract from equation (5.22) for our general problem with $d_0 \neq 0$ the same equation which we know must hold for the Ivantsov solution with $d_0 = 0$.

$$-\frac{d_0}{\rho} f(\mathbf{x}, \alpha) K(\zeta(\mathbf{x})) = p\Gamma_2(p, \mathbf{x}, \zeta(\mathbf{x})) - p\Gamma_2(p, \mathbf{x}, \zeta_{\text{Ivantsov}}(\mathbf{x})). \tag{5.24}$$

Let us introduce a stability parameter $\sigma = d_0/(p\rho)$:

$$-\sigma f(\mathbf{x}, \alpha) K(\zeta(\mathbf{x})) = \Gamma_2(p, \mathbf{x}, \zeta(\mathbf{x})) - \Gamma_2(p, \mathbf{x}, \zeta_{\text{Ivantsov}}(\mathbf{x})). \tag{5.25}$$

Because our new stability parameter appears as the coefficient of the highest derivative in the equation (in the equation for the curvature), Barbieri, Hong, and Langer [2] point out that we have reason to believe that solutions may only exist for specific values of σ. Therefore, (5.25) is a nonlinear eigenvalue equation which determines the selection of specific values of σ. In an attempt to find values for σ, we will linearize (5.25) in terms of the deviation of the interface shape from the Ivantsov parabola:

$$\zeta_0(\mathbf{x}) = \zeta(\mathbf{x}) - \zeta_{\text{Ivantsov}}(\mathbf{x}). \tag{5.26}$$

The result, in the limit of small Peclet number, is

$$\sigma \approx \sigma \frac{d^2\zeta_0}{dx^2} - \frac{3\sigma x}{1+x^2}\frac{d\zeta_0}{dx} - \frac{\left(1+x^2\right)^{3/2}}{2\pi f\left(x,\alpha\right)}\int_{-\infty}^{\infty}\frac{\left(x+x'\right)\left(\zeta_0\left(x\right)-\zeta_0\left(x'\right)\right)}{\left(x-x'\right)\left(1+\left(x+x'\right)^2/4\right)}dx'. \tag{5.27}$$

Langer [31] suggests that we eliminate the first derivative on the right-hand side by writing:

$$\zeta_0 = \left(1+x^2\right)^{3/4} Z\left(x\right). \tag{5.28}$$

This gives a linear and inhomogeneous integro-differential equation

$$\frac{\sigma}{\left(1+x^2\right)^{3/4}} = \sigma\frac{d^2Z}{dx^2} + \frac{\left(1+x^2\right)^{1/2}}{f\left(x,\alpha\right)}Z + \frac{\left(1+x^2\right)^{3/4}}{2\pi f\left(x,\alpha\right)}\mathrm{P}\int_{-\infty}^{\infty}\frac{\left(x+x'\right)\left(\zeta_0\left(x\right)-\zeta_0\left(x'\right)\right)}{\left(x-x'\right)\left(1+\left(x+x'\right)^2/4\right)}dx'. \tag{5.29}$$

Here P denotes the Cauchy principal value of the integral. For the existence of a nontrivial solution, we need the function on the left-hand side of (5.29) to be orthogonal to the zero eigenvector $\widetilde{Z}\left(x\right)$ of the adjoint of the operator on the right-hand side of the same equation [37].

$$\int_{-\infty}^{\infty}\frac{\widetilde{Z}\left(x;\sigma,\alpha\right)}{\left(1+x^2\right)^{3/4}}dx = 0. \tag{5.30}$$

Let us call this integral Θ:

$$\Theta\left(\sigma,\alpha\right) \equiv \int_{-\infty}^{\infty}\frac{\widetilde{Z}\left(x;\sigma,\alpha\right)}{\left(1+x^2\right)^{3/4}}dx. \tag{5.31}$$

The WKB method is used by many people [2], [31], [37] to obtain $\widetilde{Z}\left(x;\sigma,\alpha\right)$ and $\Theta\left(\sigma,\alpha\right)$ can then be found to behave for small σ and α as

$$\Theta\left(\sigma,\alpha\right) \sim \exp\left(-C/\sqrt{\sigma}\right)\cos\left(\frac{\pi}{2}\sqrt{\frac{\sigma_0\alpha^{7/4}}{\sigma}}\right), \tag{5.32}$$

where σ_0 is a constant of order unity. We are interested in solutions where $\Theta\left(\sigma,\alpha\right) \sim 0$:

$$\sqrt{\frac{\sigma_0\alpha^{7/4}}{\sigma}} \sim 1+2n. \tag{5.33}$$

$$\frac{\sigma_0 \alpha^{7/4}}{(1+2n)^2} \sim \sigma. \tag{5.34}$$

Linear stability analysis around these solutions shows that the largest value of σ satisfying $\Theta(\sigma, \alpha) \sim 0$ identifies the dynamically selected needle crystal. The infinitely many smaller σ's describe unstable solutions of little significance. This selects a particular stability parameter

$$\sigma \sim \sigma_0 \alpha^{7/4}. \tag{5.35}$$

σ_0 should be of order unity [31]. Substituting $\sigma = d_0/(p\rho)$ and $p = \rho v/2\kappa$, gives us a relationship between the tip radius, velocity, and coefficient of anisotropy:

$$\rho^2 v \sim \frac{d_0 2\kappa}{\sigma_0} \alpha^{-7/4}. \tag{5.36}$$

Figure 5.28 shows the results of runs at separate values of undercooling. For a fixed value of undercooling, we can find the velocity v and tip radius ρ. We expect $\rho^2 v$ to scale as $\alpha^{-7/4}$. We expect each line in Figure 5.29 corresponding to a fixed value of undercooling to have a slope of approximately $-7/4$. Our average slope of -1.72 is consistent with our relationship (5.36). We expect our curves to be independent of undercooling, which they obviously are not. However, as the undercooling decreases the lines do converge. It may be necessary to explore the behaviour of $\rho^2 v$ vs α at higher values of undercooling.

Additionally, in the limit of small Peclet number, $\Delta \approx \sqrt{\pi p}$. Therefore, for a constant anisotropy, we also have a relationship between velocity and undercooling after the substitutions into (5.35) of $\sigma = d_0/(p\rho)$, $\rho = 2\kappa p/v =$, and $p = \Delta^2/\pi$:

$$v \sim \frac{2\kappa\sigma_0}{d_0 \pi^2} \alpha^{7/4} \Delta^4. \tag{5.37}$$

Figure 5.30 shows the results of runs at separate values of anisotropy. For a fixed value of anisotropy, we can find the velocity v. We expect velocity to scale as Δ^4. We expect each line in Figure 5.31 corresponding to a value of a fixed undercooling to have a slope of approximately 4. Our average slope of 4.06 is consistent with our

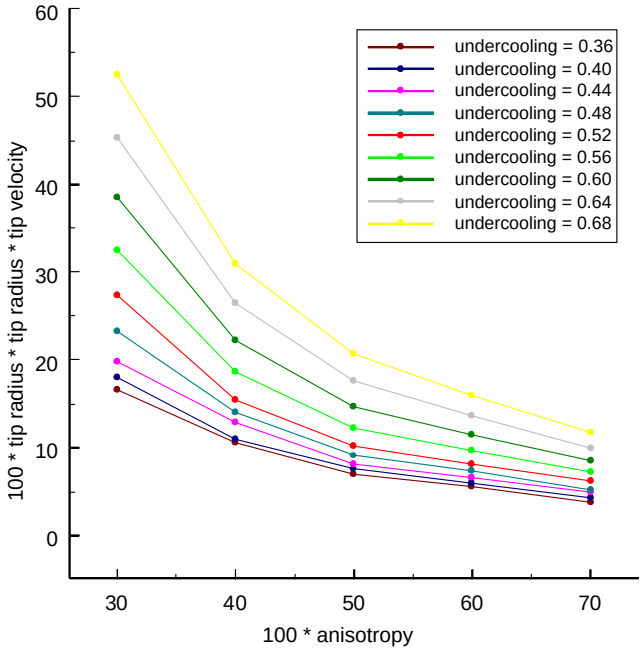

Figure 5.28: Plot of (tip velocity) $\times$ (tip radius)^2 vs. anisotropy for various undercoolings.

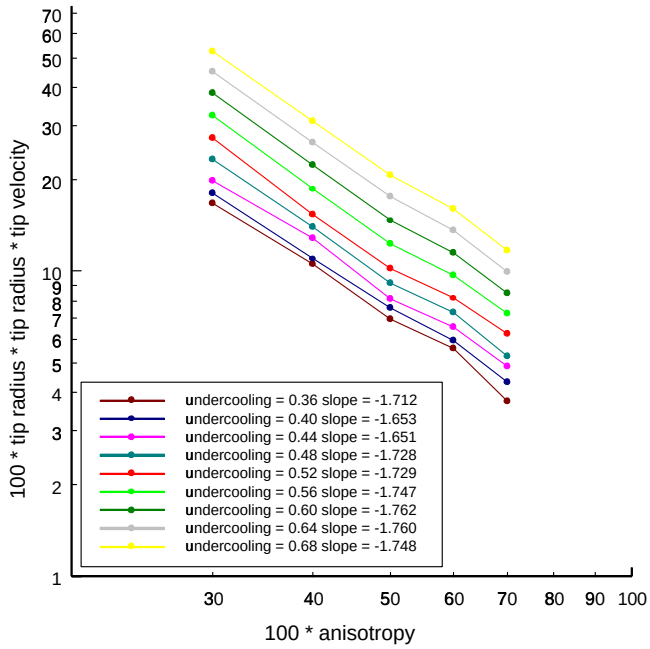

Figure 5.29: Plot of (tip velocity) $\times$ (tip radius)^2 vs. anisotropy for various undercoolings.

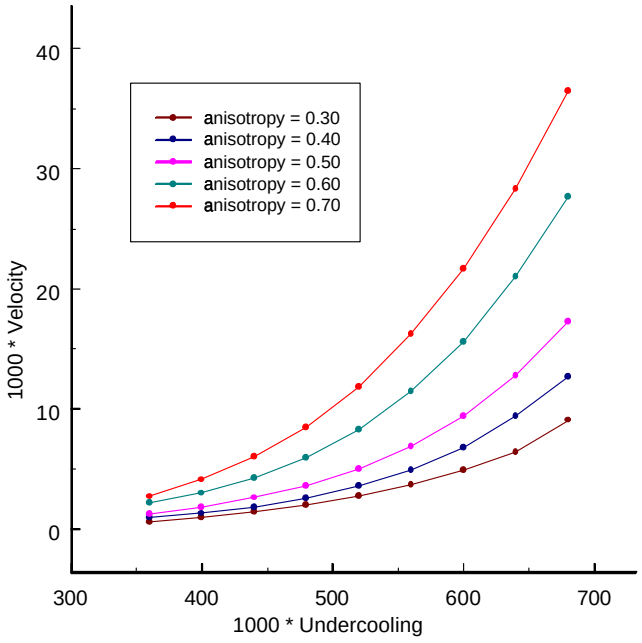

Figure 5.30: Plot of tip velocity vs. undercooling for various values of anisotropy.

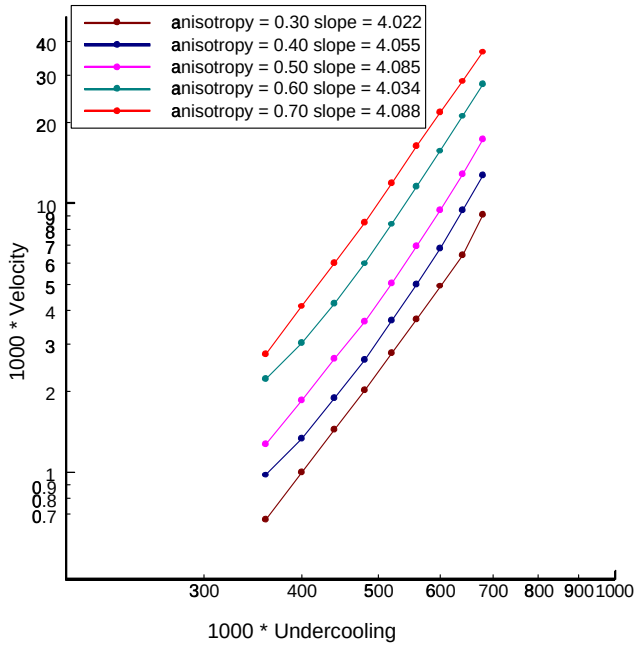

Figure 5.31: Plot of tip velocity vs. undercooling for various values of anisotropy.

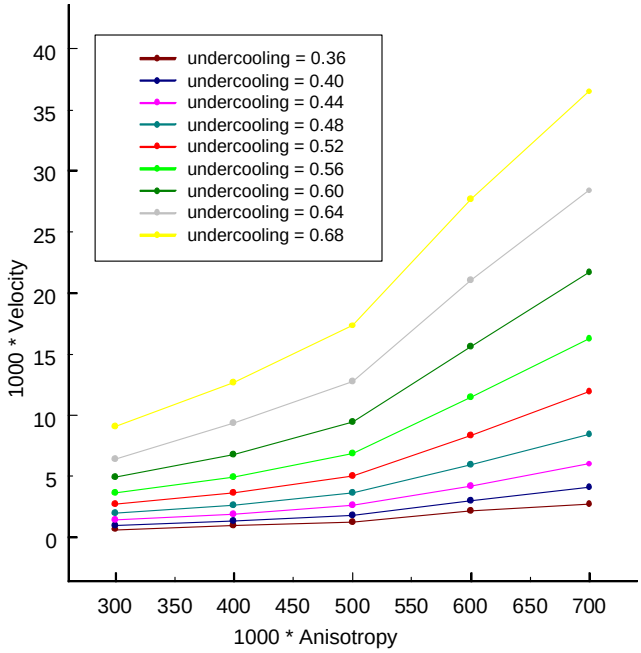

Figure 5.32: Plot of tip velocity vs. anisotropy for various values of undercooling.

relationship (5.37).

Figure 5.32 shows the results of runs at separate values of undercooling. For a fixed value of undercooling, we can find the velocity v. We expect velocity to scale as $\alpha^{7/4}$. We expect each line in Figure 5.33 corresponding to a value of a fixed undercooling to have a slope of approximately 1.75. Our average slope of 1.73 is consistent with this relationship (5.37).

LaCombe, Koss, and Glicksman [15] observed the growth of pivalic acid (PVA) dendrites in microgravity at six different undercoolings in the range of $0.13K$ to $1.25K$. Estimates for anisotropy were not given. The data presented was obtained at $0.41K$ and it shows that the tip does not approach a truly constant velocity. The non-steady-state velocities observed suggest that there may be features of the process that are not well described by current theory. However, the authors note that thermal interactions between dendrites and neighboring tips or container walls may

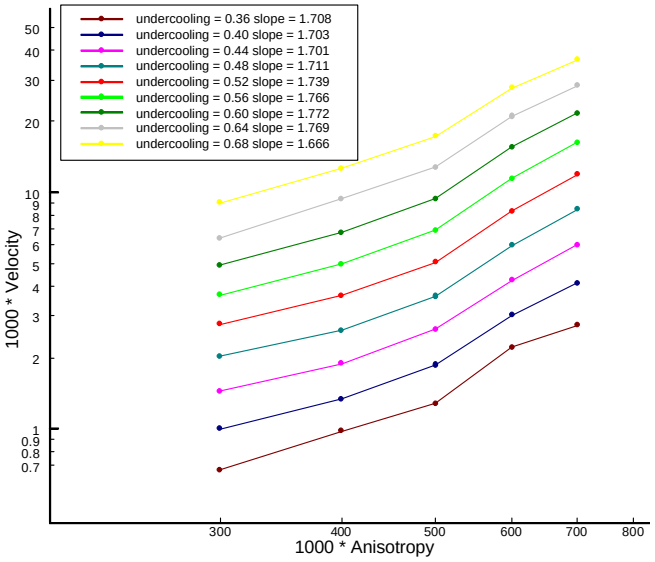

Figure 5.33: Plot of tip velocity vs. anisotropy for various values of undercooling.

account for differences between the observed velocity and the velocity predicted for a dendrite with the thermal boundary conditions set at infinity. At low undercoolings, the diffusion length is high and may compound these problems.

By converting to dimensionless quantities using Equation 2.4, the range of experimental undercoolings is approximately equal to the range 0.01 to 0.14 in our dimensionless undercooling, Δ. We cannot compare the tip velocities we calculated to those that they observed because the experiments do not achieve a constant tip velocity. Our calculations were also run at much higher values for Δ in the range of 0.4 to 0.8. A detailed comparison between the time dependent data at $0.41K$ or approximately $\Delta = 0.05$ is a subject for future work.

Chapter 6 Numerical Algorithm for the 2-D nonsymmetric Case

6.1 Two-Sided Case

The numerical method for the nonsymmetric case is nearly identical to that for the symmetric case, though it now needs to be done for both of the integral equations in (2.33) and (2.34) separately. Recall from (2.33) and (2.34) that we have the following coupled set of integral equations.

$$\begin{aligned}\frac{1}{2}\Delta = &\frac{1}{2}d_0 f\left(s,t\right)K\left(s,t\right) \\ &+\int_{V_S(t_0)} u_S\left(\mathbf{x}',t_0\right)G_S\left(\mathbf{x}',t;\zeta\left(s,t\right),t_0\right)dV' \\ &+\int_{t_0}^{t}\int_{S(t')} u_S\left(\mathbf{x}',t'\right)G_S\left(\mathbf{x}',t;\zeta\left(s,t\right),t'\right)\left(\mathbf{v}'\cdot\mathbf{n}'\right)ds'dt' \\ &+\kappa_S\int_{t_0}^{t}\int_{S(t')} G_S\left(\mathbf{x}',t;\zeta\left(s,t\right),t'\right)\left(\nabla' u_S\left(\mathbf{x}',t'\right)\cdot\mathbf{n}'\right)ds'dt' \\ &-\kappa_S\int_{t_0}^{t}\int_{S(t')} u_S\left(\mathbf{x}',t'\right)\left(\nabla' G_S\left(\mathbf{x}',t;\zeta\left(s,t\right),t'\right)\cdot\mathbf{n}'\right)ds'dt'.\end{aligned} \tag{6.1}$$

$$\begin{aligned}\frac{1}{2}\Delta = &\frac{1}{2}d_0 f\left(s,t\right)K\left(s,t\right) \\ &+\int_{V_L(t_0)} u_L\left(\mathbf{x}',t_0\right)G_L\left(\mathbf{x}',t;\zeta\left(s,t\right),t_0\right)dV' \\ &-\int_{t_0}^{t}\int_{S(t')} u_L\left(\mathbf{x}',t'\right)G_L\left(\mathbf{x}',t;\zeta\left(s,t\right),t'\right)\left(\mathbf{v}'\cdot\mathbf{n}'\right)ds'dt' \\ &-\kappa_L\int_{t_0}^{t}\int_{S(t')} G_L\left(\mathbf{x}',t;\zeta\left(s,t\right),t'\right)\left(\nabla' u_L\left(\mathbf{x}',t'\right)\cdot\mathbf{n}'\right)ds'dt' \\ &+\kappa_L\int_{t_0}^{t}\int_{S(t')} u_L\left(\mathbf{x}',t'\right)\left(\nabla' G_L\left(\mathbf{x}',t;\zeta\left(s,t\right),t'\right)\cdot\mathbf{n}'\right)ds'dt'.\end{aligned} \tag{6.2}$$

These equations are now coupled by the conditions on the interface dictating the conservation of heat at the interface:

$$\mathbf{v} \cdot \mathbf{n} = \kappa_S \nabla u_S(s,t) \cdot \mathbf{n} - \kappa_L \nabla u_L(s,t) \cdot \mathbf{n}. \tag{6.3}$$

The pieces of the integral equations may be different, but the steps remain the same and are summarized as follows:

1. Separate the problem into a part with a singularity and a part which is smooth and satisfies the heat equation. This introduces an underlying smooth temperature field $\overline{u}(\mathbf{x}, t_1, t)$, which must be evaluated at all points throughout the domain of the problem.

2. Approximate the remaining unknown integrals with the singularities in terms of the interface position at the current time.

3. Calculate the interface position at the current time.

4. Update the underlying smooth temperature field using the diffusion equation to advance to the next time step.

5. Compute the contribution of the time integral to the smooth temperature distribution for the next time step.

6.1.1 Step 1: Separate into Singular and Smooth Parts

As in the symmetric case, there will be a discontinuity in the temperature field at the interface due to the release of latent heat during solidification. However, the underlying temperature field will be smooth if no additional heat is released. Therefore, we can separate our integral equations (6.1) and (6.2) into one component with a singularity at the current time and one component which stops short of the current

time and is smooth with derivatives of all orders.

$$\begin{aligned}\frac{1}{2}\Delta = & \frac{1}{2}d_0 f(s,t)\, K(s,t) \\ & + \int_{V_S(t_0)} u_S(\mathbf{x}',t_0)\, G_S(\mathbf{x}',t;\zeta(s,t),t_0)\, dV' \\ & + \int_{t_0}^{t-N\Delta t}\int_{S(t')} u_S(\mathbf{x}',t')\, G_S(\mathbf{x}',t;\zeta(s,t),t')\,(\mathbf{v}'\cdot\mathbf{n}')\, ds'dt' \\ & + \int_{t-N\Delta t}^{t}\int_{S(t')} u_S(\mathbf{x}',t')\, G_S(\mathbf{x}',t;\zeta(s,t),t')\,(\mathbf{v}'\cdot\mathbf{n}')\, ds'dt' \\ & + \kappa_S \int_{t_0}^{t-N\Delta t}\int_{S(t')} G_S(\mathbf{x}',t;\zeta(s,t),t')\,(\nabla' u_S(\mathbf{x}',t')\cdot\mathbf{n}')\, ds'dt' \\ & + \kappa_S \int_{t-N\Delta t}^{t}\int_{S(t')} G_S(\mathbf{x}',t;\zeta(s,t),t')\,(\nabla' u_S(\mathbf{x}',t')\cdot\mathbf{n}')\, ds'dt' \\ & - \kappa_S \int_{t_0}^{t-N\Delta t}\int_{S(t')} u_S(\mathbf{x}',t')\,(\nabla' G_S(\mathbf{x}',t;\zeta(s,t),t')\cdot\mathbf{n}')\, ds'dt' \\ & - \kappa_S \int_{t-N\Delta t}^{t}\int_{S(t')} u_S(\mathbf{x}',t')\,(\nabla' G_S(\mathbf{x}',t;\zeta(s,t),t')\cdot\mathbf{n}')\, ds'dt'. \end{aligned} \tag{6.4}$$

$$\begin{aligned}\frac{1}{2}\Delta = & \frac{1}{2}d_0 f(s,t)\, K(s,t) \\ & + \int_{V_L(t_0)} u_L(\mathbf{x}',t_0)\, G_L(\mathbf{x}',t;\zeta(s,t),t_0)\, dV' \\ & - \int_{t_0}^{t-N\Delta t}\int_{S(t')} u_L(\mathbf{x}',t')\, G_L(\mathbf{x}',t;\zeta(s,t),t')\,(\mathbf{v}'\cdot\mathbf{n}')\, ds'dt' \\ & - \int_{t-N\Delta t}^{t}\int_{S(t')} u_L(\mathbf{x}',t')\, G_L(\mathbf{x}',t;\zeta(s,t),t')\,(\mathbf{v}'\cdot\mathbf{n}')\, ds'dt' \\ & - \kappa_L \int_{t_0}^{t-N\Delta t}\int_{S(t')} G_L(\mathbf{x}',t;\zeta(s,t),t')\,(\nabla' u_L(\mathbf{x}',t')\cdot\mathbf{n}')\, ds'dt' \\ & - \kappa_L \int_{t-N\Delta t}^{t}\int_{S(t')} G_L(\mathbf{x}',t;\zeta(s,t),t')\,(\nabla' u_L(\mathbf{x}',t')\cdot\mathbf{n}')\, ds'dt' \\ & + \kappa_L \int_{t_0}^{t-N\Delta t}\int_{S(t')} u_L(\mathbf{x}',t')\,(\nabla' G_L(\mathbf{x}',t;\zeta(s,t),t')\cdot\mathbf{n}')\, ds'dt' \\ & + \kappa_L \int_{t-N\Delta t}^{t}\int_{S(t')} u_L(\mathbf{x}',t')\,(\nabla' G_L(\mathbf{x}',t;\zeta(s,t),t')\cdot\mathbf{n}')\, ds'dt'. \end{aligned} \tag{6.5}$$

We are able to define two functions (one for the integral equation in the solid and one for the integral equation in the liquid) which satisfy the heat equation and which have finite derivatives of all orders at the interface.

$$\begin{aligned}\overline{u}_S(\mathbf{x},t_1,t) = &\int_{V_S(t_0)} u_S(\mathbf{x}',t_0)\, G_S(\mathbf{x}',t;\zeta(s,t),t_0)\, dV' \\ &+ \int_{t_0}^{t-N\Delta t}\int_{S(t')} u_S(\mathbf{x}',t')\, G_S(\mathbf{x}',t;\zeta(s,t),t')\,(\mathbf{v}'\cdot\mathbf{n}')\, ds'dt' \\ &+ \kappa_S \int_{t_0}^{t-N\Delta t}\int_{S(t')} G_S(\mathbf{x}',t;\zeta(s,t),t')\,(\nabla' u_S(\mathbf{x}',t')\cdot\mathbf{n}')\, ds'dt' \\ &- \kappa_S \int_{t_0}^{t-N\Delta t}\int_{S(t')} u_S(\mathbf{x}',t')\,(\nabla' G_S(\mathbf{x}',t;\zeta(s,t),t')\cdot\mathbf{n}')\, ds'dt'.\end{aligned} \tag{6.6}$$

$$\begin{aligned}\overline{u}_L(\mathbf{x},t_1,t) + &\int_{V_L(t_0)} u_L(\mathbf{x}',t_0)\, G_L(\mathbf{x}',t;\zeta(s,t),t_0)\, dV' \\ &- \int_{t_0}^{t-N\Delta t}\int_{S(t')} u_L(\mathbf{x}',t')\, G_L(\mathbf{x}',t;\zeta(s,t),t')\,(\mathbf{v}'\cdot\mathbf{n}')\, ds'dt' \\ &- \kappa_L \int_{t_0}^{t-N\Delta t}\int_{S(t')} G_L(\mathbf{x}',t;\zeta(s,t),t')\,(\nabla' u_L(\mathbf{x}',t')\cdot\mathbf{n}')\, ds'dt' \\ &+ \kappa_L \int_{t_0}^{t-N\Delta t}\int_{S(t')} u_L(\mathbf{x}',t')\,(\nabla' G_L(\mathbf{x}',t;\zeta(s,t),t')\cdot\mathbf{n}')\, ds'dt'.\end{aligned} \tag{6.7}$$

Because we can calculate $\overline{u}_S(\mathbf{x},t_1,t)$ and $\overline{u}_L(\mathbf{x},t_1,t)$ throughout our domain, the integral equations (6.1) and (6.2) have each been reduced to having only three unknown integrals which are over a much smaller range. Unfortunately, we do not reduce this to one unknown integral as in the symmetric case. Here instead we have,

$$\begin{aligned}\frac{1}{2}\Delta = &\frac{1}{2} d_0 f(s,t)\, K(s,t) + \overline{u}_S(\zeta(s,t),t-N\Delta t,t) \\ &+ \int_{t-N\Delta t}^{t}\int_{S(t')} u_S(\mathbf{x}',t')\, G_S(\mathbf{x}',t;\zeta(s,t),t')\,(\mathbf{v}'\cdot\mathbf{n}')\, ds'dt' \\ &+ \kappa_S \int_{t-N\Delta t}^{t}\int_{S(t')} G_S(\mathbf{x}',t;\zeta(s,t),t')\,(\nabla' u_S(\mathbf{x}',t')\cdot\mathbf{n}')\, ds'dt' \\ &- \kappa_S \int_{t-N\Delta t}^{t}\int_{S(t')} u_S(\mathbf{x}',t')\,(\nabla' G_S(\mathbf{x}',t;\zeta(s,t),t')\cdot\mathbf{n}')\, ds'dt'.\end{aligned} \tag{6.8}$$

$$\begin{aligned}\frac{1}{2}\Delta = &\frac{1}{2}d_0 f\left(s,t\right)K\left(s,t\right)+\overline{u}_L\left(\zeta\left(s,t\right),t-N\Delta t,t\right) \\ &-\int_{t-N\Delta t}^{t}\int_{S(t')}u_L\left(\mathbf{x}',t'\right)G_L\left(\mathbf{x}',t;\zeta\left(s,t\right),t'\right)\left(\mathbf{v}'\cdot\mathbf{n}'\right)ds'dt' \\ &-\kappa_L\int_{t-N\Delta t}^{t}\int_{S(t')}G_L\left(\mathbf{x}',t;\zeta\left(s,t\right),t'\right)\left(\nabla' u_L\left(\mathbf{x}',t'\right)\cdot\mathbf{n}'\right)ds'dt' \\ &+\kappa_L\int_{t-N\Delta t}^{t}\int_{S(t')}u_L\left(\mathbf{x}',t'\right)\left(\nabla' G_L\left(\mathbf{x}',t;\zeta\left(s,t\right),t'\right)\cdot\mathbf{n}'\right)ds'dt'.\end{aligned} \tag{6.9}$$

6.1.2 Step 2: Approximate the Singular Integrals

In order to find the interface position from our integral equation, we need to be able to numerically compute the remaining memory integrals, those holding information from time $t-N\Delta t$ to t. There are several memory integrals involved in the nonsymmetric case. If we know the interface position at previous time steps and an approximation to the interface position at the current time, then we can find the integrals of interest. We will define our integral equations (6.8) and (6.9) in terms of the unknown integrals:

$$\begin{aligned}\frac{1}{2}\Delta = &\frac{1}{2}d_0 f\left(s,t\right)K\left(s,t\right)+\overline{u}_S\left(\zeta\left(s,t\right),t-N\Delta t,t\right) \\ &+Q_S\left(\zeta\left(s,t\right),t-N\Delta t,t\right) \\ &+R_S\left(\zeta\left(s,t\right),t-N\Delta t,t\right) \\ &-T_S\left(\zeta\left(s,t\right),t-N\Delta t,t\right).\end{aligned} \tag{6.10}$$

$$\begin{aligned}\frac{1}{2}\Delta = &\frac{1}{2}d_0 f\left(s,t\right)K\left(s,t\right)+\overline{u}_L\left(\zeta\left(s,t\right),t-N\Delta t,t\right) \\ &-Q_L\left(\zeta\left(s,t\right),t-N\Delta t,t\right) \\ &-R_L\left(\zeta\left(s,t\right),t-N\Delta t,t\right) \\ &+T_L\left(\zeta\left(s,t\right),t-N\Delta t,t\right),\end{aligned} \tag{6.11}$$

where our unknown integrals are

$$Q\left(\zeta\left(s,t\right),t_1,t\right)=\int_{t_1}^{t}\int_{S(t')}u\left(\mathbf{x}',t'\right)G\left(\mathbf{x}',t;\zeta\left(s,t\right),t'\right)\left(\mathbf{v}'\cdot\mathbf{n}'\right)ds'dt'. \tag{6.12}$$

$$R\left(\zeta\left(s,t\right),t_1,t\right)=\kappa\int_{t_1}^{t}\int_{S(t')}G\left(\mathbf{x}',t;\zeta\left(s,t\right),t'\right)\nabla u\left(\mathbf{x}',t'\right)\cdot\mathbf{n}'ds'dt'. \tag{6.13}$$

$$T\left(\zeta\left(s,t\right),t_1,t\right)=\kappa\int_{t_1}^{t}\int_{S(t')}u_S\left(\mathbf{x}',t'\right)\nabla G\left(\mathbf{x}',t;\zeta\left(s,t\right),t'\right)\cdot\mathbf{n}'ds'dt'. \tag{6.14}$$

$Q\left(\zeta\left(s,t\right),t_1,t\right)$ is very similar to $Q\left(\zeta\left(s,t\right),t_1,t\right)$ from the symmetric case. In the symmetric case, the kernel is not multiplied by the temperature field on the interface. However, we can assume that Δt is small enough such that for any t' in our range, we can approximate $u\left(\mathbf{x}',t'\right)$ by $u\left(\mathbf{x}',t\right)$. And the temperature field will only need to be applied at specific points on the interface. Therefore, the evaluation of $Q\left(\zeta\left(s,t\right),t_1,t\right)$ from the symmetric case (3.41) can be evaluated in a similar fashion in the nonsymmetric case.

$$Q\approx\sum_{j=0}^{I-1}\sum_{g=1}^{G}w_g\left[\frac{\left[u\left(s',t\right)\left(\mathbf{v}'\cdot\mathbf{n}'\right)\right]_{s'=s_{j+1/2}}\exp\left(\frac{B_j^2-4A_jC_j}{16\kappa C_j\beta^2}\right)}{2\sqrt{\pi\kappa C_j}}\operatorname{erf}\left(\frac{B_j+2C_j\Delta s}{4\beta\sqrt{\kappa C_j}}\right)\right]_{\beta=\beta_g} \tag{6.15}$$

$$-\sum_{j=0}^{I-1}\sum_{g=1}^{G}w_g\left[\frac{\left[u\left(s',t\right)\left(\mathbf{v}'\cdot\mathbf{n}'\right)\right]_{s'=s_{j+1/2}}\exp\left(\frac{B_j^2-4A_jC_j}{16\kappa C_j\beta^2}\right)}{2\sqrt{\pi\kappa C_j}}\operatorname{erf}\left(\frac{B_j}{4\beta\sqrt{\kappa C_j}}\right)\right]_{\beta=\beta_g}.$$

We will next look at the integral $R\left(\zeta\left(s,t\right),t_1,t\right)$ (6.13). This integral is similar to our integral Q from Chapter 3. However, we are looking at the behavior of the temperature field at the interface $\nabla u\left(\mathbf{x}',t'\right)\cdot\mathbf{n}'$ instead of the velocity of the interface as in Q (3.25).

$$R\left(\zeta\left(s,t\right),t_1,t\right)=\kappa\int_{t_1}^{t}\int_{S(t')}G\left(\mathbf{x}',t;\zeta\left(s,t\right),t'\right)\nabla u\left(\mathbf{x}',t'\right)\cdot\mathbf{n}'ds'dt', \tag{6.16}$$

where

$$\begin{aligned} x &= \zeta(s,t)\cos s, \\ y &= \zeta(s,t)\sin s, \\ x' &= \zeta(s',t')\cos s', \\ y' &= \zeta(s',t')\sin s'. \end{aligned} \tag{6.17}$$

We define a function

$$F(x',y',t') = \nabla u(x',y',t')\cdot \mathbf{n}'. \tag{6.18}$$

We assume that if $t - t_1$ is sufficiently small, that $F(x',y',t')$ can be approximated over the range $t' = [t_1, t]$ by a polynomial.

$$F(x',y',t') \approx F_0(x',y',t) + (t'-t)F_1(x',y',t) + (t'-t)^2 F_2(x',y',t) + \ldots. \tag{6.19}$$

For a first approximation, we will look only at on the first term in each series, though the method could be extended by including additional terms:

$$R \approx \kappa \int_{t_1}^{t}\int_{-\pi}^{\pi} \frac{F_0(x',y',t)}{4\pi\kappa(t-t')} \exp\left(-\frac{(x-x')^2+(y-x')^2}{4\kappa(t-t')}\right) ds'dt'. \tag{6.20}$$

Make the change of variables $\beta = 1/(t-t')$,

$$R \approx \int_{1/(t-t_1)}^{\infty}\int_{-\pi}^{\pi} \frac{F_0(x',y',t)}{4\pi\beta} \exp\left(-\beta\frac{(x-x')^2+(y-y')^2}{4\kappa}\right) ds'd\beta. \tag{6.21}$$

Change the order of integration:

$$R \approx \int_{-\pi}^{\pi} \frac{F_0(x',y',t)}{4\pi} \int_{1/(t-t_1)}^{\infty} \frac{1}{\beta} \exp\left(-\beta\frac{(x-x')^2+(y-y')^2}{4\kappa}\right) d\beta ds'. \tag{6.22}$$

Using the exponential integral $E_1(z) = \int_{z/\alpha}^{\infty} \frac{\exp(-\alpha u)}{u} du$, the integral over β can now be

evaluated

$$R \approx \int_{-\pi}^{\pi} \frac{F_0(x', y', t)}{4\pi} E_1\left(\frac{(x-x')^2 + (y-y')^2}{4\kappa(t-t_1)}\right) ds'. \tag{6.23}$$

We notice the log singularity which is introduced by the exponential function, E_1. To deal with this singularity, we will subtract a function with a similar singularity which we are able to evaluate in closed form. We find this new function in the vicinity of $s = s'$.

$$\begin{aligned} R \approx & \int_{-\pi}^{\pi} \frac{F_0(x', y', t)}{4\pi} E_1\left(\frac{(x-x')^2 + (y-y')^2}{4\kappa(t-t_1)}\right) ds' \\ & - \frac{F_0(x, y, t)}{4\pi} \int_{-\pi}^{\pi} E_1\left(\frac{(x_s + y_s)^2 (s-s')^2}{4\kappa(t-t_1)}\right) ds' \\ & + \frac{F_0(x, y, t)}{4\pi} \int_{-\pi}^{\pi} E_1\left(\frac{(x_s + y_s)^2 (s-s')^2}{4\kappa(t-t_1)}\right) ds'. \end{aligned} \tag{6.24}$$

We will now evaluate the new integral. This subtraction allows us to remove the log singularity while providing a good approximation as $t_1 \to t$.

$$I = \int_{-\pi}^{\pi} E_1\left(\frac{(x_s + y_s)^2 (s-S')^2}{4\kappa(t-t_1)}\right) ds'. \tag{6.25}$$

Define a function $\alpha(s)$.

$$\alpha(\theta) = \frac{(x_s + y_s)^2}{4\kappa(t-t_1)}. \tag{6.26}$$

The unknown integral becomes

$$I = \int_{-\pi}^{\pi} E_1\left(\alpha(s-s')^2\right) ds'. \tag{6.27}$$

Make the change of variables $\gamma = \alpha(s-S')^2$,

$$I = \int_{\alpha(s+\pi)^2}^{\alpha(s-\pi)^2} E_1(\gamma)\left(-\frac{1}{2\sqrt{\alpha\gamma}}\right) d\gamma = \frac{1}{2\sqrt{\alpha}} \int_{\alpha(s-\pi)^2}^{\alpha(s+\pi)^2} \int_{t}^{\infty} \frac{1}{\sqrt{\gamma}} \frac{e^{-t}}{t} dt\, d\gamma. \tag{6.28}$$

Changing the order of integration $a = \alpha\,(s-\pi)^2$ and $b = \alpha\,(s+\pi)^2$,

$$I = \frac{1}{2\sqrt{\alpha}}\left[\int_a^b \frac{e^{-t}}{t}\int_a^t \frac{1}{\sqrt{\gamma}}d\gamma dt \;+\int_b^\infty \frac{e^{-t}}{t}\int_a^b \frac{1}{\sqrt{\gamma}}d\gamma dt\right]. \tag{6.29}$$

$$I = \frac{2}{2\sqrt{\alpha}}\left[\int_a^b \frac{e^{-t}}{t}\left[\sqrt{\gamma}\right]_{\gamma=a}^{\gamma=t} dt \;+\int_b^\infty \frac{e^{-t}}{t}\left[\sqrt{\gamma}\right]_{\gamma=a}^{\gamma=b} dt\right]. \tag{6.30}$$

$$I = \frac{1}{\sqrt{\alpha}}\left[\int_a^b \frac{e^{-t}}{t}\sqrt{t}dt \;-\int_a^b \frac{e^{-t}}{t}\sqrt{a}dt + \int_b^\infty \frac{e^{-t}}{t}\sqrt{b}dt \;-\int_b^\infty \frac{e^{-t}}{t}\sqrt{a}dt\right]. \tag{6.31}$$

$$I = \frac{1}{\sqrt{\alpha}}\left[\int_a^b \frac{e^{-t}}{\sqrt{t}}dt \;-\sqrt{a}\int_a^b \frac{e^{-t}}{t}dt + \sqrt{b}\int_b^\infty \frac{e^{-t}}{t}dt \;-\sqrt{a}\int_b^\infty \frac{e^{-t}}{t}dt\right]. \tag{6.32}$$

$$I = \frac{1}{\sqrt{\alpha}}\left[\int_a^b \frac{e^{-t}}{\sqrt{t}}dt \;-\sqrt{\alpha}\,(s-\pi)\int_a^\infty \frac{e^{-t}}{t}dt + \sqrt{\alpha}\,(s+\pi)\int_b^\infty \frac{e^{-t}}{t}dt\right]. \tag{6.33}$$

Our integral can be evaluated in closed form:

$$\begin{aligned} I = {} & \frac{\pi}{\sqrt{\alpha}}\left[\operatorname{erf}\left(\sqrt{\alpha}\,(s+\pi)\right)\frac{\pi}{\sqrt{\alpha}}\operatorname{erf}\left(\sqrt{\alpha}\,(s-\pi)\right)\right] \\ & + (\pi-s)\,E_1\left(\alpha\,(s-\pi)^2\right) + (s+\pi)\,E_1\left(\alpha\,(s+\pi)^2\right). \end{aligned} \tag{6.34}$$

Making the substitutions for the endpoints:

$$\begin{aligned} I = {} & \frac{2\pi\sqrt{\kappa\,(t-t_1)}}{x_s^2+y_s^2}\operatorname{erf}\left(\frac{x_s^2+y_s^2}{2\sqrt{\kappa\,(t-t_1)}}\,(s+\pi)\right) \\ & - \frac{2\pi\sqrt{\kappa\,(t-t_1)}}{x_s^2+y_s^2}\operatorname{erf}\left(\frac{x_s^2+y_s^2}{2\sqrt{\kappa\,(t-t_1)}}\,(s-\pi)\right) \\ & + (\pi-s)\,E_1\left(\frac{\left(x_s^2+y_s^2\right)^2}{4\kappa\,(t-t_1)}\,(s-\pi)^2\right) \\ & + (s+\pi)\,E_1\left(\frac{\left(x_s^2+y_s^2\right)^2}{4\kappa\,(t-t_1)}\,(s+\pi)^2\right). \end{aligned} \tag{6.35}$$

So the integral of interest (6.13) can be evaluated by

$$
\begin{aligned}
R \approx & \int_{-\pi}^{\pi} \frac{F_0(x', y', t)}{4\pi} E_1\left(\frac{(x-x')^2 + (y-y')^2}{4\kappa(t-t_1)}\right) ds' \\
& - \frac{F_0(x, y, t)}{4\pi} \int_{-\pi}^{\pi} E_1\left(\frac{(x_s+y_s)^2 (s-s')^2}{4\kappa(t-t_1)}\right) ds' \\
& + \frac{F_0(x, y, t)}{2} \frac{\sqrt{\kappa(t-t_1)}}{x_s^2+y_s^2} \operatorname{erf}\left(\frac{x_s^2+y_s^2}{2\sqrt{\kappa(t-t_1)}}(s+\pi)\right) \\
& - \frac{F_0(x, y, t)}{2} \frac{\sqrt{\kappa(t-t_1)}}{x_s^2+y_s^2} \operatorname{erf}\left(\frac{x_s^2+y_s^2}{2\sqrt{\kappa(t-t_1)}}(s-\pi)\right) \\
& + \frac{F_0(x, y, t)}{4\pi}(\pi - s) E_1\left(\frac{(x_s^2+y_s^2)^2}{4\kappa(t-t_1)}(s-\pi)^2\right) \\
& + \frac{F_0(x, y, t)}{4\pi}(s+\pi) E_1\left(\frac{(x_s^2+y_s^2)^2}{4\kappa(t-t_1)}(s+\pi)^2\right).
\end{aligned} \tag{6.36}
$$

Next, we look at the integral $T(\zeta(s,t), t_1, t)$ (6.14).

$$
T(\zeta(s,t), t_1, t) = \kappa \int_{t_1}^{t} \int_{S(t')} u_S(\mathbf{x}', t') \nabla G(\mathbf{x}', t; \zeta(s,t), t') \cdot \mathbf{n}' ds' dt', \tag{6.37}
$$

where

$$
\begin{aligned}
x &= \zeta(s,t) \cos s, \\
y &= \zeta(s,t) \sin s, \\
x' &= \zeta(S', t') \cos s', \\
y' &= \zeta(S', t') \sin s'.
\end{aligned} \tag{6.38}
$$

We define a function

$$
H(x', y', t') = u(x', y', t'). \tag{6.39}
$$

We assume that if $t - t_1$ is sufficiently small, that $H(x', y', t')$ can be approximated

over the range $t' = [t_1, t]$ by a polynomial.

$$H(x', y', t') \approx H_0(x', y', t) + (t' - t) H_1(x', y', t) + (t' - t)^2 H_2(x', y', t) + \dots . \quad (6.40)$$

For a first approximation, we will look only at on the first term in each series, though the method could be extended by including additional terms:

$$T \approx \kappa \int_{t_1}^{t} \int_{S(t')} H_0(x', y', t) \nabla G(x', y', t; x, y, t') \cdot \mathbf{n}' ds' dt'. \quad (6.41)$$

$$T \approx \kappa \int_{t_1}^{t} \int_{-\pi}^{\pi} H_0(x', y', t) \left(-\frac{\partial y'}{\partial S'} \frac{\partial}{\partial x'} + \frac{\partial x'}{\partial S'} \frac{\partial}{\partial y'} \right) G \, ds' dt'. \quad (6.42)$$

The derivatives can be evaluated.

$$T \approx \int_{t_1}^{t} \int_{-\pi}^{\pi} \frac{H_0(x', y', t) \left[\frac{\partial x'}{\partial S'} (y - y') - \frac{\partial y'}{\partial S'} (x - x') \right]}{8\pi\kappa (t - t')^2} e^{-\frac{(y-y')^2 + (x-x')^2}{4\kappa(t-t')}} ds' dt'. \quad (6.43)$$

Again make the change of variables $\beta = 1/(t - t')$,

$$T \approx \int_{1/(t-t_1)}^{\infty} \int_{-\pi}^{\pi} \frac{H_0(x', y', t) \left[\frac{\partial x'}{\partial S'} (y - y') - \frac{\partial y'}{\partial S'} (x - x') \right]}{8\pi\kappa} e^{-\beta \frac{(y-y')^2 + (x-x')^2}{4\kappa}} ds' d\beta. \quad (6.44)$$

Change the order of integration

$$T \approx \int_{-\pi}^{\pi} \frac{H_0(x', y', t) \left[\frac{\partial x'}{\partial S'} (y - y') - \frac{\partial y'}{\partial S'} (x - x') \right]}{8\pi\kappa} \int_{1/(t-t_1)}^{\infty} e^{-\beta \frac{(y-y')^2 + (x-x')^2}{4\kappa}} d\beta ds'. \quad (6.45)$$

The integral over β can be easily evaluated.

$$T = \int_{-\pi}^{\pi} \frac{H_0(x', y', t) \left[\frac{\partial x'}{\partial S'} (y - y') - \frac{\partial y'}{\partial S'} (x - x') \right]}{8\pi\kappa} \left[-\frac{4\kappa e^{-\beta \frac{(y-y')^2 + (x-x')^2}{4\kappa}}}{(x - x')^2 + (y - y')^2} \right]_{1/(t-t_1)}^{\infty} ds' . \quad (6.46)$$

$$T = \int_{-\pi}^{\pi} \frac{H_0\left(x', y', t\right)\left[\frac{\partial x'}{\partial S'}\left(y - y'\right) - \frac{\partial y'}{\partial S'}\left(x - x'\right)\right]}{2\pi\left[\left(x - x'\right)^2 + \left(y - y'\right)^2\right]} \exp\left(-\frac{\left(x - x'\right)^2 + \left(y - y'\right)^2}{4\kappa\left(t - t_1\right)}\right) ds' . \tag{6.47}$$

In (6.23), the term multiplying the exponential function was singular. This is not true in this case, however, and $\left[\frac{\partial x'}{\partial S'}\left(y - y'\right) - \frac{\partial y'}{\partial S'}\left(x - x'\right)\right] / \left[\left(x - x'\right)^2 + \left(y - y'\right)^2\right]$ obtains a finite value. There is still a problem regarding the exponential decay. Again we subtract a function which we can evaluate in closed form from our integral which has the same behavior as S' approaches our interface position, s.

(6.48)

$$\begin{aligned} T = & \int_{-\pi}^{\pi} \frac{H_0\left(x', y', t\right)\left[\frac{\partial x'}{\partial S'}\left(y - y'\right) - \frac{\partial y'}{\partial S'}\left(x - x'\right)\right]}{2\pi\left[\left(x - x'\right)^2 + \left(y - y'\right)^2\right]} \exp\left(-\frac{\left(x - x'\right)^2 + \left(y - y'\right)^2}{4\kappa\left(t - t_1\right)}\right) ds' \\ & - \frac{H_0\left(x, y, t\right)}{2\pi} \frac{x_s y_{ss} - y_s x_{ss}}{x_s^2 + y_s^2} \int_{-\pi}^{\pi} \exp\left(-\frac{\left(x_s^2 + y_s^2\right)\left(s - s'\right)^2}{4\kappa\left(t - t_1\right)}\right) ds' \\ & + \frac{H_0\left(x, y, t\right)}{2\pi} \frac{x_s y_{ss} - y_s x_{ss}}{x_s^2 + y_s^2} \int_{-\pi}^{\pi} \exp\left(-\frac{\left(x_s^2 + y_s^2\right)\left(s - s'\right)^2}{4\kappa\left(t - t_1\right)}\right) ds'. \end{aligned}$$

We can evaluate the new integral in closed form where $\alpha = \left(x_s^2 + y_s^2\right) / \left[4\kappa\left(t - t_1\right)\right]$:

$$\begin{aligned} J &= \int_{-\pi}^{\pi} \exp\left(-\frac{\left(x_s^2 + y_s^2\right)\left(s - s'\right)^2}{4\kappa\left(t - t_1\right)}\right) ds' \\ &= \frac{1}{2}\left[\sqrt{\frac{\pi}{\alpha}}\,\mathrm{erf}\left(\sqrt{\alpha\left(s - s'\right)}\right)\right]_{s\prime=-\pi}^{s\prime=\pi} \\ &= \frac{1}{2}\sqrt{\frac{\pi}{\alpha}}\left[\mathrm{erf}\left(\sqrt{\alpha}\left(s - \pi\right)\right) - \mathrm{erf}\left(\sqrt{\alpha}\left(s + \pi\right)\right)\right]. \end{aligned} \tag{6.49}$$

So our approximation for $T\left(\zeta\left(s,t\right),t_1,t\right)$ becomes

$$
\begin{aligned}
T = & \int_{-\pi}^{\pi} \frac{H_0\left(x',y',t\right)\left[\frac{\partial x'}{\partial S'}\left(y-y'\right)-\frac{\partial y'}{\partial S'}\left(x-x'\right)\right]}{2\pi\left[\left(x-x'\right)^2+\left(y-y'\right)^2\right]} \exp\left(-\frac{\left(x-x'\right)^2+\left(y-y'\right)^2}{4\kappa\left(t-t_1\right)}\right) ds' \\
& - \frac{H_0\left(x,y,t\right)}{2\pi}\frac{x_s y_{ss}-y_s x_{ss}}{x_s^2+y_s^2}\int_{-\pi}^{\pi} \exp\left(-\frac{\left(x_s^2+y_s^2\right)\left(s-s'\right)^2}{4\kappa\left(t-t_1\right)}\right) ds' \\
& + H_0\left(x,y,t\right)\frac{x_s y_{ss}-y_s x_{ss}}{x_s^2+y_s^2}\sqrt{\frac{\kappa\left(t-t_1\right)}{4\pi\left(x_s^2+y_s^2\right)}}\,\mathrm{erf}\left(\sqrt{\frac{x_s^2+y_s^2}{4\kappa\left(t-t_1\right)}}\left(s-\pi\right)\right) \\
& - H_0\left(x,y,t\right)\frac{x_s y_{ss}-y_s x_{ss}}{x_s^2+y_s^2}\sqrt{\frac{\kappa\left(t-t_1\right)}{4\pi\left(x_s^2+y_s^2\right)}}\,\mathrm{erf}\left(\sqrt{\frac{x_s^2+y_s^2}{4\kappa\left(t-t_1\right)}}\left(s+\pi\right)\right).
\end{aligned}
\tag{6.50}
$$

6.1.3 Step 3: Find the Interface Position

We can now use Newton's method to solve for the new interface position. We have an equation describing the position of each point on the interface in both the solid and liquid phases (6.10) and (6.11):

$$
\begin{aligned}
\frac{1}{2}\Delta = & \frac{1}{2}d_0 f\left(s_j,t\right)K\left(s_j,t\right)+\overline{u}_S\left(\zeta\left(s_j,t\right),t-N\Delta t,t\right) \\
& + Q_S\left(\zeta\left(s_j,t\right),t-N\Delta t,t\right) \\
& + R_S\left(\zeta\left(s_j,t\right),t-N\Delta t,t\right) \\
& - T_S\left(\zeta\left(s_j,t\right),t-N\Delta t,t\right),
\end{aligned}
\tag{6.51}
$$

$$
\begin{aligned}
\frac{1}{2}\Delta = & \frac{1}{2}d_0 f\left(s_j,t\right)K\left(s_j,t\right)+\overline{u}_L\left(\zeta\left(s_j,t\right),t-N\Delta t,t\right) \\
& - Q_L\left(\zeta\left(s_j,t\right),t-N\Delta t,t\right) \\
& - R_L\left(\zeta\left(s_j,t\right),t-N\Delta t,t\right) \\
& + T_L\left(\zeta\left(s_j,t\right),t-N\Delta t,t\right).
\end{aligned}
\tag{6.52}
$$

There will be an equation for each $j = 0, \ldots, I-1$. In the nonsymmetric case, there are many more unknowns to be found. Each equation depends on known quantities such as the position of the interface at previous times and the physical parameters of the system. And as in the symmetric case, the unknown values of the current interface position $(X_0, X_1, \ldots, X_j, \ldots, X_{I-1}, Y_0, Y_1, \ldots, Y_j, \ldots, Y_{I-1})$ are also necessary for evaluation. However, in the nonsymmetric case, we also need to know the value of $\nabla u \cdot n$ at each point on the interface as approached from both the solid and liquid. We can again rewrite the left-hand side of (3.46) and call it g_j. We can write equations (6.51) and (6.52) as a sum of known coefficients multiplied by our unknown quantities.

$$g_j = \sum_{i=0}^{I-1} \alpha_{ij} X_i + \beta_{ij} Y_i + \gamma_{ij} \nabla u_S \left(s_j, t\right) \cdot n. \tag{6.53}$$

$$h_j = \sum_{i=0 \alpha ij}^{I-1} \Lambda_{ij} X_i + \Upsilon_{ij} Y_i + \Gamma_{ij} \nabla u_L \left(s_j, t\right) \cdot n.$$

These coefficients are quite complex, but can be found using the methods in the previous section.

We will use the same prescriptions for point motion on the interface as we use in the symmetric case. We will set the tangential velocity of the first point to zero.

$$\left[\mathbf{v} \ \cdot \mathbf{t}\right]_{s=-\pi} = 0. \tag{6.54}$$

This equation (6.54) also depends only on the unknown values of the current interface position $(X_0, X_1, \ldots, X_j, \ldots, X_{I-1}, Y_0, Y_1, \ldots, Y_j, \ldots, Y_{I-1})$ and known quantities such as the position of the interface at previous times and the physical parameters of the system. Similarly, we can write equation (6.54) as a sum of known coefficients multiplied by our unknown quantities. We will call this new value h_0.

$$p_0 = \sum_{i=0}^{I-1} \mu_{i0} X_i + \nu_{i0} Y_i. \tag{6.55}$$

These coefficients are determined by finding the tangential velocity of point t in terms of the current and previous interface positions.

The remaining equations are found by assuming that the points are equally spaced along the interface.

$$\text{arclen}(\zeta(s_j,t),\zeta(s_{j+1},t)) - \text{arclen}(\zeta(s_0,t),\zeta(s_1,t)) = 0. \tag{6.56}$$

We are comparing the arc length between point s_j and its next neighbor with the arc length between the first two points on the interface. There is an equation for each $j = 1,\ldots,I-1$, and each of these equations depends only on the unknown values of the current interface position $(X_0, X_1, \ldots, X_j, \ldots, X_{I-1}, Y_0, Y_1, \ldots, Y_j, \ldots, Y_{I-1})$ and known quantities such as the position of the interface at previous times and the physical parameters of the system. We write the quantity on the left-hand side of equation (6.56) as h_j. Only the position of the current and previous interface should be necessary to evaluate this expression:

$$p_j = \sum_{i=0}^{I-1} \mu_{ij} X_i + \nu_{ij} Y_i. \tag{6.57}$$

Finally, our integral equation is coupled at the interface by the Stefan condition (2.7).

$$[\mathbf{v}\cdot\mathbf{n}]_{s=s_j} - \kappa_S \nabla u_S(s_j,t)\cdot\mathbf{n} - \kappa_L \nabla u_L(s_j,t)\cdot\mathbf{n} = \mathbf{0}. \tag{6.58}$$

In the symmetric case, this was implicitly involved in the integral equation. However, in the nonsymmetric case it must be directly applied while solving for the integral equation. There will be an equation for each $j = 0,\ldots,I-1$. Each equation depends only on known quantities and the unknown quantities previously described $(X_j, Y_j, \nabla u_S(s_j,t)\cdot\mathbf{n}, \nabla u_L(s_j,t)\cdot\mathbf{n})$. We can rewrite the left-hand side of (6.58) as a sum of only known coefficients multiplied by our unknown quantities.

$$q_j = \sum_{i=0}^{I-1} \rho_{ij} X_i + \sigma_{ij} Y_i + \tau_{ij} \nabla u_S(s_j,t)\cdot n + \omega_{ij} \nabla u_L(s_j,t)\cdot n. \tag{6.59}$$

Although much larger and significantly more complex, our system may again be approximated by a matrix equation.

$$\mathbf{F}\mathbf{x} = \mathbf{0}, \tag{6.60}$$

where

$$\mathbf{x} = [X_0 \ldots X_{I-1}, Y_0 \ldots Y_{I-1}, \nabla u_{0,\text{solid}} \ldots \nabla u_{I-1,\text{solid}}, \nabla u_{0,\text{liquid}} \ldots \nabla u_{I-1,\text{liquid}}]^T. \tag{6.61}$$

$$F = \begin{bmatrix} \text{coefficients for } g_0 \\ \vdots \\ \text{coefficients for } g_{I-1} \\ \text{coefficients for } h_0 \\ \vdots \\ \text{coefficients for } h_{I-1} \\ \text{coefficients for } p_0 \\ \vdots \\ \text{coefficients for } p_{I-1} \\ \text{coefficients for } q_0 \\ \vdots \\ \text{coefficients for } q_{I-1} \end{bmatrix}.$$

We can now use Newton's method to solve for the new interface position in the same way that we did in the symmetric case in Section 3.1.3.

6.1.4 Step 4: Diffuse the Smooth Temperature Field

In Section 3.1.4, we discussed in detail how to diffuse the smooth temperature field. Exactly the same process can be used for the nonsymmetric case, except in the non-symmetric case there are two smooth temperature fields which require advancement

using the diffusion equation. We advance each smooth temperature field separately using the diffusion coefficient appropriate in each phase.

6.1.5 Step 5: Find the New Contribution

We need to advance our smooth temperature fields in both phases to the next time step (6.6) and (6.7):

$$\overline{u}_S\left(\mathbf{x}, t - N\Delta t + \Delta t, t + \Delta t\right) = \tag{6.62}$$

$$\begin{aligned}
&\int_{V_S(t_0)} u_S\left(\mathbf{x}', t_0\right) G_S\left(\mathbf{x}', t; \zeta\left(s,t\right), t_0\right) dV' \\
&+ \int_{t_0}^{t-N\Delta t} \int_{S(t')} u_S\left(\mathbf{x}', t'\right) G_S\left(\mathbf{x}', t; \zeta\left(s,t\right), t'\right) \left(\mathbf{v}'\cdot\mathbf{n}'\right) ds'dt' \\
&+ \kappa_S \int_{t_0}^{t-N\Delta t} \int_{S(t')} G_S\left(\mathbf{x}', t; \zeta\left(s,t\right), t'\right) \left(\nabla' u_S\left(\mathbf{x}', t'\right)\cdot\mathbf{n}'\right) ds'dt' \\
&- \kappa_S \int_{t_0}^{t-N\Delta t} \int_{S(t')} u_S\left(\mathbf{x}', t'\right) \left(\nabla' G_S\left(\mathbf{x}', t; \zeta\left(s,t\right), t'\right)\cdot\mathbf{n}'\right) ds'dt' \\
&+ \int_{t-N\Delta t}^{t-(N-1)\Delta t} \int_{S(t')} u_S\left(\mathbf{x}', t'\right) G_S\left(\mathbf{x}', t; \zeta\left(s,t\right), t'\right) \left(\mathbf{v}'\cdot\mathbf{n}'\right) ds'dt' \\
&+ \kappa_S \int_{t-N\Delta t}^{t-(N-1)\Delta t} \int_{S(t')} G_S\left(\mathbf{x}', t; \zeta\left(s,t\right), t'\right) \left(\nabla' u_S\left(\mathbf{x}', t'\right)\cdot\mathbf{n}'\right) ds'dt' \\
&- \kappa_S \int_{t-N\Delta t}^{t-(N-1)\Delta t} \int_{S(t')} u_S\left(\mathbf{x}', t'\right) \left(\nabla' G_S\left(\mathbf{x}', t; \zeta\left(s,t\right), t'\right)\cdot\mathbf{n}'\right) ds'dt',
\end{aligned}$$

$$\overline{u}_L\left(\mathbf{x}, t - N\Delta t + \Delta t, t + \Delta t\right) = \tag{6.63}$$

$$
\begin{aligned}
&\int_{V_L(t_0)} u_L\left(\mathbf{x}', t_0\right) G_L\left(\mathbf{x}', t; \zeta\left(s,t\right), t_0\right) dV' \\
&- \int_{t_0}^{t-N\Delta t} \int_{S(t')} u_L\left(\mathbf{x}', t'\right) G_L\left(\mathbf{x}', t; \zeta\left(s,t\right), t'\right) \left(\mathbf{v}'\cdot\mathbf{n}'\right) ds'dt' \\
&- \kappa_L \int_{t_0}^{t-N\Delta t} \int_{S(t')} G_L\left(\mathbf{x}', t; \zeta\left(s,t\right), t'\right) \left(\nabla' u_L\left(\mathbf{x}', t'\right)\cdot\mathbf{n}'\right) ds'dt' \\
&+ \kappa_L \int_{t_0}^{t-N\Delta t} \int_{S(t')} u_L\left(\mathbf{x}', t'\right) \left(\nabla' G_L\left(\mathbf{x}', t; \zeta\left(s,t\right), t'\right)\cdot\mathbf{n}'\right) ds'dt' \\
&- \int_{t-N\Delta t}^{t-(N-1)\Delta t} \int_{S(t')} u_L\left(\mathbf{x}', t'\right) G_L\left(\mathbf{x}', t; \zeta\left(s,t\right), t'\right) \left(\mathbf{v}'\cdot\mathbf{n}'\right) ds'dt' \\
&- \kappa_L \int_{t-N\Delta t}^{t-(N-1)\Delta t} \int_{S(t')} G_L\left(\mathbf{x}', t; \zeta\left(s,t\right), t'\right) \left(\nabla' u_L\left(\mathbf{x}', t'\right)\cdot\mathbf{n}'\right) ds'dt' \\
&+ \kappa_L \int_{t-N\Delta t}^{t-(N-1)\Delta t} \int_{S(t')} u_L\left(\mathbf{x}', t'\right) \left(\nabla' G_L\left(\mathbf{x}', t; \zeta\left(s,t\right), t'\right)\cdot\mathbf{n}'\right) ds'dt'.
\end{aligned}
$$

The value of the underlying temperature field from time t diffused one time step to $t+\Delta t$ was found in the previous section (Section 6.1.4) and gave us the contribution corresponding to the first four integrals in each of the equations (6.62) and (6.63).

Next we need to find the new contribution to the underlying temperature fields which correspond to the final three integrals in each of the equations (6.62) and (6.63). These additional integrals are actually our familiar functions from Section 6.1.2: $Q\left(\mathbf{x},t-\left(N-1\right)\Delta t, t-N\Delta t\right)$ in the solid and liquid, $R\left(\mathbf{x},t-\left(N-1\right)\Delta t, t-N\Delta t\right)$ in the solid and liquid, and $T\left(\mathbf{x},t-\left(N-1\right)\Delta t, t-N\Delta t\right)$ in the solid and liquid. To complete $\overline{u}_S\left(\mathbf{x}, t-N\Delta t+\Delta t, t+\Delta t\right)$ and $\overline{u}_L\left(\mathbf{x}, t-N\Delta t+\Delta t, t+\Delta t\right)$ over the entire domain, these integrals need to be evaluated at each point in the domain for both the solid and liquid temperature fields. We have shown in great detail the evaluation of these integrals previously and that evaluation can now conveniently be used again to find the newest pieces of $\overline{u}_S\left(\mathbf{x}, t-N\Delta t+\Delta t, t+\Delta t\right)$ and $\overline{u}_L\left(\mathbf{x}, t-N\Delta t+\Delta t, t+\Delta t\right)$. However, Q, R, and T are very complicated and computationally intensive functions to evaluate, and because they must be evaluated at every point in the domain twice (once for the solid temperature field and once for the liquid), this becomes the most costly step in the numerical method. However, it does maintain a constant operation count between time steps and does not grow as time

progresses as a direct integral equation solver would.

Because each step also satisfies the heat equation, we can continue to step the method forward in this manner.

6.2 One-Sided Model

The numerical model could also be applied to a one-sided model. In a one-sided model, no diffusion occurs in the solid phase. Setting $\kappa_S = 0$ throughout Section 6.1 significantly reduces the amount of work that is required. However, the numerical method remains unchanged.

Brattkus and Meiron [4] were able to use the one-sided, one-dimensional model to simulate the rapid directional solidification of a binary alloy. The controlling factor for growth in the solidification of metal alloys is the distribution of the solute which is dissolved in the liquid. Mass diffusion in the limiting mechanism. For an alloy being directionally solidified at a pulling speed of V with a temperature gradient G, the diffusion equation becomes

$$\frac{\partial C}{\partial t} = D\frac{\partial^2 C}{\partial z^2} + V\frac{\partial C}{\partial z}, \tag{6.64}$$

where C is the concentration of the solute and D is its diffusivity. Additional boundary conditions are given by

$$D\frac{\partial C}{\partial z} = v\,(k-1)\,C, \tag{6.65}$$

where k is equal to the ratio of concentration across the interface and v is the velocity of the interface, which is given by

$$v = V + \frac{\partial \zeta}{\partial t}. \tag{6.66}$$

Also the temperature of the front T_I is fixed by

$$T_I = T_M + mC + \mu_0 v, \tag{6.67}$$

where m is the slope of the liquidus, $1/\mu_0$ is a characteristic velocity representing nonequilibrium attachment kinetics, and T_M is the melting temperature. Although the model is quite complicated, it can be represented by an integral equation which resembles the one that we have dealt with in this thesis. Their integral equation at the interface $\zeta(t)$ becomes

$$\frac{1}{2}u(\zeta) = \int_0^t u(\zeta') \frac{\partial G(\zeta, t; \zeta', t')}{\partial z} dt' \tag{6.68}$$

$$+ \int_0^t \left(1 + \frac{\partial \zeta'}{\partial t}\right) \left[ku(\zeta') - \frac{k_E(1-k)}{1-k_E}\right] G(\zeta, t; \zeta', t')\, dt'$$

$$+ \int_{-\infty}^{\infty} u_0(z')\, G(\zeta, t; z', 0)\, dz', \tag{6.69}$$

where

$$G(z, t; z', t') = \frac{1}{\sqrt{4\pi(t-t')}} \exp\left[-\frac{(z - z' + t - t')^2}{4(t-t')}\right] \tag{6.70}$$

and k_E is the equilibrium value of k. A relaxation oscillatory instability in the steadily moving front discovered and discussed by Coriell and Sekerka [13] and Merchant and Davis [36] is confirmed by the numerical results.

Chapter 7 Summary and Ideas for Future Work

We implemented a numerical algorithm for the symmetric case in two dimensions. The results obtained agreed well with microscopic solvability theory as well as the similarity solution for the expanding circle case. An extension of the numerical was also derived for the nonsymmetric case.

Additionally, a stability analysis was done for the Ivantsov solution showing increasingly oscillatory behavior for the interface with increasing eigenvalues.

Obviously, an implementation of the two-dimensional, nonsymmetric numerical method would be the next logical step to pursue in continuance of the numerical algorithm. The numerical method would require more time and computing power than was required for the symmetric method, but the algorithm has been developed and should be fairly straightforward to implement.

Additionally, there is nothing in the algorithm which prevents extension of this method to three dimensions. Extending either the symmetric or nonsymmetric cases to three dimensions would be possible. Also noise could be added to stimulate the growth of side branches.

Bibliography

[1] V. Alexiades and A. D. Solomon, *Mathematical Modeling of Melting and Freezing Processes*, Hemisphere, 1993.

[2] A. Barbieri, D. C. Hong, and J. S. Langer, *Velocity selection in the symmetric model of dendritic crystal growth*, Phys. Rev. A, **35**(4), pp. 1802-1808 (1987).

[3] E. Anderson, Z. Bai, C. Bischof, J. Demmel, J. Dongarra, J. Du Croz, A. Greenbaum, S. Hammarling, A. McKenney, S. Ostrouchov, and D. Sorensen, *LAPACK Users' Guide, second edition.* SIAM, 1992.

[4] K. Brattkus and D. I. Meiron, *Numerical simulations of unsteady crystal growth*, SIAM J. Appl. Math., **52**(5), pp. 1303-1320 (1992).

[5] G. Caginalp and P. C. Fife, *Dynamics of Layered Interfaces Arising from Phase Boundaries*, SIAM J. Appl. Math. **48**(4), pp. 506-518 (1988).

[6] G. Caginalp, *Stefan and Hele-Shaw type models as asymptotic limits of the phase-field equations*, Phys. Rev. A, **39**, pp. 5887-5896 (1989).

[7] B. Caroli and H. Müller-Krumhaar, *Recent advances in the theory of free dendritic growth*, ISIJ Intl., **35**, pp. 1541-1550 (1995).

[8] B. Caroli, C. Caroli, B. Roulet, and J. S. Langer, *Solvability condition for needle crystals at large undercooling in a nonlocal model of solidification*, Phys. Rev. A, **33**, pp. 442-452 (1986).

[9] B. Caroli, C. Caroli, and B. Roulet, Notes from: Instabilities of Planar Solidification Fronts, 1989.

[10] H. S. Carslaw and J. C. Jaeger, *Conduction of Heat in Solids.* Oxford University Press, 1959.

[11] J. Chadham and P. Ortoleva, *The stabilizing effect of surface tension on the development of the free boundary in a planar, one-dimensional, Cauchy-Stefan problem*, IMA J. Appl. Math, **30**, pp. 57-66 (1983).

[12] S. Chen, B. Merriman, S. Osher, and P. Smereka, *A simple level set method for solving Stefan problems*, J. Comp. Physics, **135**, pp. 8-29 (1997).

[13] S. R. Coriell and R. F. Sekerka, *Oscillatory morphological instabilities due to non-equilibrium segregation*, J. Crystal Growth, **61**, pp. 499-508 (1983).

[14] M. E. Glicksman, M. B. Koss, L. T. Bushnell, J. C. LaCombe, and E. A. Winsa, *Dendritic growth of succinonitrile in terrestrial and microgravity conditions as a test of theory*, ISIJ Intl., **35**, pp. 604-610 (1995).

[15] J. C. LaCombe, M. B. Koss, and M. E. Glicksman, *Nonconstant Tip Velocity in Microgravity Dendritic Growth*, Physical Review Letters, **83**(15), pp. 2997-3000 (1999).

[16] L. Greengard and J. Strain, *A fast algorithm for the evaluation of heat potentials*, Comm. Pure Appl. Math., **43**, pp. 949-963 (1990).

[17] G. P. Ivantsov, *Mathematical Physics*. Dokl. Akad. Nauk, SSSR, 58, p. 567 (1947). Translated by G. Horvey, Report No. 60-RL-(2511M), G. E. research lab, New York, 1960.

[18] D. Juric and G. Tryggvason. *A front-tracking method for dendritic solidification*, J. Comp. Phys., **123**, pp. 127-148 (1996).

[19] A. Karma and W. Rappel, *Numerical simulation of three-dimensional dendritic growth*, Phys. Rev. Letters, **77**, pp. 4050-4053 (1996).

[20] A. Karma and W. Rappel, *Phase-field simulation of three-dimensional dendrites: Is microscopic solvability theory correct?*, J. Crystal Growth, **174**, pp. 54-64 (1997).

[21] A. Karma and W. Rappel, *Quantitative phase-field modelling of dendritic growth in two and three-dimensions*, Phys. Rev. E, **57**(4), pp. 4323–4349 (1998).

[22] R. Kobayashi, *Modelling and numerical simulations of dendritic crystal growth*, Physica D, **63**(3), pp. 410-423 (1993).

[23] M. D. Kunka, M. R. Foster, and S. Tanveer, *Dendritic crystal growth for weak undercooling*, Phys. Rev. E, **56**, pp. 3068-3100 (1997).

[24] P. M. Lahey, *A Fixed-Grid Numerical Method for Dendritic Solidification with Natural Convection*. PhD thesis, Department of Applied and Applied and Computational Mathematics, California Institute of Technology, 1999.

[25] J. S. Langer and H. Müller-Krumbhaar, *Stability effects in dendritic crystal growth*, J. Crystal Growth, **42**, pp. 11-14 (1977).

[26] J. S. Langer and H. Müller-Krumbhaar, *Theory of dendritic growth-I. Elements of a stability analysis*, Acta Metallurgica, **26**, pp. 1681-1687 (1978).

[27] J. S. Langer and H. Müller-Krumbhaar, *Theory of dendritic growth-II. Instabilities in the limit of vanishing surface tension*, Acta metallurgica, **26**, pp. 1689-1695 (1978).

[28] J. S. Langer and H. Müller-Krumbhaar, *Theory of dendritic growth-III. Effects of surface tension*, Acta metallurgica, **26**, pp. 1697-1708 (1978).

[29] J. S. Langer, *Instabilities and pattern formation in crystal growth*, Rev. Modern Phys., **52**, pp. 1-28.

[30] J. S. Langer, *Existence of needle crystals in local models of solidification*, Phys. Rev. A, **33**, pp. 435-441 (1986).

[31] J. S. Langer, *Lectures in the Theory of Pattern Formation*, 1987.

[32] R. B. Lehoucq, *Analysis and Implementation of an Implicitly Restarted Arnoldi Iteration*. PhD thesis, Department of Computational and Applied Mathematics, Rice University, 1995.

[33] D. I. Meiron, *Boundary integral formulation of the two-dimensional symmetric model of dendritic growth*, Physica D, **23**(1-3), pp. 329-339 (1986).

[34] D. I. Meiron, Private Communication, 1996.

[35] D. I. Meiron, *Selection of steady states in the two-dimensional symmetric model of dendritic growth.* Phys. Rev. A, **33**(4), pp. 2704-2715, (1986).

[36] G. J. Merchant and S. H. Davis, *Morphological instability in rapid directional solidification*, Acta metall. mater., **38**, pp. 2683 (1990).

[37] Y. Saito, *Statistical Physics of Crystal Growth*, World Scientific, 1996.

[38] A. Schmidt, *Computation of three-dimensional dendrites with finite elements*, J. Comp. Phys., **125**, pp. 293-312 (1996).

[39] J. A. Sethian, *Curvature and the evolution of fronts*, Comm. Math. Phys., **101**, pp. 487-499 (1985).

[40] J. A. Sethian and J. Strain, *Crystal growth and dendritic solidification*, J. Comp. Phys., **98**, pp. 231-253 (1992).

[41] D. C. Sorensen, *Implicit application of polynomial filters in a k-step Arnoldi method*, SIAM J. Matrix Analysis and Appl., **13**(1), pp. 357:385, (1992).

[42] J. Strain, *A boundary integral approach to unstable solidification*, J. Comp., Phys., **85**, pp. 342-389 (1989).

[43] J. Strain, *Velocity effects in unstable solidification*, SIAM J. Appl. Math., **50**, pp. 1-15 (1990).

[44] J. M. Sullivan Jr., D. R. Lynch, and K. O'Neill, *Finite Element Simulation of Planar Instabilities during Solidification of an Undercooled Melt*, J. Comp., Phys., **69,** pp. 81-111 (1987).

[45] C. Yang, D. C. Sorenson, D. I. Meiron, and B. Wedeman, Numerical computation of the linear stability of the diffusion model for crystal growth simulation, preprint of article presented at conference.